Estimation of Iceberg Density in the Grand Banks of Newfoundland

by

Robert Kelly

A Thesis Submitted to the Faculty of Graduate Studies and Research
in partial fulfilment of the requirements of the degree of
Master of Engineering

Department of Civil Engineering and Applied Mechanics
McGill University, Montréal
March, 1996

ISBN 0-612-12122-4

Abstract

Icebergs offshore Newfoundland represent hazards to both ships and constructed facilities, such as off-shore oil production facilities. Collision with icebergs represent hazards for both surface and sub-surface facilities. In the latter case, hazards are associated with seabed scouring by the iceberg keel. In both cases, hazard analysis requires estimation of the flux of icebergs and their size distribution. Estimates of the flux of icebergs can be achieved by obtaining separate estimates of iceberg densities and of drift patterns of iceberg velocities. The objective of this thesis is to develop and apply estimation procedures for the density of icebergs using presently available data sets. The most comprehensive of these data sets is compiled by the International Ice Patrol (IIP), starting in 1960. The IIP database comprises data from several sources and for icebergs of varying sizes. In addition, the spatial coverage of surveys does not appear to be uniform throughout the year. Several non-parametric density estimation procedures are investigated. The objective is to eliminate any apparent high densities in the estimates due to the non-uniform coverage of the region during surveys and retain statistically significant features in the spatial variation of densities.

Several kernel estimators are examined: (1) a uniform square kernel, (2) a uniform circular kernel, (3) a Normal kernel, and (4) an adaptive kernel. Uniform kernels have the advantage of computational efficiency, however, they do not account for spatial variations in the densities and produce over-smoothing in regions of peak iceberg densities and under-smoothing in regions of low iceberg densities. The adaptive kernel is computationally more demanding, but appears to fulfill all the desired requirements for preserving significant features and eliminating erratic estimates.

Résumé

Les icebergs au large de Terre-Neuve représentent un risque potentiel pour la navigation et les structures autant temporaires que permanentes. Les risques de collision sont importants autant pour les installations en surface que pour les installations submergées. Dans ce dernier cas, les risques sont associés aux sillons creusés par les icebergs dans le sol marin. Dans tous les cas, les analyses de risque requièrent une estimation du flux des icebergs et leur distribution en grosseur. L'estimation du flux des icebergs peut être obtenue par l'intermédiaire de l'estimation de la densité des icebergs et de la charactérization de leur dérive. L'objectif de la thèse est de développer et d'appliquer des méthodes d'estimation pour la densité des icebergs en utilisant les données présentement disponibles. La base de données la plus complète sur les icebergs est celle compilée par le International Ice Patrol (IIP) depuis 1960. Cette base de données comprend des observations de plusieurs sources (navire, AES, etc.) sur des icebergs de taille diverse. De plus, la couverture spatiale des reconnaissances n'est pas toujours uniforme au cours de l'année ou d'une année à l'autre. Plusieurs méthodes d'estimation non-paramétrique de la densité sont analysées. L'objectif de l'estimation est d'éliminer tout estimé apparemment élevé de la densité associé à une reconnaissance préférentielle de la region et de retenir toute variation spatiale jugée statistiquement significative.

Plusieures procédures d'estimation utilisant des fonctions de type kernel sont étudiées: (1) kernel carré uniforme, (2) kernel circulaire uniforme, (3) kernel à distribution Normale, et (4) kernel carré variable. Les fonctions à kernel uniforme ont l'avantage au niveau du calcul numérique mais négligent la variation spatiale de la densité, ce qui résulte à un sur-lissage des estimés dans les régions où les icebergs sont abondants et à un sous-lissage des estimés dans les régions où les icebergs sont peu nombreux. Les fonctions à kernel variable sont plus exigeantes du point de vue calcul mais semblent remplir toutes les exigences au niveau du lissage optimal des estimés.

Table of Contents

List of Figures

List of Tables

List of Symbols

Note that the absence of parentheses after a definition indicates that it applies throughout the text, otherwise the definition, or symbol, is particular only to the indicated section.

Latin Symbols

A	:	Area;
$E(\cdot)$	:	Expected value of $\cdot$;
F_{dr}	:	Cumulative distribution function of iceberg keel depth (3.5.3);
L	:	Length of sonar track (3.5.1);
	:	Perimeter;
N	:	Number of new scours (3.5.1);
N^*	:	Number of observed lines (4.2);
N_R	:	Number of report days;
NG	:	Number of new groundings (3.5.2);
$P(\cdot)$	:	Probability of $\cdot$;
P_D	:	Probability of detection;
R_{max}	:	Maximum kernel radius;
$\Re^n$	:	n-dimension space;
S	:	Sample region;
$K(\cdot)$	:	Kernel function;
T	:	Year (5.3);
X	:	Set of objects(4.3);
	:	Random vector coordinates;
$V(\cdot)$	:	Coefficient of variation of $\cdot$;
d	:	Water depth (3.5.3);
	:	Distance from a point to line (4.2);
	:	Distance from the centre of a kernel to a point (5.1.2);
f, f_x	:	Probability distribution function; Probability distribution function of x;
h	:	Histogram bin width (4.3);
	:	Kernel bandwidth;
i, j	:	Indexing variables.;
n	:	Number of observations (4.3);
r	:	Correlation coefficient (5.2);
t	:	Time of year (month) (5.3);
$\underline{t}$	:	Vector Coordinates;
t_1, t_2	:	Axes labels;
$\underline{x}$	:	Vector Coordinates;
x_1, x_2	:	Axes labels;
$\underline{y}$	:	Vector coordinates;

Greek Symbols

Θ	:	Sample space;
ΔT	:	Elapsed time between repetitive mapping surveys (3.5.1);
	:	Length of observation period (3.5.2);
Ω	:	Random set of lines;
Δt	:	Time period (5.3.1);
α	:	Angle;
δ	:	Smoothing factor (5.4);
ϕ	:	Flux of icebergs (bergs/km-day) (3.5.3);
λ	:	Rate of scouring (Section 3.5);
	:	Intensity function (Chapter 4);
	:	Iceberg density (Chapter 5);
μ	:	Mean;
ν	:	Iceberg drift velocity;
π	:	Pi;
ρ	:	Corelation Coefficient (5.4);
θ	:	Vector coordinates;
σ	:	Standard deviation;
υ	:	Iceberg crossing rate (5.3);

Acknowledgments

It is with deep appreciation that I acknowledge my research advisor, Luc E. Chouinard, for his invaluable insight and assistance. His enthusiastic interest and constant cooperation deserves the heartiest of acknowledgements.

I would also like to express my gratitude towards Gary Sonnichsen and Michael Lewis of the Geological Survey of Canada (Atlantic), who were able to provide the data for this study, as well as some financial assistance.

Finally, I would like to send my warmest regards to my parents, family and friends, just for being themselves.

1. Introduction

Currently, there is substantial interest in the estimation of iceberg related hazards in the Grand Banks of Newfoundland. The discovery of oil reserves in this region has made the Grand Banks a potentially viable source of oil, however the presence of icebergs and pack-ice in this region represent a hazard to development. Drifting icebergs represent a hazard for both surface and subsurface production systems. In both cases, hazard analysis requires estimates of the flux of icebergs, their size and shape distributions, and their drift velocities, as a function of location.

Hazard analysis for Hibernia has focused mainly on characterizing collision between the fixed production structure and icebergs. However future developments at Hibernia, Terra Nova and Whiterose will rely extensively on sub-sea production systems which can be adversely affected by iceberg scouring, which has not been well characterized to date.

Only sparse data is currently available in order to characterize the frequency and severity of scouring over the Grand Banks. Scouring models based on a characterization of icebergs drift and size distribution can greatly reduce the uncertainty on the estimates of iceberg hazards. These models can be used to eliminate relict scours, to estimate in-filling rates of scours and to interpolate over locations where scouring data is not available.

An important element of the scouring model is the flux of icebergs at a given location which can be estimated from data on the spatial density and drift characteristics of icebergs.

This thesis focuses on the estimation of the density of icebergs in the vicinity of the Grand Banks. Several density estimation methods are examined in an attempt to develop an optimal procedure for the available data. The proposed methods of estimation are based on kernel density estimators for point patterns. The results should help in developing an iceberg scouring hazard model, which may be achieved by coupling estimated regional iceberg densities with regional probability distribution function for iceberg draft and regional drift velocities.

1.1 Icebergs

The estimation of regional iceberg densities has recently gained more attention because of the inherent risk caused by the presence of icebergs and an anticipated increase in the level of activity in the region. Risk of collision between a vessel and icebergs has been studied extensively (Blenkarn and Knapp, 1969; Evans-Hamilton, 1975; Crocker *et al*, 1995). Similar to iceberg-vessel collisions, the risk of iceberg scouring increases with the concentration of icebergs. Although, for iceberg scouring, only icebergs with large drafts are of significance. Other factors involved in iceberg scouring and collision include iceberg drift patterns (Garrett *et al*, 1985) and the probability distribution of iceberg sizes (Wadhams, 1983). The estimation of iceberg densities for the purpose of estimating collision probability focuses on the lower end of the probability distributions of iceberg sizes. The emphasis on smaller icebergs, which are much more numerous than large icebergs, is related to the inability to detect the smaller ice features in a wave environment to prevent collision. In contrast, scouring hazards are exclusively related to large icebergs, which are relatively unimportant for navigation because of their high probability of detection.

1.1.1 Sources of Iceberg Data

Two data sets were available for analysis: (1) the International Ice Patrol (IIP) database; and (2) the Husky Oil data sets.

The IIP was established in 1913, one year after the sinking of the Titanic and has since been responsible for determining the limits of iceberg hazards for navigation in the Grand Banks. IIP compiled a digitized database of iceberg locations that dates back to 1960. This represents the largest and most comprehensive iceberg database available for the Grand Banks. Iceberg databases have also been compiled by the Canadian Atmospheric and Environmental Agency (AES) and oil companies drilling in the Grand Banks, but are not as comprehensive. Husky Oil performed exploratory drilling on the northern edge of the Grand Banks between 1984 and 1988, during which they collected a database of iceberg statistics. This database is more limited in scope and range than the IIP database and is useful only for estimating regional iceberg characteristics close to the drilling sites.

1.2 Scours

Scours are long furrows caused when the keels of pressure ridges embedded in ice floes, or icebergs drag along the seafloor. Scouring may disrupt or damage sub-sea structures, such as pipelines, wellheads and cables. Scouring was originally identified as a potential impediment to development in the Beaufort Sea in 1970, where scours are produced by drifting ice floes (Pelletier and Shearer, 1972). Soon after, icebergs drifting off eastern Canada were also recognized as a hazard to development (Harris, 1974; Harris and Jollymore, 1974; Lewis and Keen, 1990).

Several methods for estimating scouring rates off eastern Canada have been developed, including repetitive mapping, inference through iceberg groundings, inference through iceberg keel size distribution, iceberg flux, scour degradation and scour dating (Lewis and Keen, 1990). However, these methods typically use data obtained over a relatively short period of time and a small region, and may not be representative of long term regional scouring rate trends. By using the IIP database, estimates of iceberg densities for the entire Grand Banks region may be obtained using a sample that includes 34 years of observations and which may be more representative of long term trends in regional iceberg densities.

1.3 Density Estimation

Estimates of iceberg densities are obtained by idealizing iceberg locations on a given day as a point pattern process and then analyzing the data with kernel estimators. Kernel density estimators are non-parametric estimators which include, as a special case, histograms.

Difficulties associated with the estimation of iceberg densities are related to the variability of the process spatially and in time, both intra-annually and inter-annually, and to the surveying and reporting procedures for the icebergs included in the data sets. For the IIP database, the main difficulties are associated with the different sources reporting icebergs, the non-uniform rate of surveying across the region, and the lack of information with respect to the size and location of the surveys. Issues related to temporal and spatial variations in the densities are not as important given the extent of the database both in time and space. Conversely, the Husky Oil data set is more homogeneous from the reporting point of view, given that all icebergs within 100 km of a drilling site are thought to have been reported. However, the data set is too limited in space and time to develop reliable estimates of regional long term trends in iceberg densities.

1.4 Thesis Outline

Chapter 2 presents a literature review on iceberg occurrences over the Grand Banks and of their characteristics. This is followed by a detailed description of the IIP and Husky Oil data sets.

In Chapter 3, the mechanics of iceberg scouring is described. A qualitative description of observed iceberg scours is presented and estimation procedures for the scouring rate are reviewed.

In Chapter 4, random line processes are described as a means of representing the drift of large icebergs. Given the nature of the available data few reliable iceberg tracks are available and the bulk of the data has to be analyzed as random points. Various non-parametric kernel density estimators are reviewed for the estimation of the density of icebergs as a function of time and location.

Chapter 5 presents the results of the analysis for both the IIP and the Husky Oil data sets. These include the estimation of the density of icebergs as a function of time and location, as well as some results for the distribution of iceberg dimensions and drift characteristics.

Finally, Chapter 6 highlights the main conclusions and offers recommendations for future research.

2. Icebergs

2.1 The Grand Banks of Newfoundland

The Grand Banks of Newfoundland are situated approximately 150 kilometers from the southeastern tip of the island of Newfoundland. It is comprised of six banks, the largest of which is the Grand Bank, a nearly flat region with bathymetries less than 100 m. It is separated from Newfoundland by the Avalon Channel, which is up to 200 m deep. The northern region of the Grand Banks has water depths of 200 m to 400 m. The eastern edge of the Grand Banks borders Flemish Pass, which is over 1000 m deep. East of Flemish Pass is Flemish Cap, an isolated area with water levels as shallow as 126 m (Figure 2.1-1). A thin layer of sand and gravel covers the Grand Banks. This surface is continually changing due to wave action, burrowing marine animals and iceberg scouring (Lewis *et al*, 1988). Traditionally, the Grand Banks have been mainly known as excellent fishing grounds. More recently, discoveries of hydro-carbon deposits has lead to the promise of the Grand Banks becoming a major source of oil production.

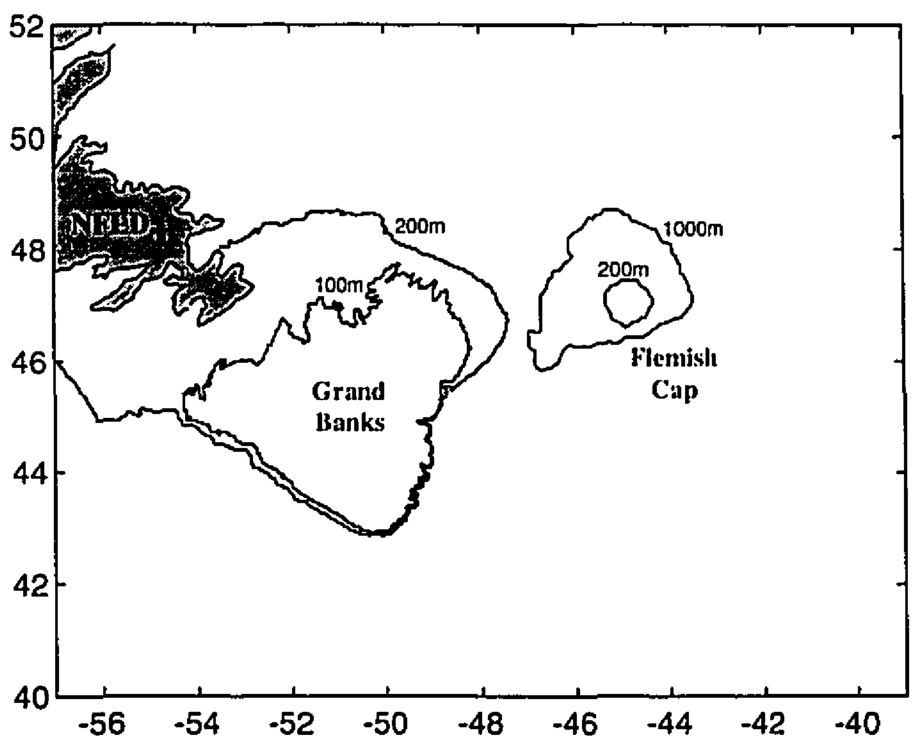

Figure 2.1-1 Grand Banks of Newfoundland.

2.2 Iceberg Sources

Calving of glaciers off Greenland's western coast is the principal source of icebergs. Icebergs are also formed by calving glaciers along Greenland's western coastline as well as Ellesmere, Bylot and Baffin Islands (Figure 2.2-1; Clark *et al*, 1990). These icebergs are carried by the strong ocean currents through Baffin Bay and south along the eastern Canadian seaboard. It is estimated that 10,000 to 30,000 icebergs are produced each year and that up to 40,000 icebergs are maintained in Baffin Bay, some of which exceed 25-30 million tonnes in mass (Clark *et al*, 1990; Lewis and Keen, 1990; Dinsmore, 1972). On average, a few hundred of these icebergs are transported as far south as the Grand Banks of Newfoundland each year, while the rest deteriorate much sooner. However, the number of icebergs which reach the Grand Banks is highly variable, both seasonally and yearly.

2.3 Drift

An iceberg's long-term drift is governed by ocean currents. However, iceberg trajectory may be influenced by such short-term factors as strong winds and tidal currents (Lewis *et al*, 1988). Icebergs originating from the south-western Greenland coast follow one of three paths (Figure 2.2-1; Marko, 1982; Marko *et al* 1986, 1987, 1994). Icebergs may flow northward along the West Greenland Current into northern Baffin Bay and then move westward, joining the swift Baffin and Labrador Currents southward. Alternatively, icebergs may follow the West Greenland Current only until Davis Strait before joining the Baffin and Labrador Currents. The third pathway accounts for those icebergs which move beyond the extent of the coastal currents (Marko *et al*, 1994). Near complete coverage of far-offshore ice during the fall and winter months allows icebergs to travel in a predominantly southerly direction with velocities of 5 to 20 km/day (Marko, 1982; Marko *et al*, 1994).

Icebergs entering the Grand Banks flow with the Labrador Current, which enters the Grand Banks with a southerly speed of 0.2 m/s. Once in the vicinity of the Grand Banks, icebergs follow one of three main paths. They may either drift east, along the northern edge of the Grand Banks and through the Flemish Cap; south-east, between the Flemish Cap and the Grand Banks, through Flemish Pass; or southward, traveling between Newfoundland and the

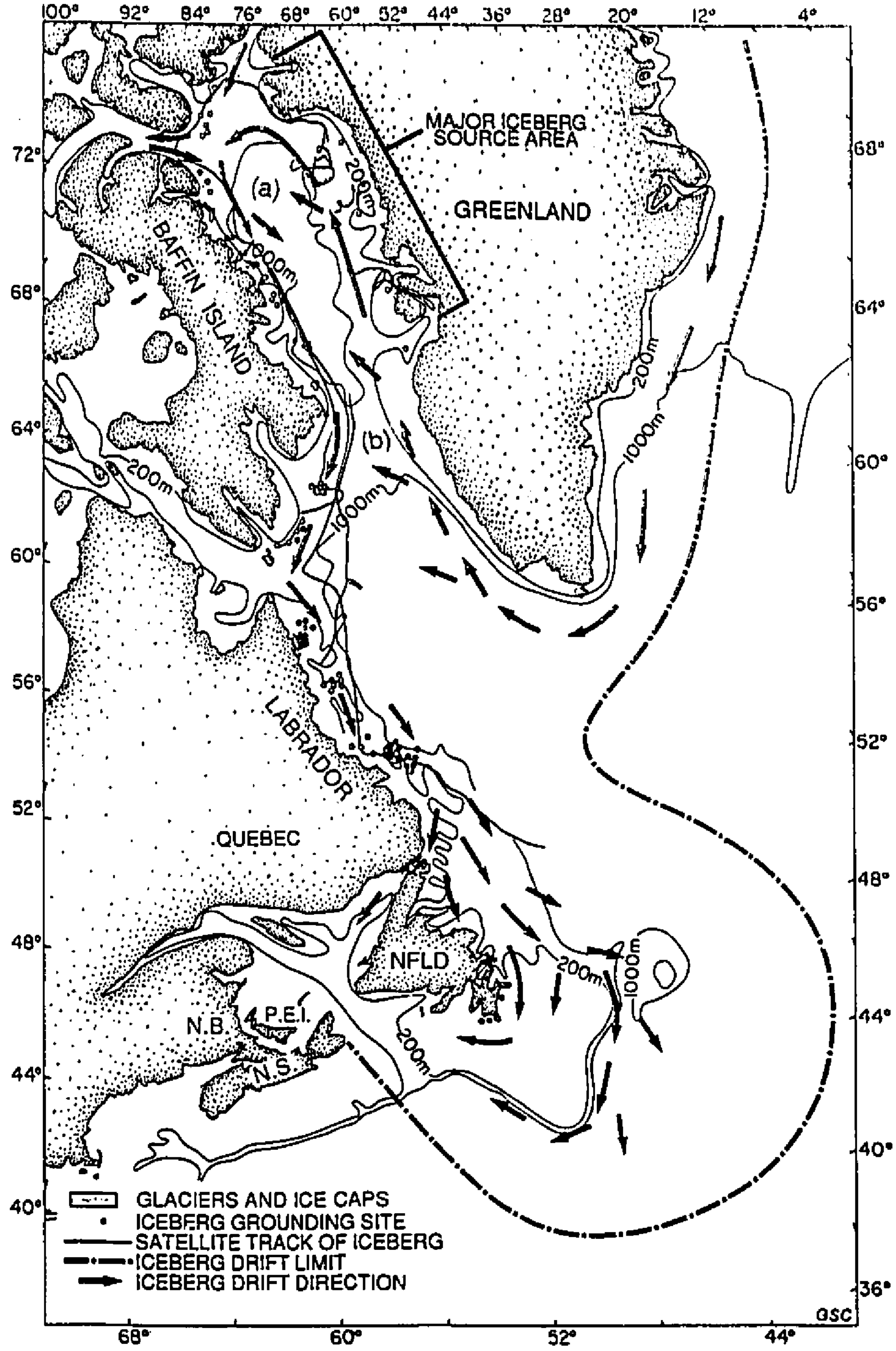

Figure 2.2-1 Iceberg drift pattern, areas of known iceberg groundings, glacial regions, paths of satellite-tracked icebergs and extreme iceberg drift limit. (a) Baffin Bay; (b) Davis Strait (from Lewis and Keen, 1990).

Grand Banks before drifting west and rounding the south-eastern tip of Newfoundland. This pattern closely resembles the flow of the Labrador Current as it enters the Grand Banks. The Labrador Current diverges into three branches: one flows south until the northern edge of the Grand Banks and then continues east, north of the Flemish Cap; another follows the contour of the Grand Banks southward through Flemish Pass and then east towards southern Newfoundland; and a third flows through Avalon Channel and follows Newfoundland's western coastline. Figure 2.3-1 shows the mean circulation pattern of currents in the Grand Banks. These currents have mean velocities of 0.2 m/s to 0.6 m/s (Lewis et al, 1988).

The distance traveled by icebergs from Greenland to the Grand Banks is approximately 1800 nautical miles and may take more than 2 years to complete (Clark *et al*, 1990).

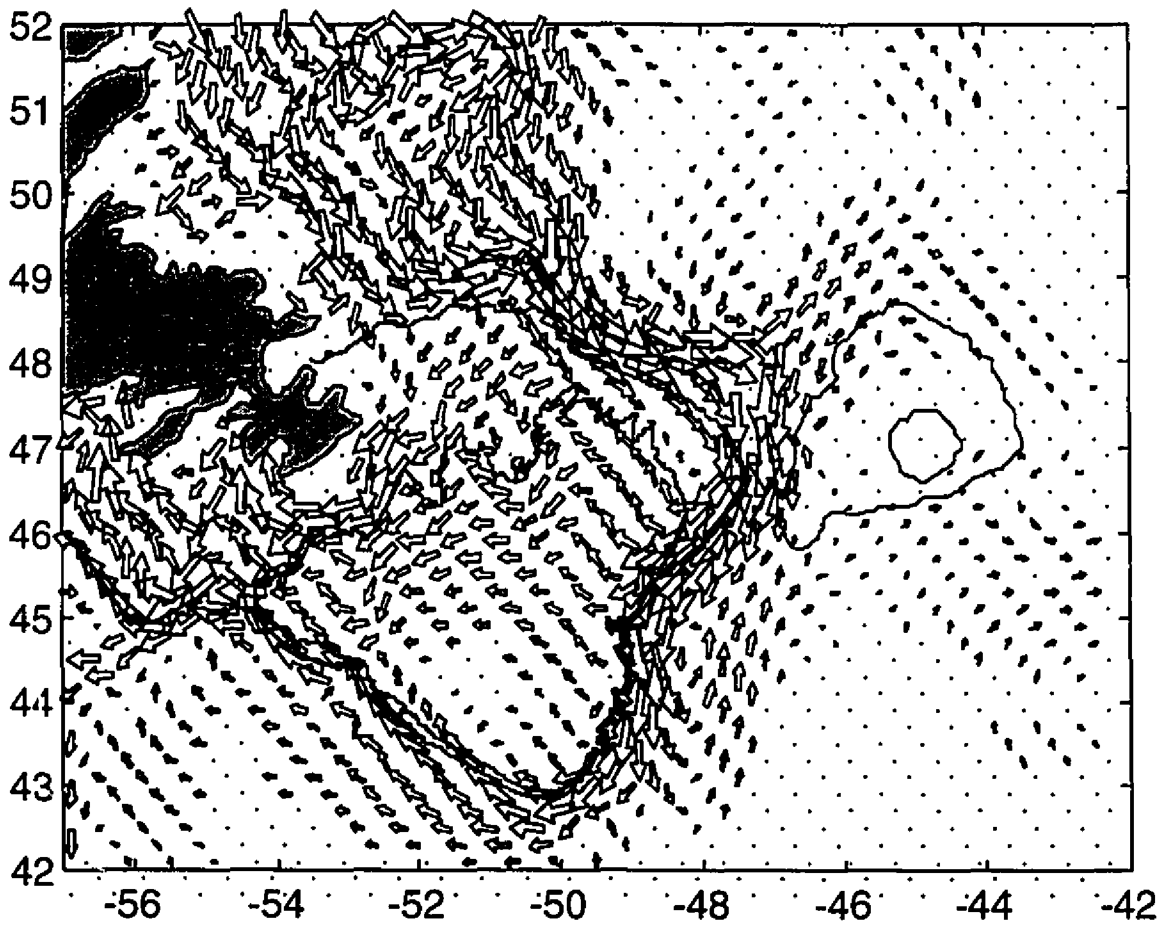

Figure 2.3-1 General current circulation pattern in the Grand Banks. (Note: to enhance small, but equally important currents, the arrows were scaled by the square root of the current magnitude).

2.4 Inter-Annual and Intra-Annual Variability

The number of icebergs drifting south of 48°N has been the traditional indicator of the severity of the iceberg season since it represents the historical boundary of trans-Atlantic shipping routes passing south of Newfoundland (Clark *et al*, 1990). Iceberg flux or densities exhibit large variabilities both inter-annually and intra-annually (Figures 2.4-1 and 2.4-2).

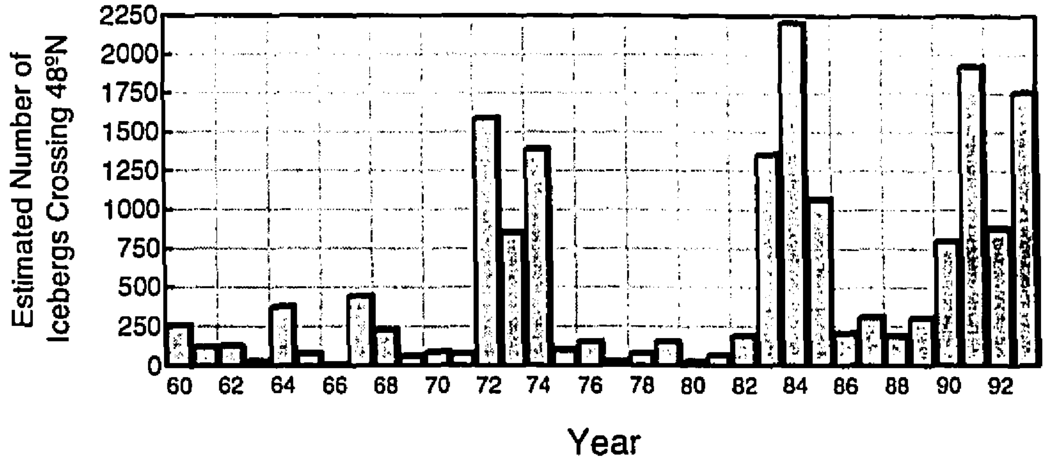

Figure 2.4-1 Number of icebergs crossing 48°N, by year, as estimated by IIP.

The intra-annual variability of iceberg flux gives rise to the notion of an iceberg season. The iceberg season extends from March to July and accounts for 91% of all reported icebergs drifting south of 48°N (Figure 2.4-2).

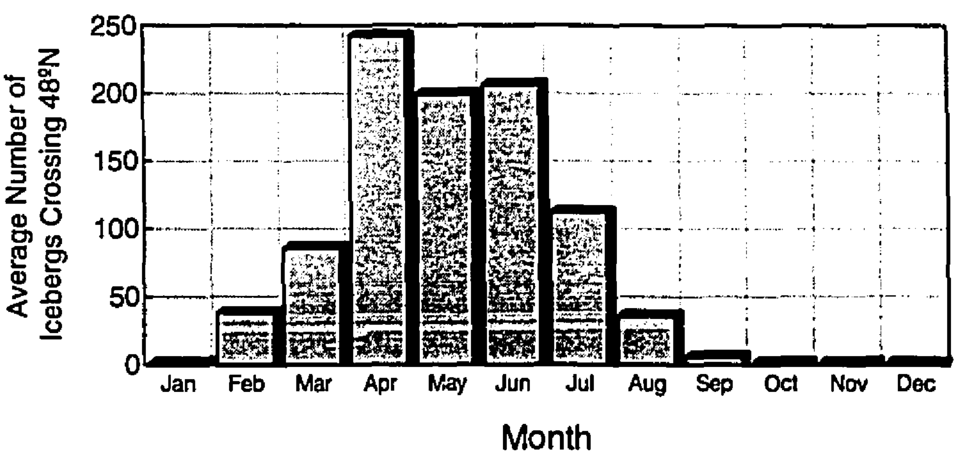

Figure 2.4-2 Monthly average of the number of icebergs crossing 48°N, as estimated by IIP.

An explanation for this phenomenon has been suggested by Marko *et al* (1994). Between August and mid-October, when there is no landfast ice along eastern Baffin Island, icebergs may drift close to shore, subsequently grounding. Grounded icebergs are not likely to drift as far south as the Grand Banks, as severe deterioration is needed before the iceberg is mobilized. Also, an iceberg may ground several more times after being remobilized. Landfast ice, which appears in early October, prevents icebergs from entering shallow waters. As a result, a greater number of icebergs avoid shallow continental shelf areas and drift south towards Davis Strait. Landfast ice can also entrap icebergs located up to 70 km from shore and prevent their release until the following summer during ice break-up. Icebergs which do not ground or are not entrapped reach Davis Strait between January and February. The presence of ice cover in Davis Strait at this time of year keeps sea water temperatures low and dampens waves, both of which are key factors in iceberg deterioration. By preventing grounding and abating deterioration, icebergs are more likely to reach the Grand Banks. In all, it is estimated that only 0.5% of icebergs formed each year by calving drift south of 48°N (Marko *et al*, 1994).

2.5 Classification of Physical Characteristics

By nature, icebergs are random in shape. Nonetheless, the International Ice Patrol (IIP) classifies the above water appearance of icebergs as either tabular or non-tabular. The non-tabular descriptor includes such shapes as growler, domed, dry-dock, pinnacle and bergy bit (Table 2.5-1). Tabular and blocky icebergs are very stable and are least susceptible to rolling and splitting. Icebergs in an advanced state of deterioration will generally exhibit rounded or pinnacled features (NORDCO, 1980). Since the Grand Banks is close to the southern limit of the iceberg corridor, icebergs are then in the final stages of deterioration and are typically non-tabular. Bergy bits and growlers are pieces from larger icebergs or icebergs in a state of near complete deterioration.

IIP has adopted a standardized size classification which it uses when reporting icebergs (Table 2.5-2). In accordance with this classification, length refers to the longest waterline dimension, while height refers to the greatest vertical dimension measured from the waterline. Estimates on iceberg drafts suggest that 50% of icebergs drifting into the Grand Banks will have drafts in excess of 60 m, but less than 10% will exceed 100 m (NORDCO, 1980).

TYPE OF ICEBERG	DESCRIPTION
TABULAR (TAB)	Horizontal, flat-topped berg with length:height ratio of 5:1 or more
BLOCKY (BLK)	Steep precipitous sides with horizontal or flat top, very solid berg, length:height ratio of 3:1 to 5:1
DOME (DOM)	Large smooth rounded top.
DRY-DOCK (DDK)	Eroded such that a large U-shaped slot is formed with twin columns or pinnacles. Slot extends under the water line or close to it.
PINNACLED (PNC)	Large central spire or pyramid of one or more spires dominating the shape. Less massive than domed-shaped icebergs of similar dimension.
BERGY BIT (BBB)	A mass of glacial ice smaller than an iceberg, but larger than a growler, about 15 m long. Small berg or large growler is the preferred usage.
GROWLER (GGG)	A mass of glacial ice that has calved from an iceberg or is the remains of an iceberg. A growler has a height of less than 1 m and a length less than 5 m.

Table 2.5-1 IIP iceberg size descriptors

TABULAR ICEBERGS		
Description	***Length***	***Height***
SMALL	Between 15 m and 60 m	Between 5 m and 15 m
MEDIUM	Between 60 m and 122 m	Between 15 m and 60 m
LARGE	Greater than 122 m	Between 50 m and 75 m
NON-TABULAR ICEBERGS		
Description	***Length***	***Height***
GROWLER	Under 5 m	Under 1 m
BERGY BIT	Between 5 m and 15 m	Between 1 m and 5 m
SMALL	Between 15 m and 60 m	Between 5 m and 15 m
MEDIUM	Between 60 m and 122 m	Between 15 m and 60 m
LARGE	Greater than 122 m	Between 50 m and 75 m

Table 2.5-2 IIP qualitative size and dimension descriptors.

2.6 Sources of Data

2.6.1 International Ice Patrol (IIP)

The IIP was formed in 1913 and is operated by the United States Coast Guard. Its mandate is to patrol the Grand Banks in order to determine the southwestern, southern and southeastern limits of the iceberg infested region. IIP's secondary objective is to maintain a database as complete as possible of iceberg locations within these limits (Anderson, 1993). The area surveyed by IIP is bounded by latitudes 40°N to 52°N and longitudes 39°W to 57°W. IIP supplements its database of iceberg locations with reports from other sources, such as reports from ships, commercial flights and from the Canadian Atmospheric Environment Service (AES). This data base is considered to be the most comprehensive source of iceberg information available, yet it is believed to underestimate the actual number of icebergs in the region (NORDCO, 1980).

IIP focuses its surveys on large icebergs and, in general, does not report growlers or bergy bits. In addition, IIP is mainly concerned with the southern extent of iceberg infested waters, which are areas with low iceberg densities. Consequently, IIP only reports icebergs in areas of high iceberg density incidentally when flying to the survey regions. The more extensive the outer limits of the iceberg infested area, the less time is available to cover interior areas, such as at the northern edge of the Grand Banks. IIP optimizes flight times by using an iceberg drift model to predict the future location of icebergs. However, this model is limited to regions where icebergs are frequently found. In years when icebergs drift further south than usual, such as in 1989, IIP must patrol more extensively southern regions because they are unable to predict iceberg movement. This leaves less time and resources to patrol the inner regions where the majority of icebergs are located. IIP's inability to survey interior regions does not affect it's mandate, however it affects reported number of icebergs crossing 48°N (Anderson, 1993).

IIP has been using aerial reconnaissance missions since 1946. Before 1946, ships were used to track icebergs. In 1983, IIP introduced the Side Looking Airborne Radar (SLAR) on its aircraft to improve iceberg detection. Previously, airborne reports had been done visually. Aircraft equipped with SLAR patrol from an elevation of 1800 m to 2400 m (6000 to 8000 feet) using a standard parallel leg type search with a 50 km (25 nautical miles) track spacing. With a SLAR range of approximately 50 km (27 nautical miles), IIP ensures 200% coverage of the interior of the regions patrolled (Anderson, 1993). Figures 2.6-1 and 2.6-2 show two flight patterns performed by the IIP in 1993 and exemplify how searches shift southward as the iceberg season progresses.

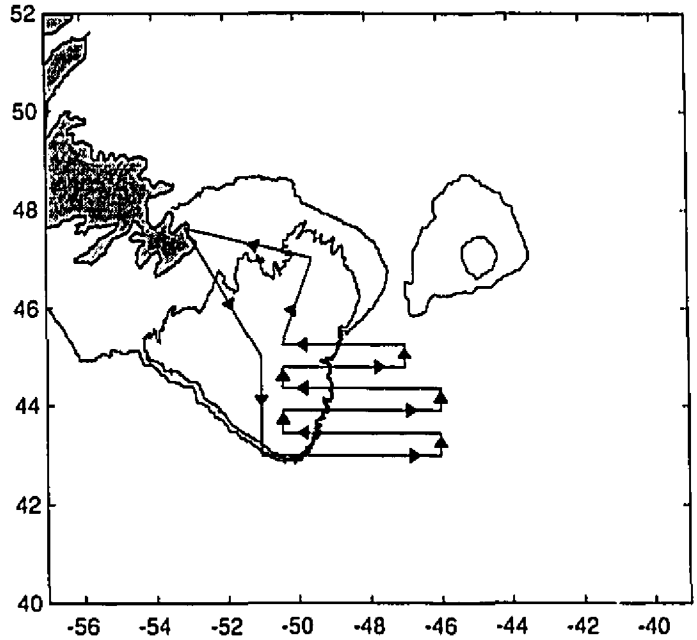

Figure 2.6-1 Typical IIP flight pattern (Flight #22, March 25 1993, 7.8 hrs).

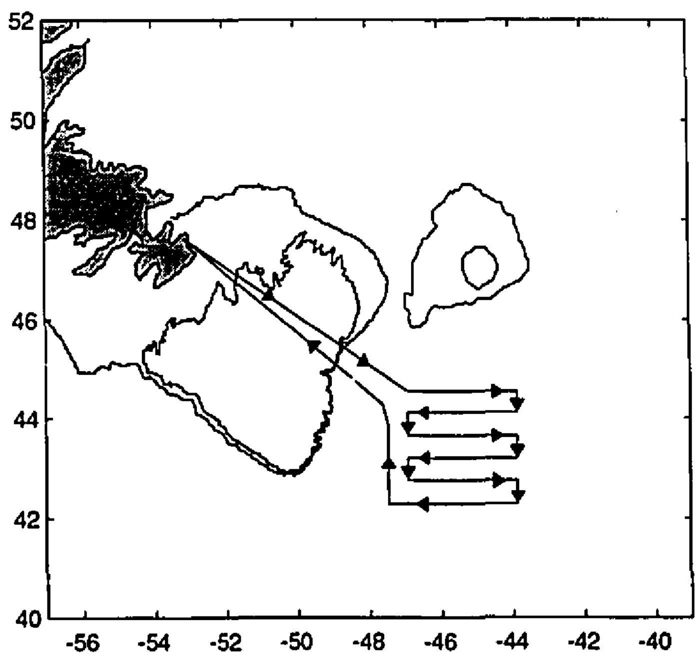

Figure 2.6-2 Typical IIP flight pattern (Flight #33, April 20 1993, 7.1 hrs).

SLAR has the advantage of not being weather dependent. The introduction of SLAR enabled IIP to perform reconnaissance flights during foul weather conditions when visibility is poor. However, a major drawback to SLAR is target discrimination. Fishing vessels and icebergs can be confused when visual confirmation is not possible. IIP tries to eliminate non-iceberg targets, but does include SLAR reports of icebergs which have not been visually confirmed in its database.

IIP includes iceberg sightings from other sources in its database, such as reports from commercial ships, commercial and military flights and coastal sightings. IIP also includes reports from the Canadian Atmospheric Environment Service. AES instituted an iceberg air reconnaissance program in the early 1980's. AES patrols regions of the Grand Banks with high iceberg densities. AES also employs SLAR, but emphasizes visual searches. As such, SLAR targets with no visual confirmation are not reported as icebergs.

Finally, IIP classifies some icebergs as resights. In order to be classified as a resight, a previously sighted iceberg must be reported in a location predicted by the drift model. As IIP may only survey a region once every two weeks, errors on resights are highly probable.

2.6.2 Oil Companies

The presence of large reserves of hydrocarbons has led to drilling exploration and development in the vicinity of the Grand Banks. Canadian drilling regulations require that iceberg surveillance be done in regions of exploration (Anderson, 1993). Oil companies searching for commercially viable sources of oil and gas comply with these regulations by conducting research into iceberg characteristics, such as size and frequency of occurrence, or flux (Crocker, 1994). Such research focuses on icebergs which may collide with gravity based structures or which may scour pipelines on the ocean floor. As a result, the compiled databases primarily document the characteristics of large icebergs. These databases are dependent on the methods used for tracking icebergs (usually a combination of radar and visual reports) as well as the location and the period of operation of the drilling platforms from which information is gathered. Exploration sites are occasionally abandoned during drilling operations due to the presence of icebergs, pack-ice invasions or for refits (Banke, 1989). As a result, it is generally recognized that these databases are incomplete due to the limited range and scope of the reported icebergs (Banke, 1989). However the databases do provide a very good source of iceberg size distributions. As opposed to IIP, which gives a qualitative estimate of iceberg dimensions, databases compiled by oil companies provide measured or estimated quantitative dimensions. In addition, the location of icebergs flowing within the observation range of oil rigs are tracked at regular intervals, providing an accurate time history of iceberg drift.

3. Scours

3.1 Introduction

Icebergs drifting into waters where the bathymetry is similar to their draft pose a threat to structures located on the seabed, such as pipelines, wellheads and under-water communication lines. Icebergs may scour the seabed and may cause failure of any structure in its path. One solution is to bury these structures. However, determining the depth to which structures need to be buried is a non-trivial dilemma. Burial depth is dependent on several factors including the scour mechanism, geology of the sea floor, and the size distribution and density of icebergs within the region (Gaskill, Nicks, Ross 1985).

3.2 Scour Characteristics

Two types of seabed disturbances can occur when an ice keel comes into contact with the sea floor: scouring or pitting. Pits are circular or elliptical in shape and may occur as an iceberg splits and rolls. Pits may also be produced as an iceberg oscillates vertically along its trajectory due to wave action or instability or due to the weight of a grounded iceberg which may cause a bearing capacity failure of the seabed (Clark *et al*, 1986; Lewis *et al*, 1987; Simms, 1993). Scours are formed as the keel of an iceberg drags along the sea floor. Scours are accompanied by the formation of small mounds on either side of the scour, called berms, which run the length of the scour. Both berms and scours can be characterized by their length, width and slope. In addition, scours are also characterized by their depth, defined as the vertical distance from the deepest point in the scour to the level of the undisturbed sea floor, and by their incision width, which is defined as the width of the scour at the level of the undisturbed sea floor. As well, berms may also be characterized by their height, defined as the vertical distance between the undisturbed sea floor and highest point of the berm. (Figure 3.2-1). Length, width and depth of scours vary for different regions. Regional geology plays an important role in scour shape and preservation. Scours formed in clays have steeper slopes and their shape is preserved for a much longer period of time than in sandy soils where hydrodynamic reworking and burrowing marine animals will act to quickly decay scour shape.

Generally, scour dimensions increase with water depth. In increasing water depths of 100 m to 200 m, the number of scours also increases (Simms, 1993). However, as water depths increase from 200 m to 225 m, the number of scours decreases, although this may be attributed to incompleteness in the surveys (Simms, 1993). Scour depths also increase with water depth, and have a maximum mean of 1.9 m in water deeper than 200 m. Finally, scour lengths can be very long, with partially scanned lengths in excess of 10 km (Comfort and Been, 1990; Simms, 1993).

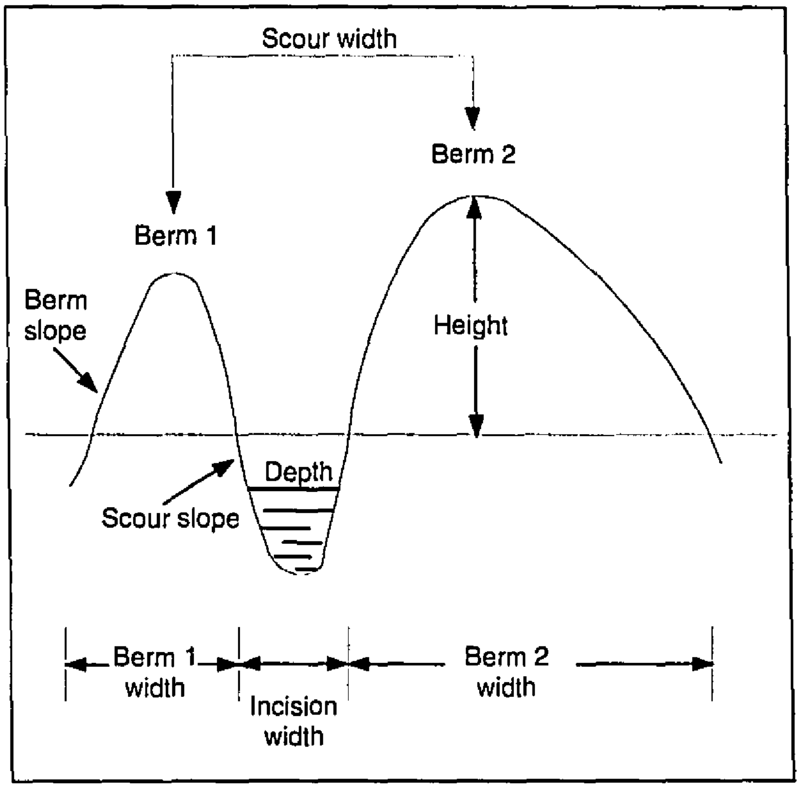

Figure 3.2-1 Scour characteristics. Note that the material excavated should be equal to the volume of the berms.

Two populations of iceberg scours can be identified in the Grand Banks. In water depths less that 110 m, a relatively young scour population is characterized by a sparse iceberg scour pattern. At water depths greater than 110 m, the pattern is dense and the scours are partially buried, suggesting that they are relict scours (Simms, 1993). Scours in water depths less than 100 m are 1 m to 2 m deep, while scours in water depths greater than 100 m are 1 m to 4 m deep (Lewis *et al*, 1987).

Estimates of scour density in the vicinity of the Grand Banks vary greatly. These vary from 40 scours/km^2 along the perimeter of the Grand Banks and in the Avalon Channel to approximately 1 scour/ km^2 along the northern edge of the Grand Banks (Lewis *et al*, 1987). However, Simms (1993) suggests, based on empirical evidence, that densities in the Grand Banks can range from 0.3 scours/km^2 to 86 scours/km^2, with a median of 2.6 scours/km^2, a mean of 6.3 scours/km^2 and a standard deviation of 9.3 scours/km^2.

3.3 Relict Scours

Relict scours are scours that were formed during the Paleocene era and are of no significance in terms of risk to sea floor structures. Typically, these scours are much deeper than modern scours, therefore including relict scour data in determining burial depth will lead to burial depths much deeper than required. It is important to identify and exclude relict scours from data sets, as the information they provide can lead to over-design. Relict scours can be easily identified if the orientation of their pattern is different from modern scour patterns, if their dimensions are different from modern scours in the region, or if modern icebergs no longer scour the sea bed either due to a decrease in iceberg size or an increase in regional bathymetry (Lewis and Keen, 1990). Relict scours have been identified in water depths of up to 750 m off the Baffin and Labrador shelves and in water depths upward of 650 m along the Flemish Pass. Relict scours have been discovered with lengths of several kilometers, widths up 90 m and depths up to 4.4 m (Pereira *et al*, 1988; Simms, 1993).

3.4 Mechanism

The interaction between an ice keel and the sea floor is a complex process involving the soil properties of the sea bed, ice characteristics and the driving forces. Icebergs are driven by the combined effect of currents, winds and waves. The scour process begins when a deep keeled iceberg is driven into an area of shallower bathymetry. The iceberg may then lift, rotate, split, scour, and/or come to rest (Comfort and Been, 1990). The iceberg will ground if the driving forces are not sufficient to sustain its drift. As scouring progresses, the soil experiences a range of deformations depending on the proximity to the ice keel. Induced stresses and strains are transferred to any structure intersecting the trajectory of a scouring iceberg, such as a pipeline. Three zones of ice-soil-pipeline interaction can be characterized as follows (Figure 3.4-1; Comfort and Been, 1990):

1. Zone 1: Large soil movements are observed as soil is displaced. A pipeline in this zone will come into direct contact with the ice keel. A pipeline located in this zone is likely to be carried forward with the iceberg.
2. Zone 2: Located close to, but beneath the base of the ice keel. Large soil movements are observed. The pipeline does not come into contact with the ice keel, but undergoes large displacements as it is carried along with the displaced soil.
3. Zone 3: Small soil displacements and strains are observed. Strains in the soil impose stresses on the pipeline. A pipeline in this zone is not expected to undergo large displacements.

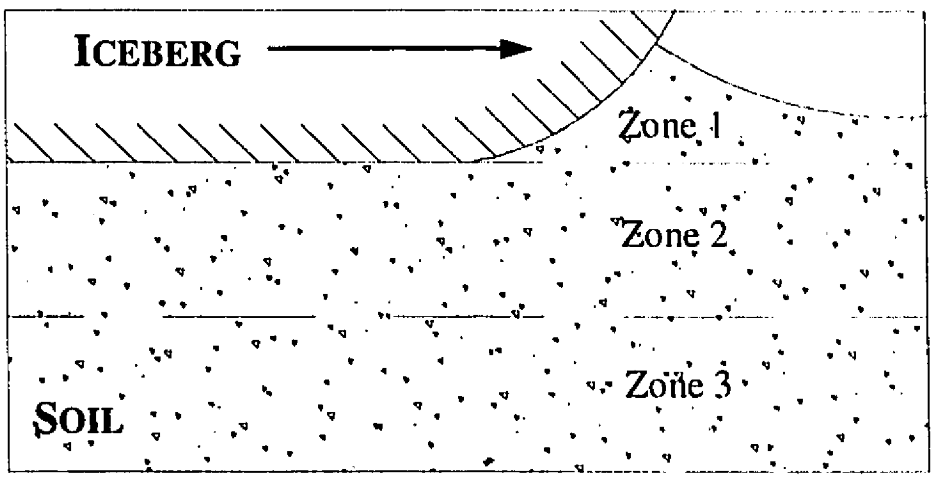

Figure 3.4-1 Scours process (adapted from Comfort and Been, 1990)

As the ice keel drags through the soil, a wedge of soil forms in front of the keel and is transported along with the ice feature. This soil acts as a "dead wedge", meaning there is little relative movement between it and the ice keel. This wedge of soil increases the cutting angle of the keel causing it to be more blunt. Soil is pushed out and in front of the keel as the iceberg moves forward. The wedge eventually stabilizes and further scouring causes excess soil to be pushed to the sides of the keel, forming berms (Figure 3.4-2).

Damage to a sea floor structure is not limited to forces induced through direct contact, but also by the large deformations caused by soil displacements. The soil displacements produced during the scouring process can create excessive strains to seabed facilities resulting in damage or failure.

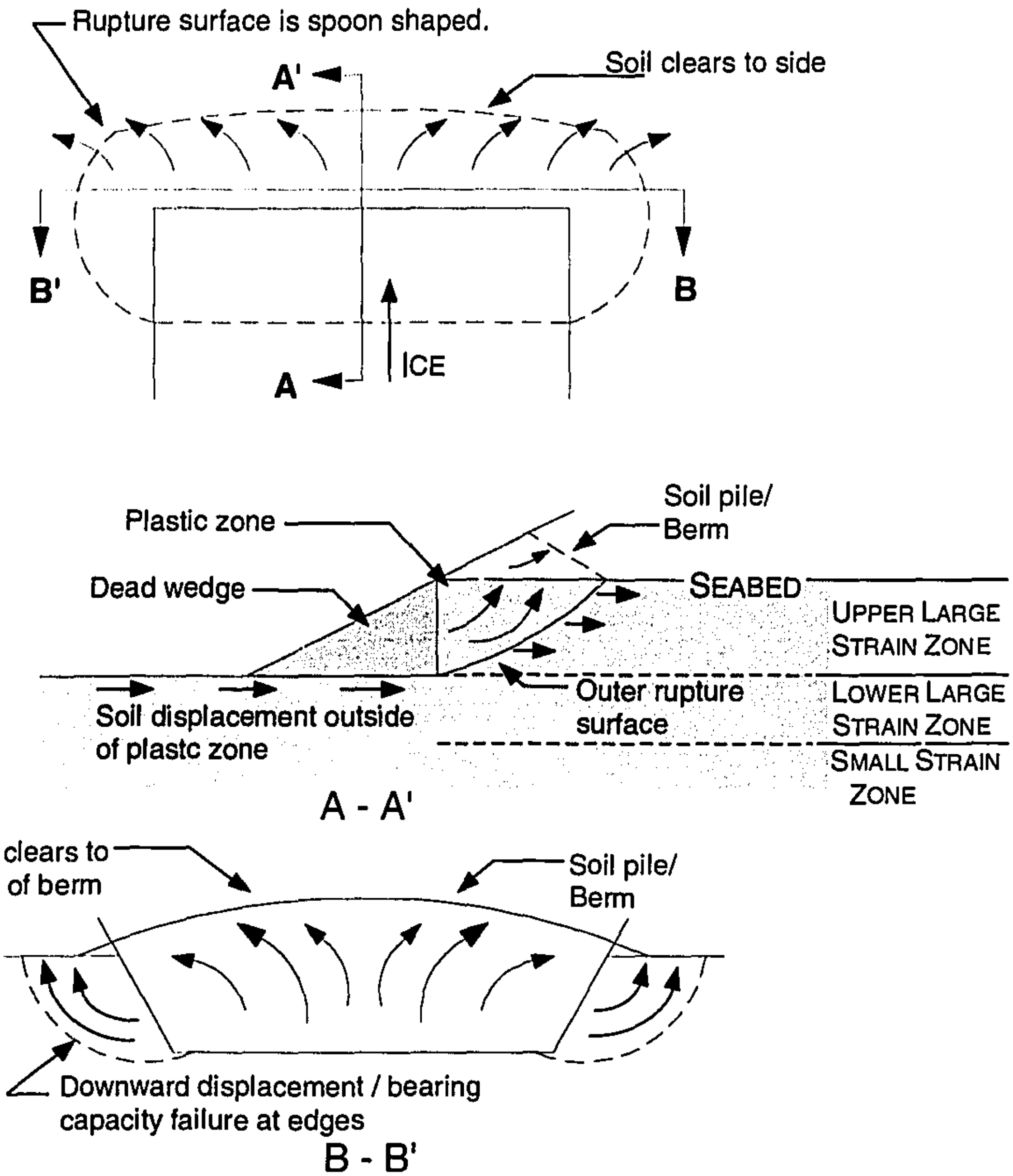

Figure 3.4-2 Berm formation through iceberg scouring (adapted from Comfort and Been, 1990).

The scouring mechanism is very different from other types of soil cutting, such as by agricultural implements. Cutting devices are sharp, rigid, are much stronger than the soil and are designed to minimize the required drag force (Been *et al* 1990). By comparison, an ice keel is blunt and does not lift soil up as it moves forward, but presses it down. Ice keels are very inefficient cutters. Finally, ice at the bottom of an iceberg is weak and may break during scouring altering the cutting surface.

3.5 Estimating scouring rates

Several methods can be used to estimate the potential of seabed scouring in a region (Lewis and Keen, 1990). The two most common methods of determining scouring rates is either by direct observation of the sea floor through repetitive mapping or through inference by measuring iceberg keel depths and combining this information with iceberg drift patterns.

3.5.1 Repetitive Mapping

Repetitive mapping involves using sonar to survey the sea floor for scour marks. Successive mapping of the same region gives detailed information as to the frequency of scouring. This method is also useful in identifying relict scours, which are cut by modern scours. Estimates of the rate of scouring are obtained from:

$$\lambda(\underline{x}) = \frac{N(\underline{x})}{\Delta T} \cdot \frac{1}{\pi \cdot L} \tag{3.5-1}$$

where $\lambda(\underline{x})$ is the rate of scouring at location $\underline{x}$, $\underline{x}$ are the coordinates in terms of longitude and latitude, $N(\underline{x})$ is the number of new scours observed in the vicinity of $\underline{x}$, ΔT is the time elapsed between two surveys, and L is the length of the line tracked by sonar.

Repetitive mapping is expensive and its accuracy is dependent on the rate of scouring, the rate of scour degradation and the time interval between mappings. Repetitive mapping is most effective in areas where the rate of scour formation exceeds the rate of scour degradation, such as in the Beaufort Sea (Lewis and Keen, 1990). Disadvantages of repetitive mapping are high cost and the relatively small sample obtained in terms of spatial coverage and time period.

3.5.2 Inferred Iceberg Groundings

Estimates of scouring rates can also be inferred from observed groundings of icebergs. An iceberg is assumed grounded when it remains motionless for one tidal cycle. The frequency of iceberg groundings is calculated as the number of inferred groundings over the number of icebergs drifting through the region during the observation period.

Estimates of the rate of scouring are obtained from:

$$\lambda(\underline{x}) = \frac{NG(\underline{x})}{\Delta T} \cdot \frac{1}{A} \tag{3.5-2}$$

where $NG(\underline{x})$ is the number of iceberg groundings in the vicinity of $\underline{x}$, ΔT is the length of the period of observation and A is the area of the region being observed. However, this procedure can underestimate the true rate of scouring given that not all scouring icebergs are observed and that not all scouring icebergs ground.

3.5.3 Ice Keel Depth and Flux

Estimates of the annual iceberg flux and of the probability distribution function of draft depth, can be used to estimate the frequency of scouring. Estimates of the rate of scouring are obtained from:

$$\lambda(\underline{x}) = \phi(\underline{x}) \cdot \left[1 - F_{dr}(d \mid \underline{x})\right] \qquad (3.5\text{-}3)$$

where $\phi(x)$ is the iceberg flux (icebergs/km-day) and $F_{dr}(d \mid \underline{x})$ is the cumulative distribution function of draft size of icebergs at location $\underline{x}$ and d is the water depth at $\underline{x}$.

The advantages of the above procedure are that:

1. it can be calibrated using iceberg and scour data;
2. it can be used to interpolate the scouring rate between regions which have been surveyed through repetitive mapping;
3. it can be used to eliminate relict scours.

Procedures for the estimation of the flux or density of icebergs as a function of location are presented in the next chapter.

4. Spatial Analysis

4.1 Introduction

The occurrence of icebergs at any given location is often modeled as a Poisson process in time for estimating design criterion for fixed offshore oil platforms, such as Hibernia. The characteristics of the Poisson probability distribution function (pdf) make it a popular choice for modeling a variety of natural phenomena. The Poisson distribution has been used to describe the random occurrence of extreme events in time , such as hurricanes and tornadoes. It has also been used to describe the spatial and temporal distribution of extreme events, such as earthquakes. The Poisson pdf is defined as follows:

$$P(X = n; \lambda) = \frac{e^{-\lambda}\lambda^{n}}{n!} \quad \text{for n = 0, 1, 2, ...} \qquad (4.1\text{-}1)$$

where λ is the intensity function and corresponds to the expected number of observations for the sample region. For a homogeneous process, λ is a non-negative constant. The following properties define a homogeneous Poisson process (Barber, 1988):

1. Occurrence of an event is independent of occurrences in any other mutually exclusive interval;
2. The probability of occurrence of an event is proportional to the interval size in which it occurs, therefore the probability of an event occurring in a small interval is small;
3. The probability of multiple occurrences in an interval approaches zero as the size of the interval is reduced;
4. The Poisson distribution is preserved when several Poisson distributions are added together, for example for earthquakes or hurricanes of different intensities.
5. The intensity factor, λ, is independent of location and is a non-negative constant.

Heterogeneous Poisson processes obey all but the last condition whereby the intensity function may vary according to location, $\underline{t}$, where $\underline{t}$ is an array of coordinates for a sub-region, or interval, in n-dimensional space ($\Re^n$) (Veneziano, 1980). For points on a line, n = 1 and $\underline{t}$ represents a segment of the line, and in $\Re^2$, $\underline{t}$ represents a surface. For the heterogeneous case, the expected number of observations in the sample region, S, is defined as:

$$E[N(S)] = \int_S \lambda(\underline{t}) \cdot d\underline{t} \qquad (4.1\text{-}2)$$

Iceberg occurrence can be modeled as a Poisson point process on a line or as a line process in $\Re^2$. In the first case, the iceberg drift is characterized, for example, as the rate of icebergs crossing a line (e.g. 48°N), which can vary as a function of longitude (Figure 4.1-1). In the second case, the two dimensional nature of iceberg drift is explicitly accounted for, which is discussed in more detail next.

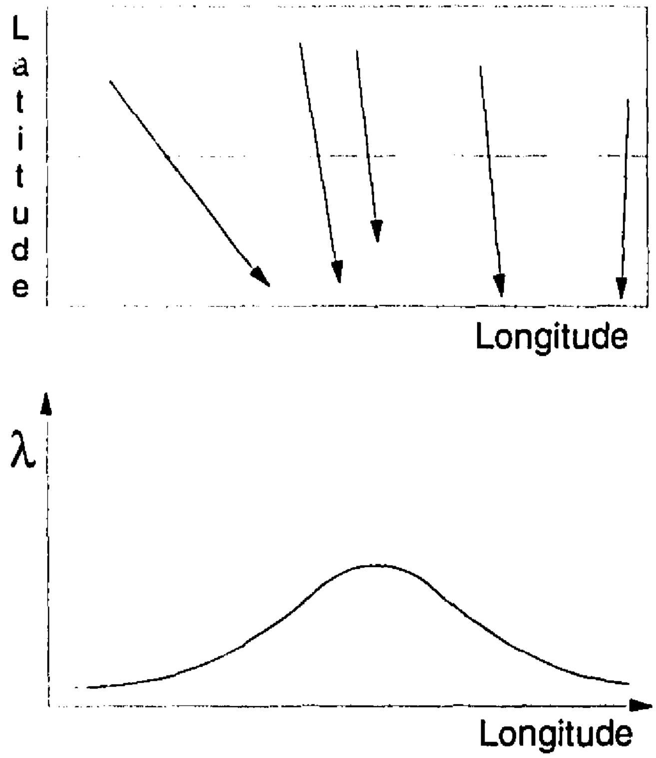

Figure 4.1-1 Iceberg drift modeled as the rate of icebergs crossing a given latitude.

4.2 Line Processes

As with a point process, a line process can be either homogeneous or heterogeneous depending if the intensity function of the process is constant (λ) or a function of location [$\lambda(\underline{x})$]. In addition, the line process can be characterized as isotropic or anisotropic, depending if the orientation of the trajectories is uniformly random or not:

$$\lambda(\underline{x},\alpha) = \lambda(\underline{x}) \cdot f(\underline{x},\alpha) \qquad (4.2\text{-}1)$$

In the case of iceberg trajectories, the line process appears to be heterogeneous and anisotropic.

Several estimation procedures can be used to estimate the properties of a line process, these are usually valid for isotropic and homogeneous processes, but can be extended to non-homogeneous, anisotropic processes under certain conditions.

In the case of icebergs, observations are usually in the form of daily reports on the location of icebergs over a defined area which is surveyed from shore, from air or from ships. There are only a few data sets (e.g. Husky Oil) which actually track individual icebergs (Figure 4.2-1). Iceberg trajectories can also be inferred from resight observations using the IIP database.

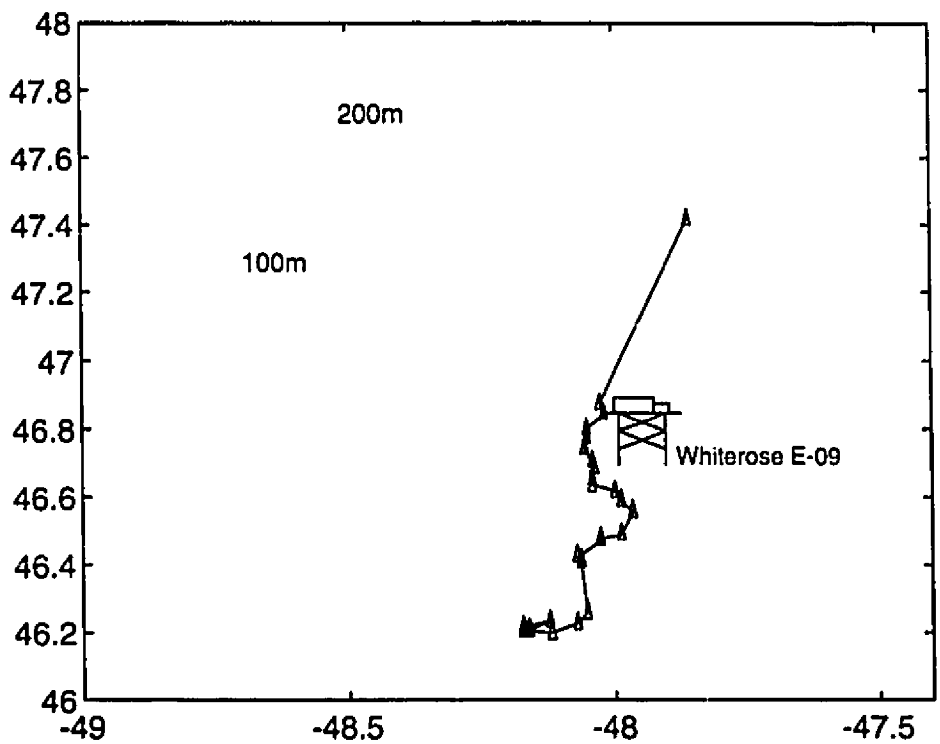

Figure 4.2-1 Trajectory of iceberg #101, observed from April 2 1988 to April 23 1988 (49 reported observations). Also included is the location wellsite Whiterose E-09.

An iceberg trajectory can be idealized as a line in $\Re^2$ and can be characterized, with respect to a given point $\underline{x} \in \Re^2$, by parameters d and α. These parameters represent, respectively, the shortest distance from the selected point to the line and the angle, measured clockwise from t_2 (Figure 4.2-2). The equation for such a line is:

$$\Omega = \{(t_1, t_2): t_1 \cdot \cos\alpha + t_2 \cdot \sin\alpha = d\} \qquad (4.2\text{-}2)$$

where Ω defines a set of random lines. The angle α ranges from 0 to π and d ranges from $-\infty$ to ∞. If Θ represents the sample space for possible values of θ, which is a vector array representing the parameters $\begin{bmatrix} d \\ \alpha \end{bmatrix}$, then:

$$\Theta = \{(d,\alpha) = -\infty < d < \infty, 0 \le \alpha < \pi\} \qquad (4.2\text{-}3)$$

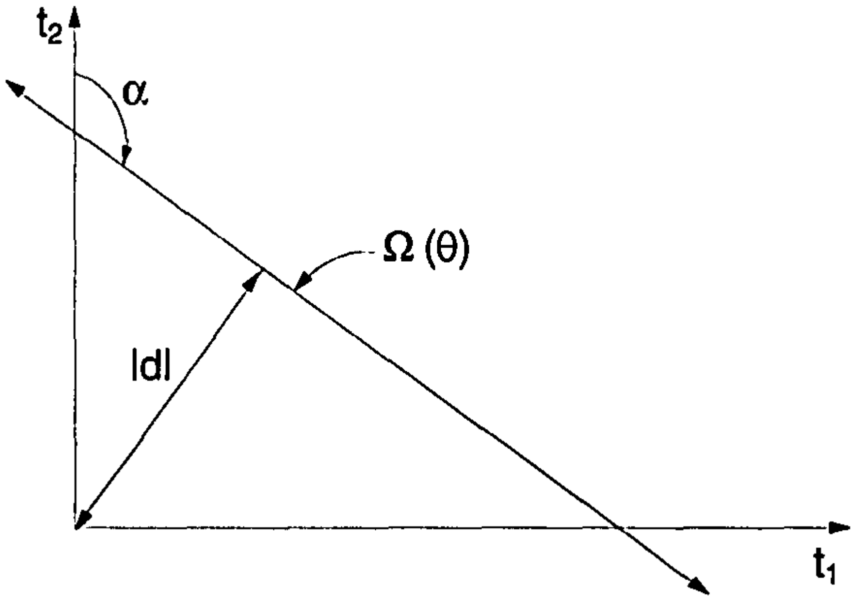

Figure 4.2-2 Paramaterization of a line in $\Re^2$.

Such a representation is very convenient when the process is analyzed for establishing design criterion with respect to the location of a oil production or exploration platform.

A set of random lines, $[\Omega(\theta)]$, has a Poisson distribution if the parameters, (θ), depict a Poisson point process in Θ. However, an homogeneous point process in θ is not a necessary condition for the line process to be homogeneous in space. A homogeneous line process requires only that the intensity function of the point process has the form:

$$\lambda(d,\alpha) = \lambda \cdot f_\alpha(\alpha) \qquad (4.2\text{-}4)$$

where λ is a positive constant and f_α is the pdf of α (Veneziano, 1980). This process is homogeneous but anisotropic, since the spacing of the lines is random, but their orientation is governed by a given pdf, f_α. If α is uniformly distributed over $[0, \pi]$, then the line process becomes isotropic, as well as homogeneous. The intensity function for an isotropic, homogeneous line process reduces to:

$$\lambda(d,\alpha) = \text{constant} = \frac{\lambda}{\pi} \qquad (4.2\text{-}5)$$

An isotropic, homogeneous line process implies that the spacing and orientation of the lines are completely random in Θ. For an anisotropic, heterogeneous line process, both the spacing of the lines and their orientation are determined by a joint pdf of (d, α).

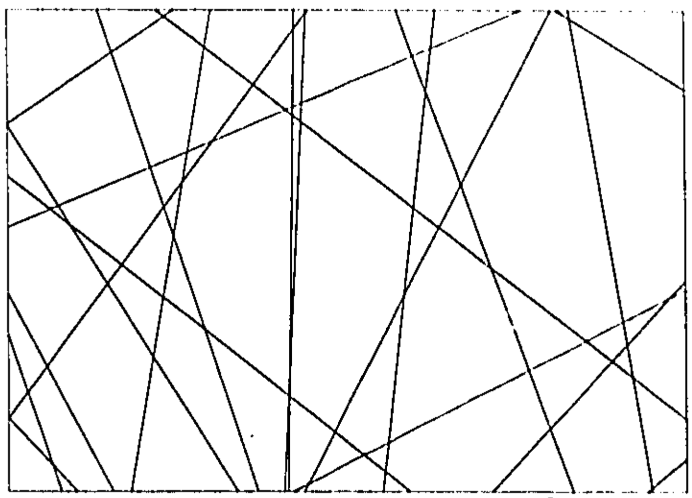

Figure 4.2-3 Poisson line process in $\Re^2$.

Estimation procedures for $\lambda(d, \alpha)$ are based on crossing rates of lines or of convex objects in space. Given a homogeneous Poisson line process, the number of lines, N, crossing through a convex figure with perimeter, L, in $\Re^2$ has a Poisson distribution with expected value (Miles, 1964; Figure 4.2-4a):

$$E[N] = \frac{\lambda \cdot L}{\pi} \qquad (4.2\text{-}6)$$

When the line process is anisotropic, the expression is only valid when the convex figure is a circle, but for the isotropic case, the figure may be any arbitrary shape. An estimate of the intensity function at a given location can be obtained by positioning a convex figure centred at the location of interest and by counting the number of observed lines, N^*, which pass through it. The intensity function can be estimated as:

$$\lambda = \frac{N^* \cdot \pi}{L} \qquad (4.2\text{-}7)$$

This last estimation is especially well adapted for the analysis of data reported by IIP. As mentioned previously, only a small fraction of the historical data set is recorded in terms of actual iceberg trajectories, the majority of the observations only provide the location of the icebergs on a given day (i.e. iceberg maps). The estimation procedure can be used in conjunction with location data by assuming that every point in the convex figure belongs to an individual trajectory. The estimate is then obtained by counting the number of points within the figure in lieu of counting the number of lines (Figure 4.2-4b). The estimation problem can then be treated using standard procedures for the estimation of the intensity function, or density, of a point process, which are discussed next.

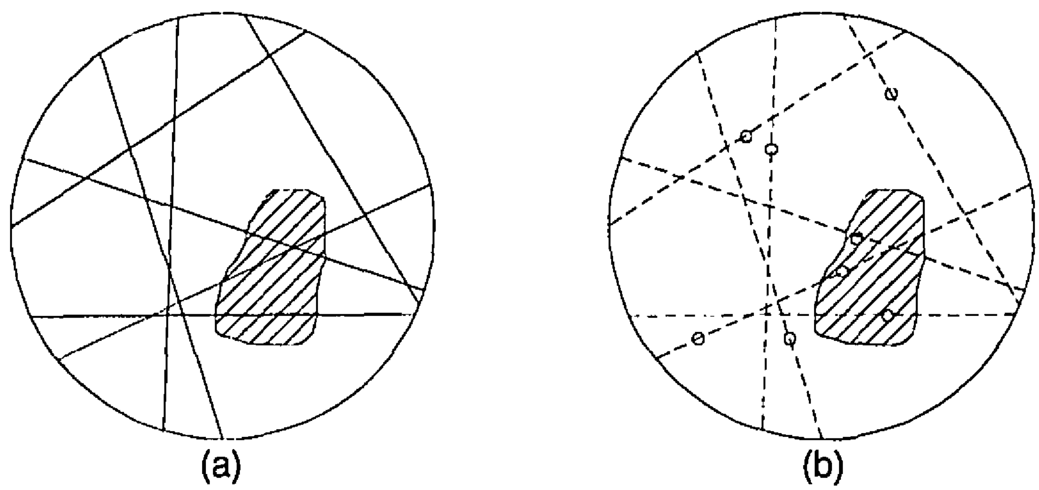

Figure 4.2-4 Poisson lines intersecting an arbitrary convex figure in $\Re^2$ modeled as (a) a line process; (b) a point process.

4.3 Point Processes

Sets of randomly distributed points are the most widely researched type of set patterns and the Poisson point process is one of the first stochastic models to have been developed (Serra, 1982). Typically, point processes describe sets of random points in $\Re^2$. The simplest point process is the homogeneous Poisson pattern, also known as complete spatial randomness (CSR). This pattern is often used as a standard for comparisons with other point processes. Two conditions are required for CSR (Boots and Getis, 1978, 1988):

1. Points are uniformly distributed over the sample region, so that the likelihood of receiving a point is equal for all sub-regions;
2. Point locations are independent of one another.

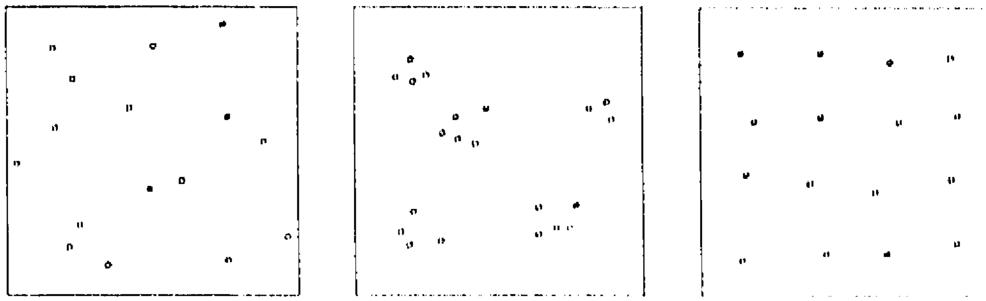

(a) (b) (c)

Figure 4.3-1 Model realizations of: (a) CSR; (b) Cluster; (c) Regular patterns.

Two other idealized models, representing opposite extremes of point patterns, are the cluster pattern and the regular pattern. The cluster pattern displays significantly more grouping than CSR, while a regular pattern displays an even distribution of points throughout the region (Figure 4.3-1). Note that the size of the sample region may influence the perceived pattern type; in Figure 4.3-2, the pattern in A appears to be regular, while the same pattern in B appears to be a cluster (Upton and Fingleton, 1985).

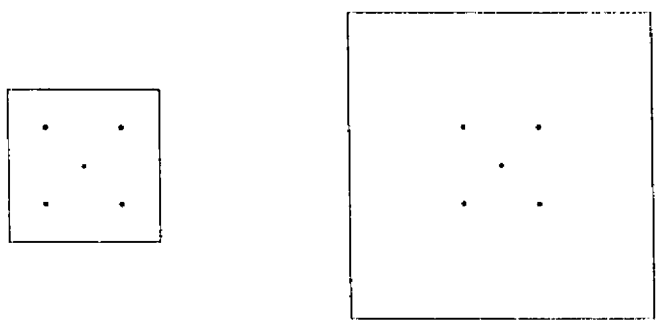

(a) (b)

Figure 4.3-2 Effect of sample area on point pattern appearance (adapted from Upton and Fingleton, 1985).

If a point exists at location θ on a plane, then it can be defined by the equation $\Omega(\theta) = 1$. Since θ represents a very small interval in the sample region, the probability of an occurrence at any point on a plane will generally be zero, $P[\Omega(\theta) = 1] \approx 0$. For this reason, the sample area is divided into smaller regions, called quadrats. The number of points in each quadrat is counted and defined as $\Omega(A)$, where A is the area of the quadrat (Ripley, 1981). The expected number of points, N, in a quadrat with area, A, can be identified as being:

$$E[N] = \lambda \cdot A \qquad (4.3\text{-}1)$$

with λ, the expected number of points per unit sample area, a positive constant. Accordingly, if n is the number of points found in a quadrat with area A, then the intensity function can be estimated as:

$$\hat{\lambda} = \frac{n}{A} \qquad (4.3\text{-}2)$$

4.4 Non-Parametric Density Estimation Using Kernels

A sample of random objects, X, in a sample space, Ω, follows a probability distribution function, f. A parametric approach to the estimation of f assumes that the parametric form of f is known and only the parameters which define f need to be estimated from X. For example, if X is assumed to be normally distributed, then only estimates of the mean, μ, and the variance, σ^2, of X are required. A non-parametric approach assumes that the exact form of the probability distribution function is unknown. It is then necessary to estimate f directly over the sample space Ω_0. Kernel estimators can be used to obtain a non-parametric estimate of f (Cressie, 1993).

Histograms are the simplest non-parametric estimator of f and are widely used to give a quick visual representation of the distribution (Silverman, 1986). Histograms consist of a set of m non-overlapping bins of equal width h, with an origin at x_0. To construct a frequency histogram, a block of width h and unit height is associated to a bin when an event falls within the bin interval (Scott, 1992). Since the area under a pdf must integrate to unity, an estimate of the data pdf can be obtained by dividing the frequency histogram by the total number of observations, n. The block associated with an observation then has dimensions of width h by height $1/n$.

Histograms can be extended to the multivariate case by defining the bins as having dimensions $h_1 \times h_2 \times \ldots \times h_d$. Therefore, in $\Re^2$, a box of width h_1, length h_2 and height $1/n$, would be placed in each bin where an observation is found. The shape of a histogram can be altered by varying the bin dimensions and the location of the origin. Increasing the bin dimensions increases smoothing of the data which eliminates some of the roughness, or "noise", inherent in a histogram plot. However, oversmoothing, can hide some the more important features of a histogram, such as the peaks and lows.

A more general form of estimator is the kernel estimator. Mathematically, a kernel estimator in $\Re^d$ with bin width h can be written simply as (Silverman, 1986):

$$\hat{f}(\mathbf{x}) = \frac{1}{n \cdot h_d} \sum_{i=1}^{n} K\left(\frac{\mathbf{x} - X_i}{h}\right) \tag{4.4-1}$$

where K(x) is a kernel function in $\Re^d$ which must satisfy the condition:

$$\int_{\Re^d} K(\mathbf{x}) = 1 \tag{4.4-2}$$

Kernel functions usually take the form of a radially symmetric, unimodal pdf (Silverman, 1986; Scott, 1992). A popular kernel function is the standard multivariate Normal distribution:

$$K(\mathbf{x}) = \frac{1}{(2\pi)^{-d/2}} \exp(-\frac{1}{2}\mathbf{x}^T\mathbf{x}) \tag{4.4-3}$$

Kernel estimators differ fundamentally from histograms in that they assign weights which are centred over the data points, while histograms are composed of a rigid mesh on which rectangular kernels are placed (Scott, 1992). Histograms can be considered as a special case of kernel estimator.

Smoothing of data through kernel estimators can be controlled by varying the window width, h. For long-tailed distributions, the choice of a constant h may present a problem: Using a small window width may cause excessive noise of the estimates in the tails of the density distribution, while a large window width may oversmooth the peak of the distribution and will introduce a bias in the estimates of the intensity function (Härdle, 1990). In order to smooth the tails without oversmoothing in regions of higher density, an adaptive kernel may be employed. The purpose of an adaptive kernel is to vary the kernel window width according to the local density of the observations. Therefore, a larger window width is preferable in regions of low density, to eliminate statistical noise, while in regions of high density, a smaller window width would be utilized to retain important features and minimize bias. In the following chapters both constant and adaptive kernels are used in the estimation of iceberg densities.

5. Data Presentation

5.1 Databases

5.1.1 International Ice Patrol (IIP)

The IIP database spans the years 1960 to 1993 and contains 92 911 reports of iceberg sightings. Each report field includes the location of the iceberg, the date and time of the sighting, the estimated size and shape of the iceberg, the type of sighting and the source of sighting. Sighting sources are grouped as being from ships, planes or other. The "other" category includes lighthouses and drilling platforms. The type of sighting indicates whether the iceberg was spotted by radar, by visual observation, or both. The various combinations of sighting source and type of sighting define all the possible modes of reporting. The size and shape of icebergs in the IIP database are qualitative estimates derived from either radar or visual observations.

The IIP database is used to estimate iceberg densities in the region bounded by latitudes 52°N and 40°N and by longitudes 52°W and 39°W, which accounts for 83 974 (90.4%) of the total number of icebergs reported in the IIP database. This region was chosen as it represents the current area covered by IIP's operations (Anderson, 1993) and because it encompasses the Grand Banks of Newfoundland, a region rich in hydrocarbon resources where iceberg scouring is a major hazard to sub-sea structures.

5.1.1.1 Limitations of IIP database

Despite many years of data, the IIP database does not exemplify an ideal sample set. It is incomplete in the sense that it comprises only partial surveys of the area: icebergs are reported only if sighted; and reports of zero sightings in a region are not included in the database. As well, the database does not contain any information on flight or navigation paths. Note that the omission of an iceberg report in a given region and at a given time does not imply that no iceberg was present. Consequently, for the purpose of density estimation, it is necessary to account for the actual region which was surveyed.

IIP performs aerial surveys of the operation area every two weeks beginning in mid-January, until the end of July. During reconnaissance flights, IIP surveys only a portion of the total area, usually using prior knowledge about the position of the icebergs. The regions typically surveyed by IIP are not necessarily the regions with high iceberg densities, but the outer limits of the region affected by icebergs. This strategy is consistent with their mandate to monitor the southern limits of the range of icebergs in the Grand Banks of Newfoundland. For these reasons, it is generally thought that the IIP reports underestimate the number of icebergs within any region of the Grand Banks by a factor of 2 to 3 (NORDCO, 1980). However, IIP supplements its databases with reports by other sources, mainly from AES and sightings from ships. Despite those deficiencies, the IIP database represents the most complete record of iceberg occurrences in the Grand Banks.

In theory, density estimates of icebergs could be obtained for each separate mode of report, for example from reports obtained exclusively from SLAR imagery. However, this is unfeasible at present, since IIP only started to use SLAR imagery on aerial patrols in 1982 and this would exclude most of the information in the IIP database. Furthermore, sighting sources are not mentioned in the IIP database for the years 1982 and 1983. For these reasons, observations from all sources were used for the analysis and assumed to be equally reliable.

Figure 5.1-1 shows the decomposition of the reported icebergs per source from 1960 to 1993. The "unknown" category refers to the years 1982 and 1983, where the source is missing from the database, while the "other" category refers to sightings reported by sources other than from ships or airplanes, such as reports by the oil industry and from lighthouses. Figure 5.1-2 shows all icebergs reported in 1974 and illustrates the incomplete nature of the surveys. In this example, two preferential survey routes, slightly above and below the 48°N latitude are apparent.

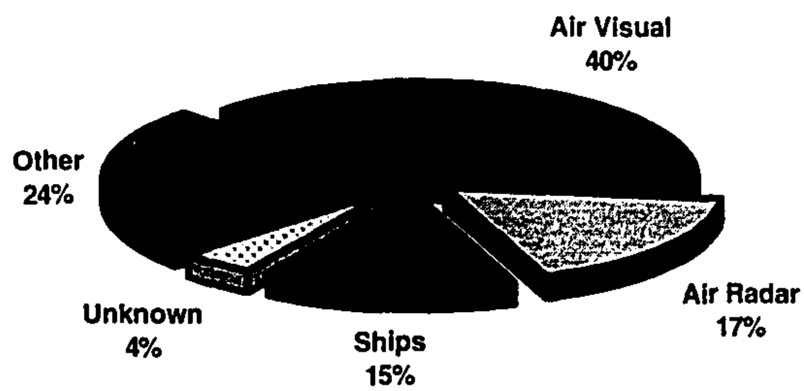

Figure 5.1-1 Decomposition of iceberg reports in IIP database by source of report.

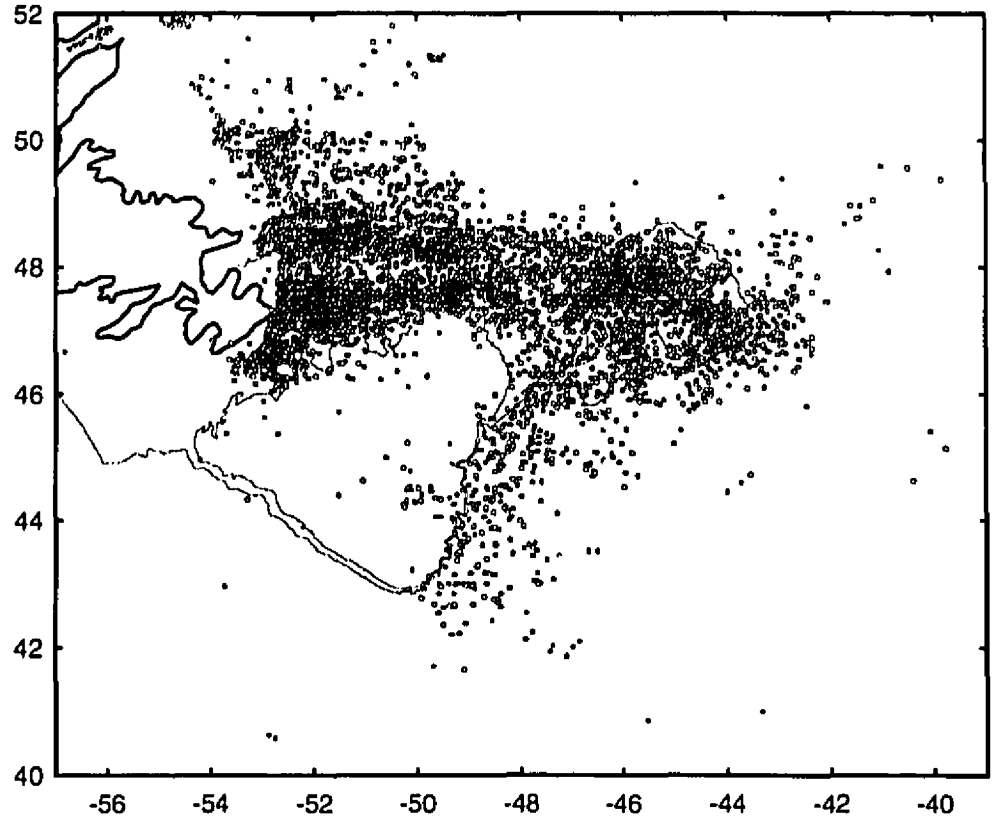

Figure 5.1-2 Iceberg locations for the 1974 iceberg season.

5.1.2 Husky Oil

Husky Oil performed exploratory drilling in the Grand Banks between 1984 and 1988. During this time, data on iceberg size characteristics and drift patterns was collected from twenty-one exploration platforms located at thirteen different sites (Figures 5.1-3 and 5.1-4; Table 5.1-1). Local bathymetries at the sites ranged from 100 m to 194 m. The Husky Oil database is composed of three separate data sets:

1. An index of drilling platforms, with their respective periods of operation and drilling, locations with local bathymetry;
2. A catalogued listing of sighted icebergs, which includes location, iceberg movement (whether drifting freely, grounded or under tow) the platform from which the iceberg was sighted, and the time and date of sighting;
3. Dimensions of each iceberg reported in data set 2, information on whether the dimensions were measured or estimated, and qualitative size and shape descriptors.

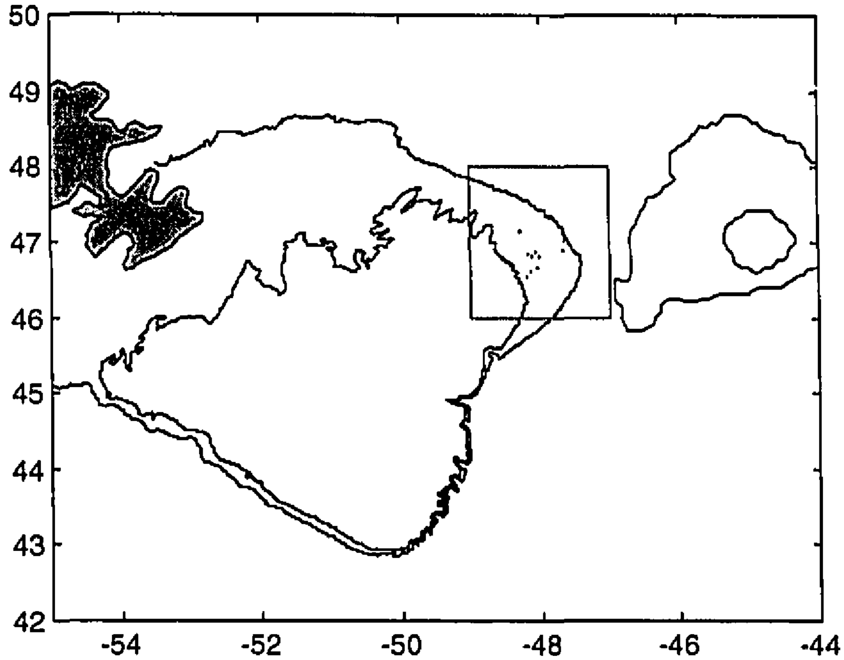

Figure 5.1-3 Husky Oil drilling sites from 1984 to 1988 in the Grand Banks of Newfoundland.

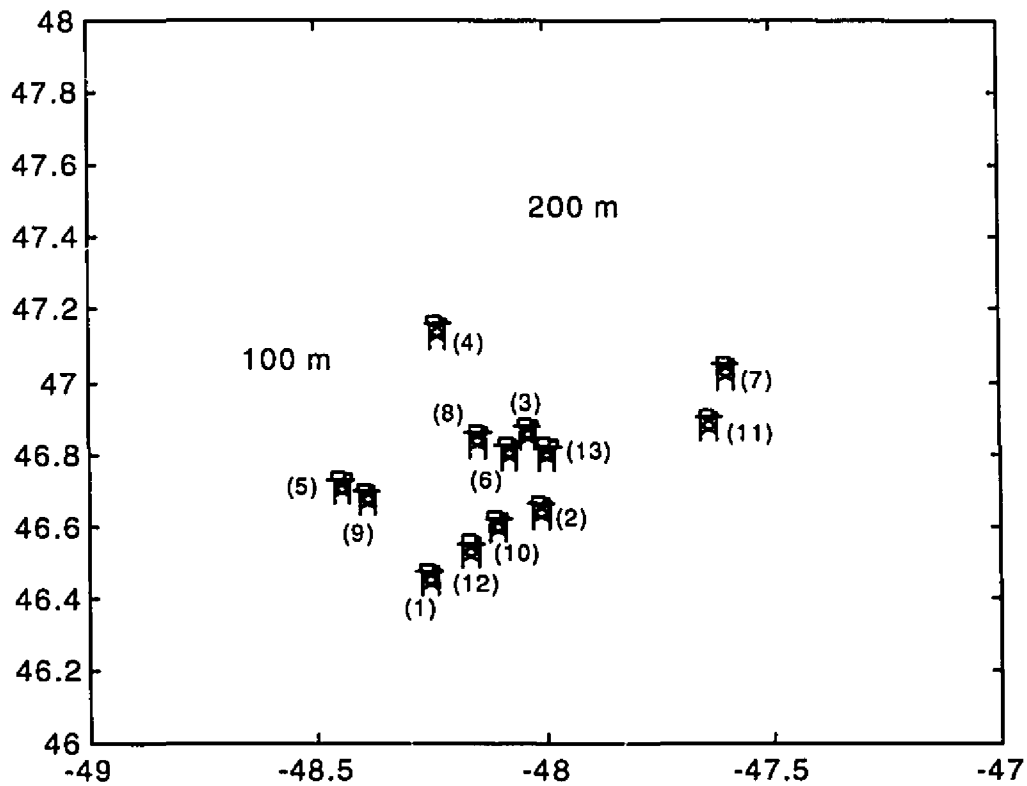

Figure 5.1-4 Enlarged region showing locations of wellsites. Wellsite numbers correspond to Table 5.1-1

Wellsite Number	Wellsite Name	Rig Name	Wellsite Latitude	Wellsite Longitude	Number of Icebergs
1	Voyager J-18	Sedco 706	46°27"32.50'N	48°17"00.49'W	82
2	Archer K-19	Bow Drill 3	46°38"43.17'N	48°02"18.42'W	8
3	Whiterose N-22	Sedco 706	46°51"47.99'N	48°03"56.51'W	8
4	Conquest k-09	Bow Drill 2	46°08"34.68'N	48°15"45.08'W	130
5	North Ben Nevis P-93	Bow Drill 3	46°42"48.10'N	48°28"34.24W	281
6	Whiterose J-49	Bow Drill 2	46°48"31.30'N	48°06"27.51'W	8
7	Panther P-52	Bow Drill 3	46°01"53.37'N	48°37"43.80'W	1
8	Whiterose L-61	Bow Drill 2	46°50"34.12'N	48°10"28.34'W	1
9	North Ben Nevis M-61	Sedco 710	46°40"53.57'N	48°25"18.60'W	3
10	Fortune G-57	Bow Drill 3	46°36"18.90'N	48°08"02.21'W	21
11	Golconda C-64	Bow Drill 3	46°53"11.62'N	48°39"56.54'W	7
12	Bonne Bay C-73	Bow Drill 3	46°32"10.74'N	48°11"30.51'W	24
13	Whiterose E-09	Bow Drill 3	46°48"26.24'N	48°01"22.65'W	15

Table 5.1-1 List of wellsite names, locations and the number of icebergs reported.

The inclusion of data on iceberg dimensions makes the Husky Oil database both unique and valuable, since it gives an estimation of the size distribution of icebergs crossing the Grand Banks. To obtain this data, Husky Oil used four levels of surveillance in tracking icebergs (Banke, 1989):

1. SLAR observations conducted by the Atmospheric Environment Service (AES) during routine ice flights. This information is also included in the IIP database;
2. Site specific radar flights. Information from AES surveys was used to deploy radar equipped aircraft to specific regions within 100 nautical miles of drilling platforms;
3. Supply vessels kept records of icebergs during routine ice sweeps near platforms and when towing away icebergs that drifted too close to the platforms;
4. Continuous local coverage near oil platforms was provided by onboard radar.

These four levels of surveillance make it very likely that all icebergs within 100 nautical miles of each platform were reported.

5.1.2.1 Limitations of Husky Oil database

Drilling operations were not continuous throughout the four and a half years of exploration (Table 5.1-2). Also, due to the risk of collision, operations were usually interrupted during the peak of the iceberg season when iceberg surveillance is most important. As a result, the database is considered to be incomplete in terms of iceberg flux through the Grand Banks and may not be representative of long term trends due to the large year to year variability in the iceberg population of the Grand Banks.

SITE	1984–1988
1	FEB 25 to APR 9
1	APR 26 to JUN 12
2	JUN 25 to DEC 16
3	JUN 26 to DEC 7
3	DEC 10 to JAN 5
4	NOV 11 to FEB 2
4	APR 21 to MAY 8
4	MAY 30 to JUL 26
5	DEC 16 to FEB 3
5	APR 8 to APR 11
5	APR 21 to NOV 1
6	JUL 25 to DEC 12
7	NOV 3 to JAN 31
8	DEC 12 to FEB 28
9	JAN 9 to APR 16
10	MAR 21 to SEP 9
11	OCT 4 to FEB 2
12	FEB 2 to FEB 27
12	MAR 16 to APR 28
12	JUN 18 to JUL 18
13	MAR 20 to JUN 30

Table 5.1-2 Husky Oil exploratory drilling schedule. Alternate shading represents a change of drilling site. Site Numbers correspond with Table 5.1-1.

In addition, even though the Husky Oil database appears to contain a large sample of iceberg dimensions, most of these are estimated from parametric relationships using visible features of the icebergs. For scouring hazards, the most important iceberg feature is keel depth. Unfortunately, only two iceberg drafts were directly measured in the Husky Oil database, all the others were estimated from the visible dimensions of the icebergs.

5.2 Iceberg Size Characteristics

Iceberg dimensions provided in the Husky Oil database are for a small region during a limited period of time. It represents the best sample presently available of iceberg dimensions entering the northern part of the Grand Banks. However, it is too limited in spatial extent to obtain accurate estimates of the spatial variation of the size distribution of icebergs. Note that regional estimates of size distributions are important to obtain an accurate assessment of scouring hazards. For example, areas with high densities of small icebergs are less susceptible to scouring than areas of lower iceberg densities but with larger dimensions. Figure 5.2-1 shows the number of observations of each iceberg dimension, while Figures 5.2-2 to 5.2-5 are histograms of each iceberg dimension. Table 5.2-1 is a list of summary iceberg statistics for the various dimensions as a function of type of data.

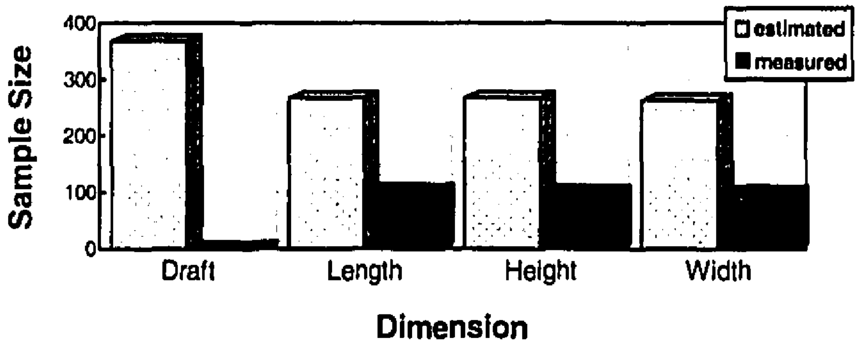

Figure 5.2-1 Sample size of iceberg dimensions in Husky Oil database.

Draft or keel refer to the lowest vertical depth of an iceberg, measured from the waterline. Note that the histogram of iceberg keel size has a distinctively different appearance than similar histograms for other iceberg dimensions. Discrepancies in the shape of the histograms may be attributed to missing data for icebergs with small drafts. Length refers to the longest projected horizontal iceberg dimension along the waterline, while width refers to the dimension along the minor axis of the iceberg along the waterline. Height is the highest vertical point of an iceberg measured from the waterline. When possible, the length, height and width of an iceberg were measured using a sextant and range technique, otherwise dimensions were estimated by visual observation (Banke, 1989). On two occasions, iceberg drafts were measured using sonar. If the measured length, height and width of an iceberg were known, the draft was calculated using an empirical formula based on these dimensions. Also, if an iceberg was assumed grounded, the draft was estimated from the known bathymetry.

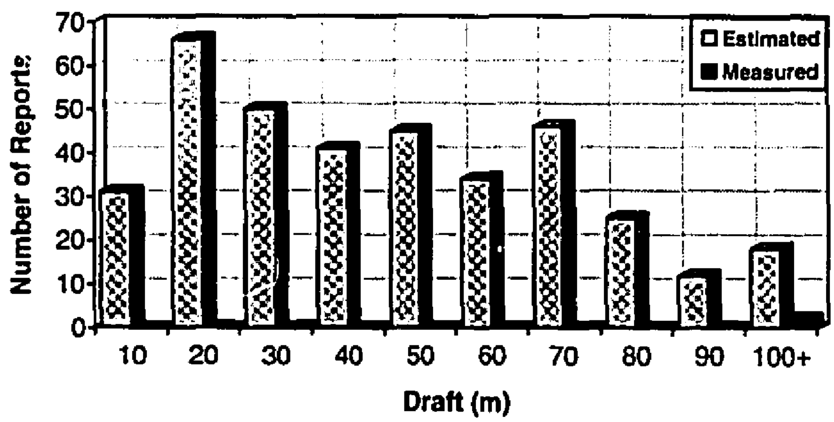

Figure 5.2-2 Histograms of measured and estimated iceberg drafts.

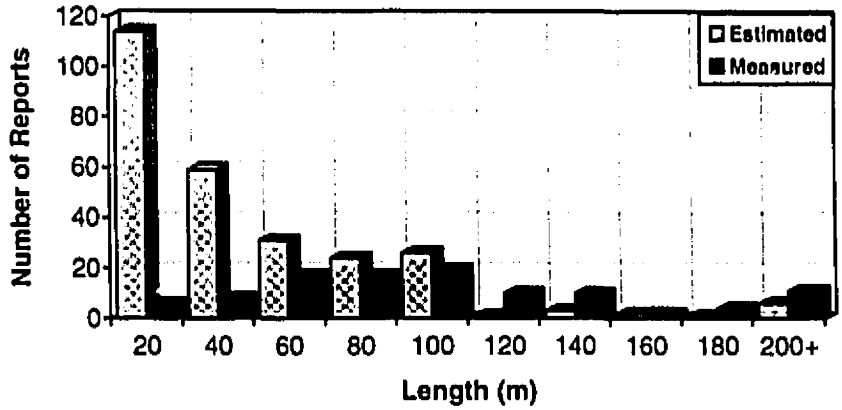

Figure 5.2-3 Histograms of measured and estimated iceberg lengths.

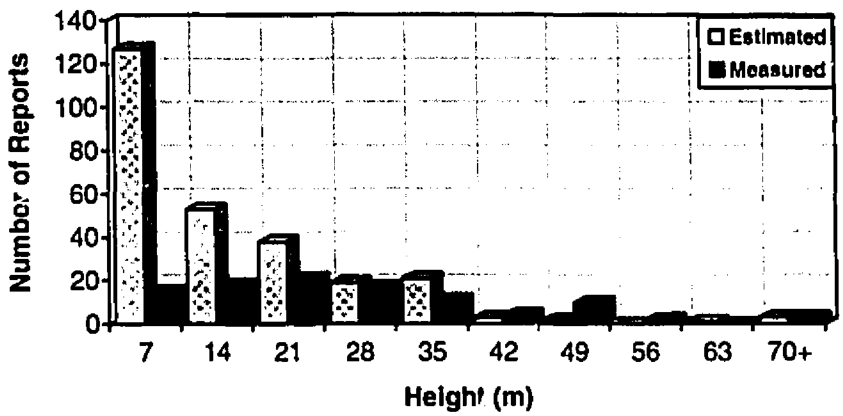

Figure 5.2-4 Histograms of measured and estimated iceberg heights.

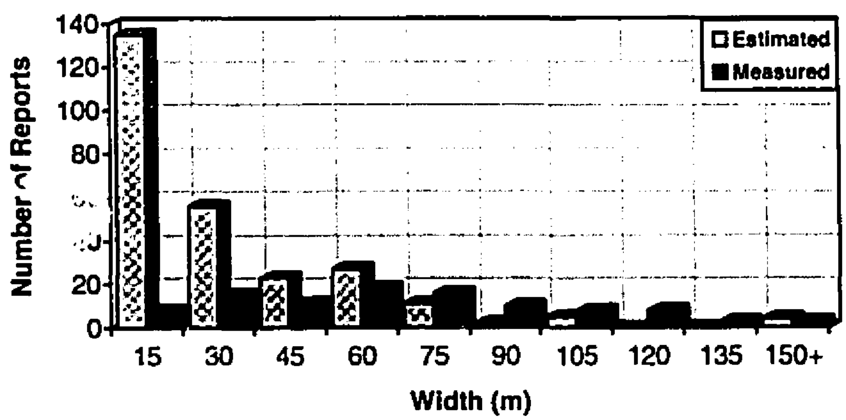

Figure 5.2-5 Histograms of measured and estimated iceberg widths.

Type of data	parameter	Length (m)	Width (m)	Height (m)	Draft (m)
ESTIMATED AND MEASURED DIMENSIONS	μ	56.05	36.50	15.17	42.69
	σ	50.36	33.40	14.54	25.84
	N	371	363	368	370
MEASURED DIMENSIONS	μ	93.32	63.16	23.91	100.00
	σ	54.08	35.16	16.83	-
	N	104	100	101	2
ESTIMATED DIMENSIONS	μ	41.53	26.37	11.87	42.38
	σ	40.50	26.46	12.05	25.56
	N	267	263	267	368

Table 5.2-1 Sample average (μ), sample standard deviation (σ) and the number (N) of icebergs represented in the Husky Oil database

Summary statistics on iceberg dimensions indicate that the mean values for measured data are much larger and display much less variance than the corresponding mean values for the estimated data (Table 5.2-1). This can be attributed to the fact that Husky Oil measured mostly large icebergs, while the dimensions of most small icebergs, growlers and bergy bits were estimated. Husky Oil also provides a qualitative size descriptor of icebergs similar to the one used by IIP (see Chapter 2.5). Figures 5.2-6 and 5.2-7 show the proportion of icebergs in each category by month for the Husky Oil and IIP data sets, respectively. The unevenness in the size distribution for the Husky Oil database is mainly due to the small sample size.

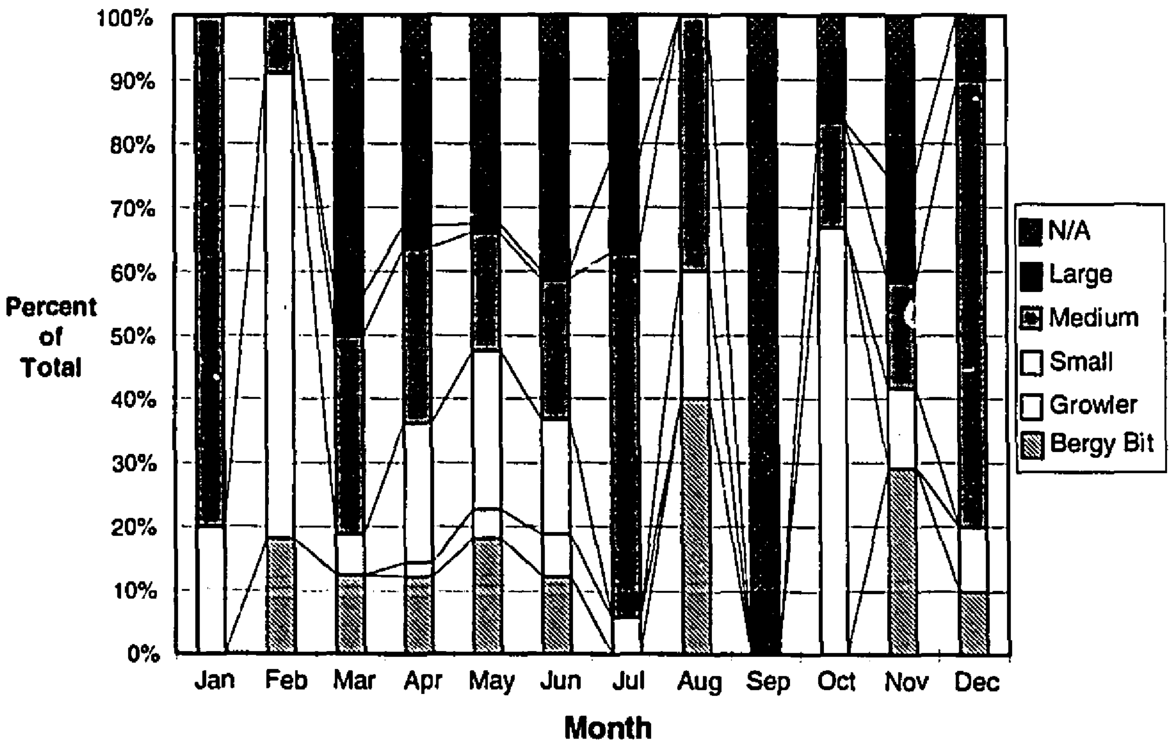

Figure 5.2-6 Decomposition of Husky Oil database by month according to qualitative descriptor of iceberg.

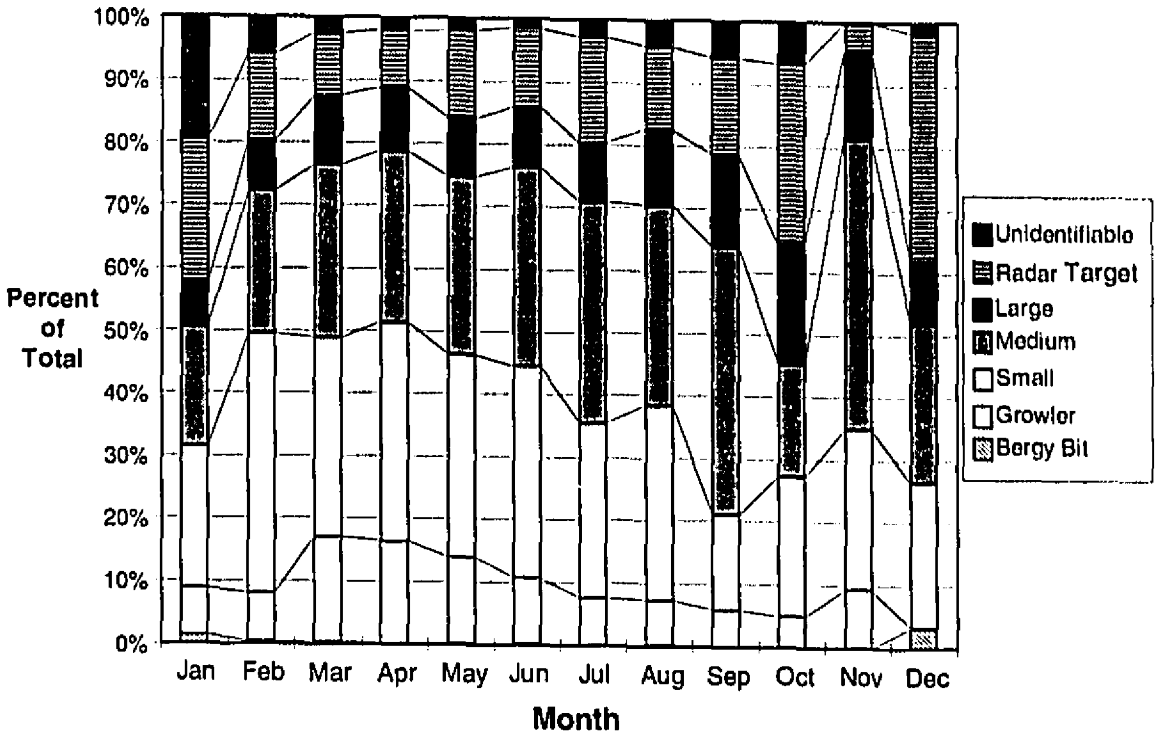

Figure 5.2-7 Decomposition of IIP database by month according to qualitative descriptor of iceberg.

Note that, for Figure 5.2-6, when the size of an iceberg was not available, it was reported as N/A in the Husky Oil database. In Figure 5.2-7, radar targets refer to SLAR images that are presumed to be icebergs, but which were not confirmed visually as being icebergs. Also, "unidentifiable" refers to all the other size categories in the IIP database, including null, garbled and general, as well as icebergs whose size descriptor is missing.

Figure 5.2-8 displays scatter plots of all possible pair-wise combinations of iceberg dimensions. The strong correlation between iceberg draft and other iceberg dimensions clearly indicates that iceberg drafts were derived using an empirical formula based on the other visible iceberg dimensions.

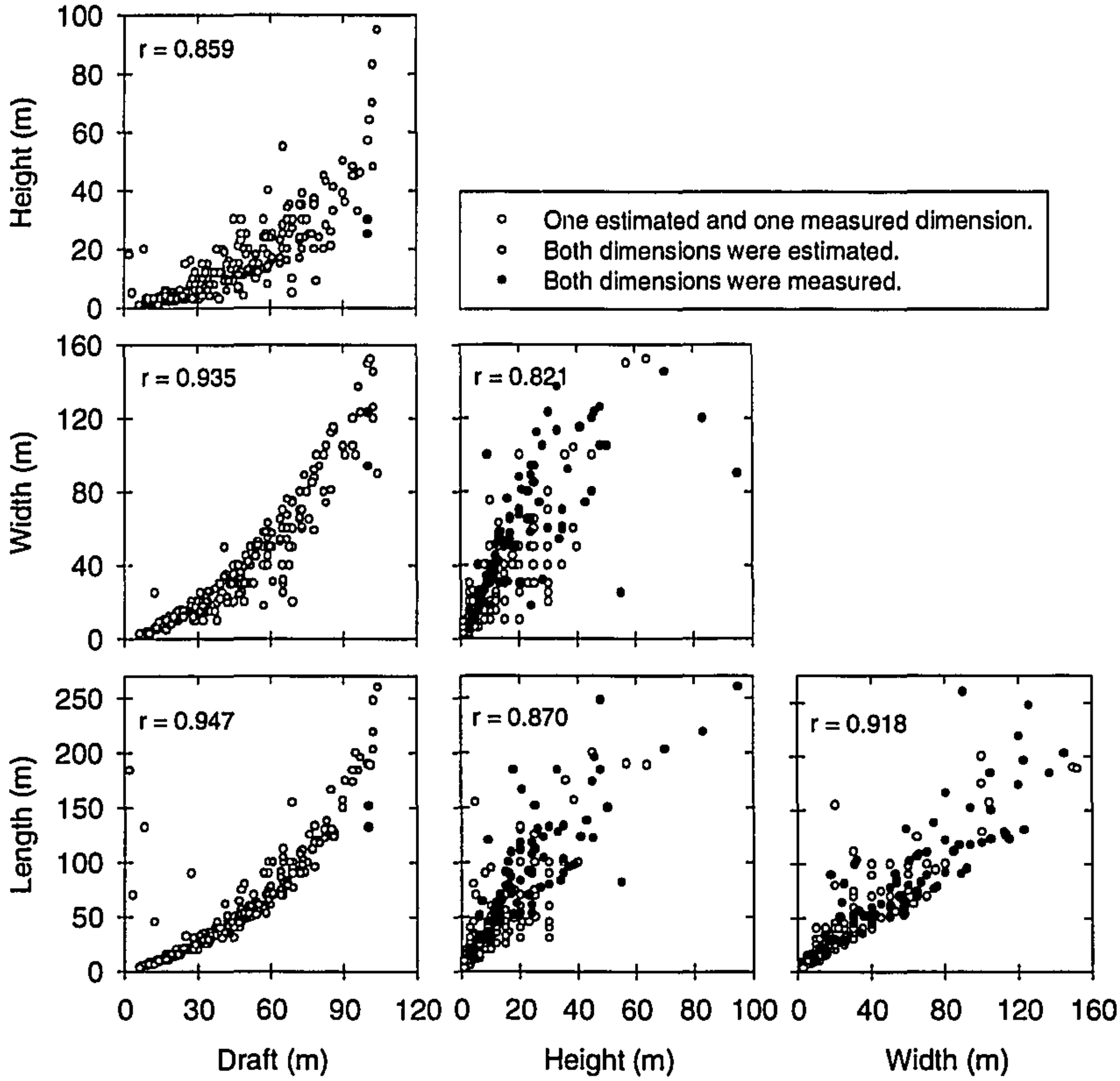

Figure 5.2-8 Scatter plots of iceberg dimensions. The linear correlation coefficient (r) is included in each plot, although the relationship between dimensions is clearly non-linear. The value of r was calculated using both estimated and measured data. Values of r for measured data are only slightly lower.

5.3 Iceberg Drift

The flow of icebergs into the Grand Banks is highly variable, both inter-annually and intra-annually (seasonally). Annual fluctuations display a slight cyclical pattern, with peaks in annual counts occurring in 3 to 4 year bundles and lows occurring at 4 to 9 year intervals (Marko *et al.*, 1994; Figure 5.3-1). Seasonally, iceberg flux has a more distinct pattern. The vast majority of icebergs are observed from April to June (Figure 5.3-2). Icebergs on the Grand Banks first appear in January. The number of icebergs on the Grand Banks increases steadily each month, reaching a peak in May, when they start decreasing. By August, the number of icebergs on the Grand Banks diminishes dramatically and remains negligible until the next season. Similarly, iceberg counts decrease as they drift southward into warmer waters. The rate at which iceberg counts decrease is gradual until 52°N in latitude. Past the 52°N latitude, the rate of iceberg crossings is significantly reduced (Figure 5.3-3).

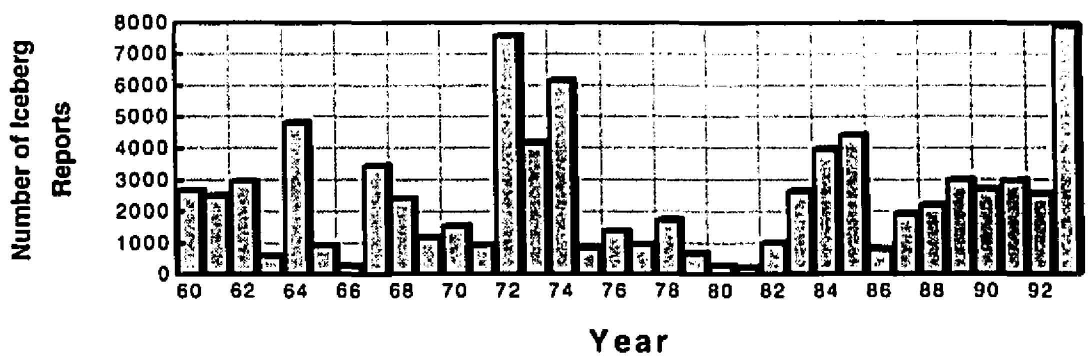

Figure 5.3-1 Decomposition of iceberg reports in IIP database by year.

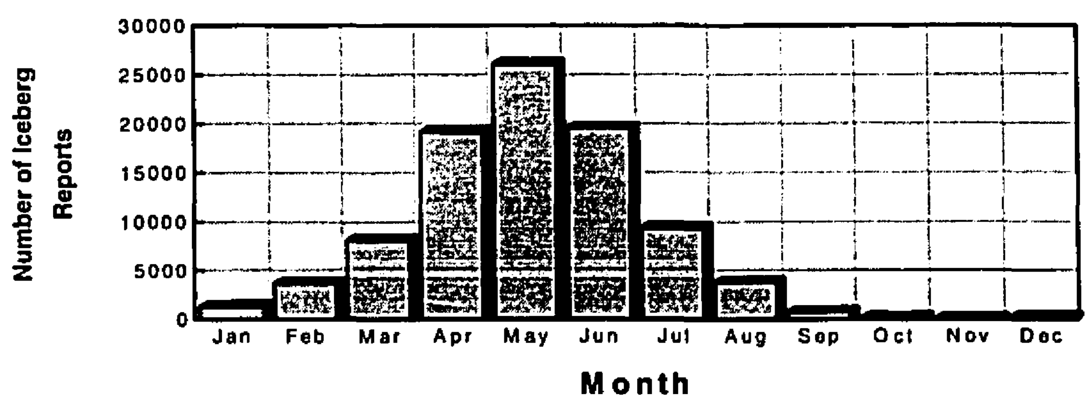

Figure 5.3-2 Decomposition of iceberg reports in IIP database by month.

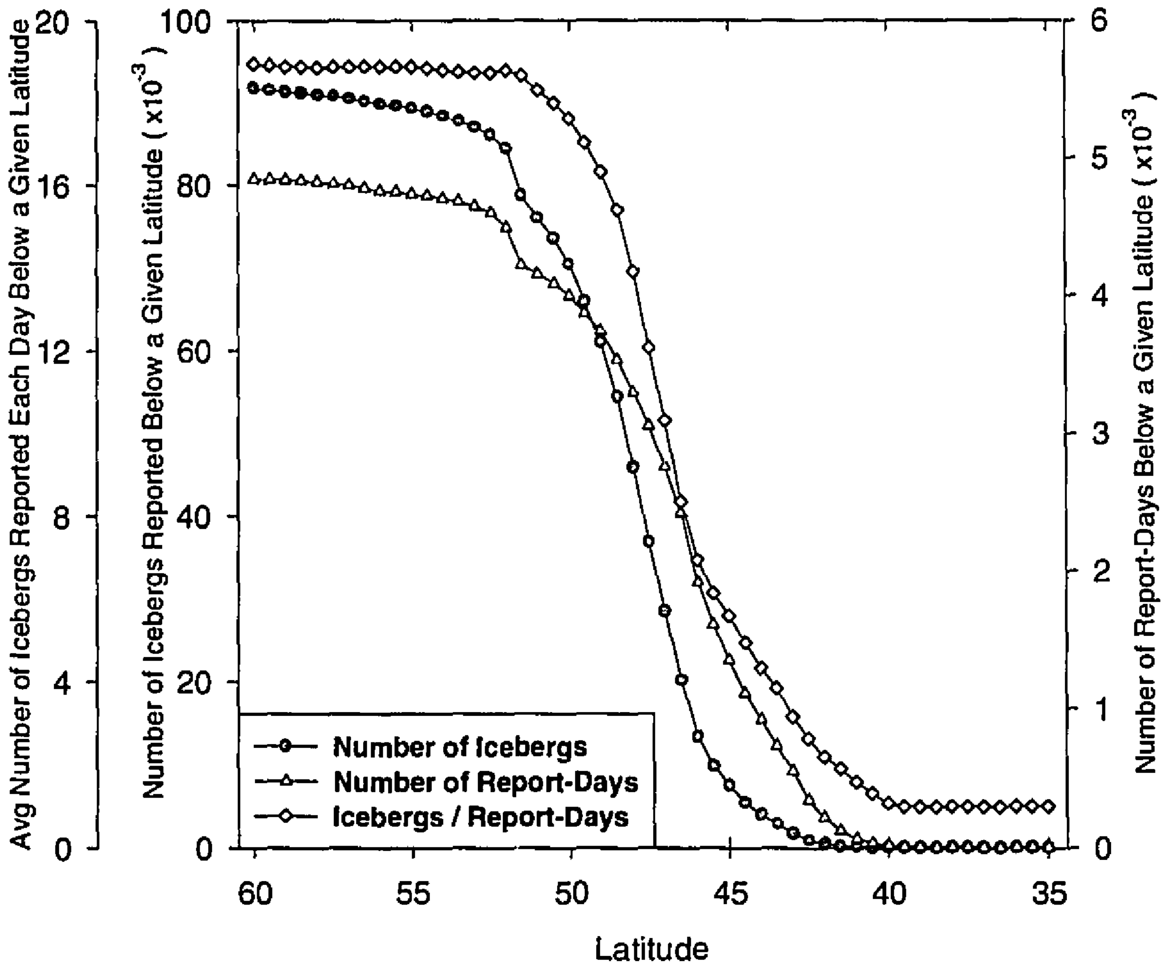

Figure 5.3-3 Number of icebergs, number of report days and average number of icebergs per report day as a function of latitude.

The number of report-days refers to the number of distinct days on which icebergs were reported in the database and is used in the calculation of spatial densities to account for the total number of surveys comprised in the database.

5.3.1 Resights

Each iceberg in both the IIP and Husky Oil databases is identified as either a new observation or a resight of a previously reported iceberg. Figures 5.3-5 and 5.3-6 show paths of resighted icebergs in the Husky Oil and IIP databases for 1987. In the Husky Oil database, icebergs were continuously monitored and icebergs marked as resights are truly resights. This is in contrast to resights in the IIP database. IIP relies on an iceberg drift model to estimate the future location of a previously observed iceberg. In following surveys, icebergs found near predicted coordinates are labeled as resights. Although IIP has refined this method over time, it can generate biased results. This method can easily result in outliers with, for example, derived drift velocities in excess of 100 km/day.

The flux of icebergs at any given location can be expressed as:

$$\phi(\underline{x}, t, T, \alpha) = v(\underline{x}, t, T, \alpha) \cdot \lambda(\underline{x}, t, T) \cdot f(\underline{x}, t, T, \alpha) \qquad (5.3\text{-}1)$$

where $\underline{x}$ is the location in longitude and latitude, t is the time of year, T is a given year, v is the drift velocity of icebergs, λ is the density of icebergs per km^2, α is the direction of drift and $f(\cdot)$ if the pdf of drift direction.

In the following sections, it will be assumed that the drift velocity is constant in time, which is a reasonable assumption for the estimation of long term hazards:

$$\phi(\underline{x}, t, T, \alpha) = v(\underline{x}, \alpha) \cdot \lambda(\underline{x}, t, T) \cdot f(\underline{x}, \alpha) \qquad (5.3\text{-}2)$$

It is further assumed that the IIP database, which contains 34 years of observations, represents a sample that is large enough to be representative of the long term average flux:

$$\phi(\underline{x}, t, \alpha) = v(\underline{x}, \alpha) \cdot \lambda(\underline{x}, t) \cdot f(\underline{x}, \alpha) \qquad (5.3\text{-}3)$$

where $\lambda(\underline{x}, t)$ represents the seasonal variation of iceberg densities over the region.

Given the uncertainty associated with the IIP resight data and the limited number of observations in the Husky Oil database, drift velocities could not be reliably estimated at this time (see Appendix A for velocities derived from the IIP database).

The crossing rate of icebergs with respect to a line with orientation α_0 can be derived from estimates of the spatial density of icebergs and of the drift velocities (Figure 5.3-4). Given a random distribution of icebergs in space with intensity function $\lambda(\underline{x})$, the intensity of the process within a strip of unit width normal to Ω_0, and with length y, is equal to:

$$\lambda(y) = \lambda(\underline{x}) \cdot 1 \qquad (5.3\text{-}4)$$

The total area swept by a strip of unit width during a time period Δt is:

$$A = v(\underline{x})\Delta t \cdot 1 \tag{5.3-5}$$

where $v(\underline{x})$ is the drift velocity at $\underline{x}$, assuming $\vec{v}(\underline{x})$ is perpendicular to Ω_0 (Figure 5.3-4). The crossing rate can be estimated as:

$$\upsilon(\underline{x})\left[\frac{\text{icebergs}}{\text{km - day}}\right] = \frac{\lambda(\underline{x})\cdot v(\underline{x})\cdot \Delta t}{\Delta t} = \lambda(\underline{x})\cdot v(\underline{x}) \tag{5.3-6}$$

If the direction of drift is random with probability distribution function $f(\underline{x}, \alpha)$, the crossing rate, in terms of α, is:

$$\upsilon(\underline{x},\alpha) = \lambda(\underline{x})\cdot v(\underline{x},\alpha)\cdot f_\alpha(\underline{x},\alpha) \tag{5.3-7}$$

Finally, the total crossing rate, with respect to some given direction α_0, is (**Milan**, 1964):

$$\upsilon_{\alpha_0}(\underline{x}) = \lambda(\underline{x})\cdot v(\underline{x},\alpha)\cdot \int_0^\pi \left|\sin(\alpha_0 - \alpha)\right| \cdot f_\alpha(\underline{x},\alpha)\, d\alpha \tag{5.3-8}$$

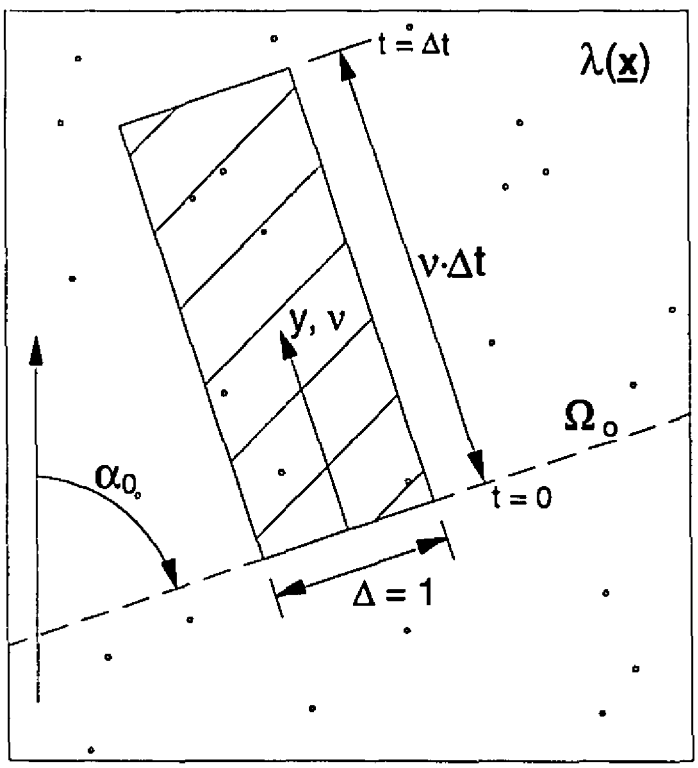

Figure 5.3-4 Idealization of the area surveyed during an iceberg search.

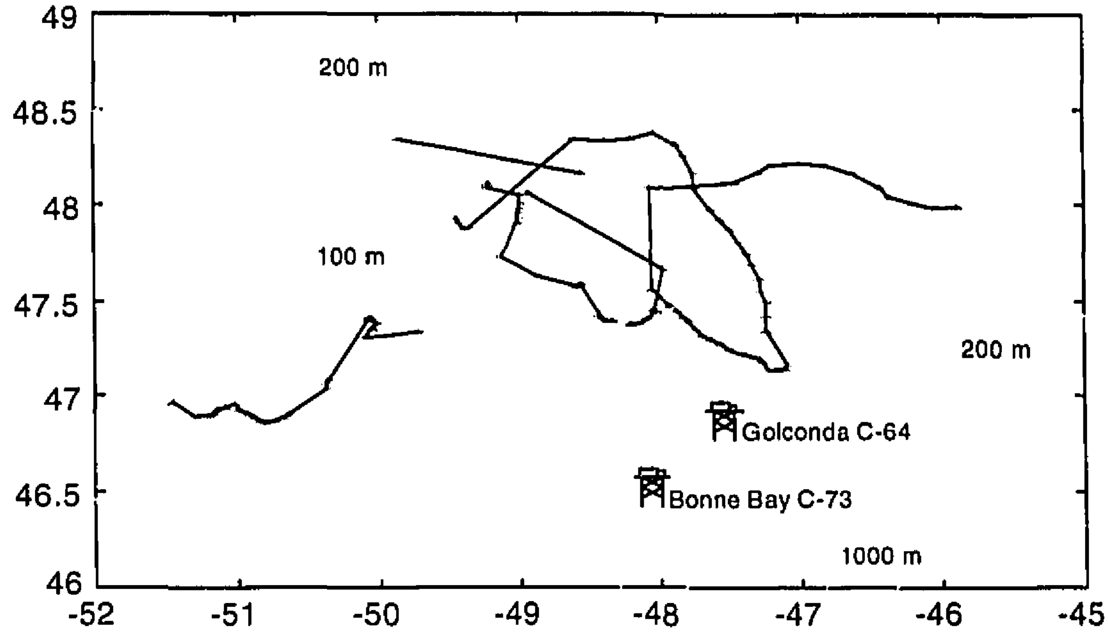

Figure 5.3-5 Some resighted icebergs, tracked by Husky Oil in 1987. Included are the locations and names of the wellsites where exploratory drilling was being performed.

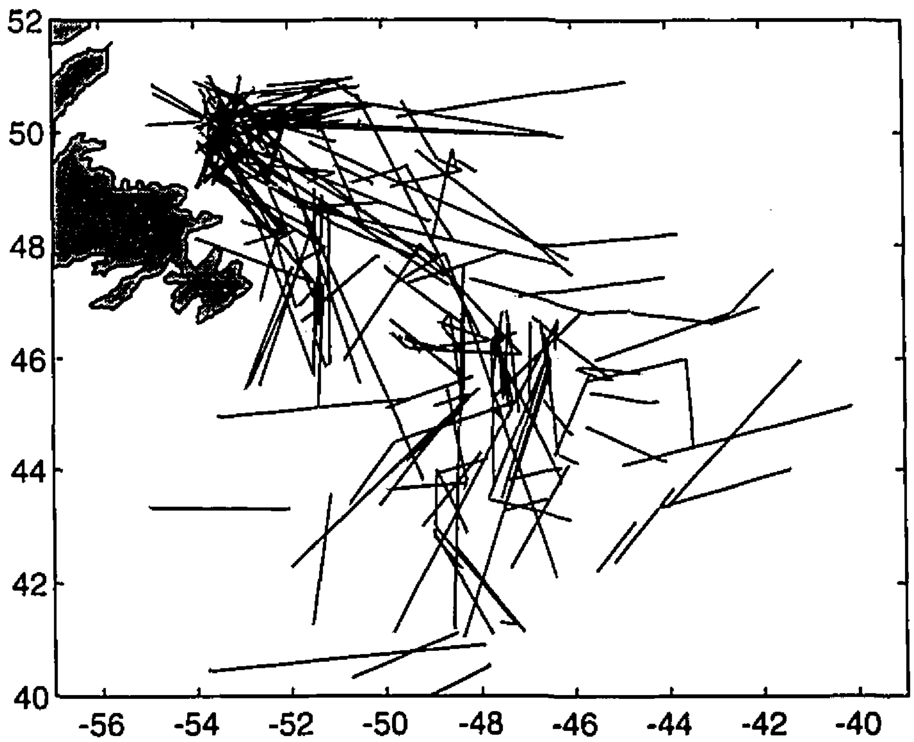

Figure 5.3-6 IIP iceberg resights in 1987

5.3.2 Groundings

The Husky Oil database records the movement of individual icebergs during drilling operations. Iceberg movement is qualified as either free, grounded or towed. When an iceberg drifted too close to an oil rig, it was towed away to avoid collision. Towed icebergs do not give valuable drift information, since they are being disrupted from their natural drift pattern.

Icebergs that appeared to be static were designated as grounded. However, this classification results in an unrealistically large number of reported groundings. Applying a criteria of no movement for 24 hours in less than 200m of water to define a definite grounding, results in only 44 groundings involving 27 large icebergs (Banke, 1987).

IIP does not report many groundings, due to their surveillance methods. Typically, IIP surveys a large area only once every two weeks, which is not frequent enough to establish if an iceberg has been grounded or not.

An attempt to infer scouring rates from reported iceberg groundings was not undertaken at this stage due to the inconsistent method of reporting grounded icebergs in the IIP and Husky Oil databases.

5.4 Density Estimation

5.4.1 Introduction

The crossing rate is used in combination with the pdf of iceberg draft to estimate scouring hazards at a given location. The crossing rate is a function of the density of icebergs and of the drift pattern (Eq 5.3-8). The following section addresses the estimation of the spatial density of icebergs, which are idealized as random points.

Estimates for the density of a homogeneous point process can be obtained as follows:

$$\hat{\lambda} = \frac{N}{A} \qquad (5.4\text{-}1)$$

where N is the total number of points contained in the region surveyed with area, A.

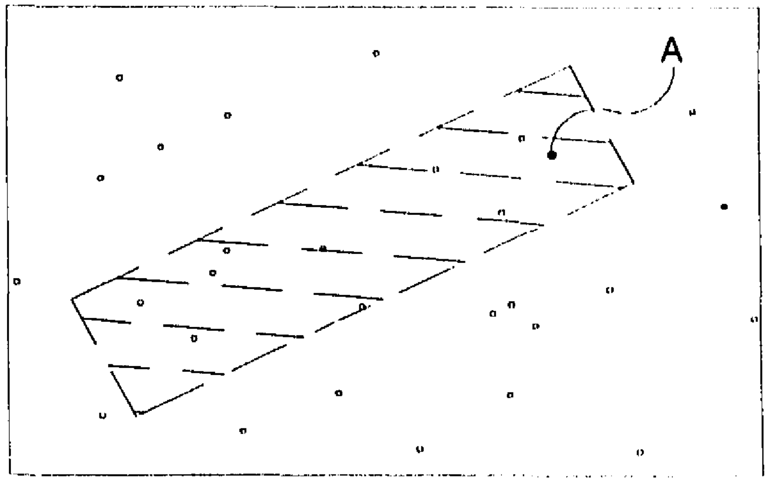

Figure 5.4-1 Idealization of a survey region with area A.

The uncertainty on the estimate decreases with an increase in the number of points contained in the surveyed area. Consequently, the uncertainty can be decreased by sampling over a larger region or by re-sampling a smaller region several times (Figure 5.4-2):

$$\hat{\lambda} = \sum_{j=1}^{m} \frac{N_j}{A_j} \qquad (5.4\text{-}2)$$

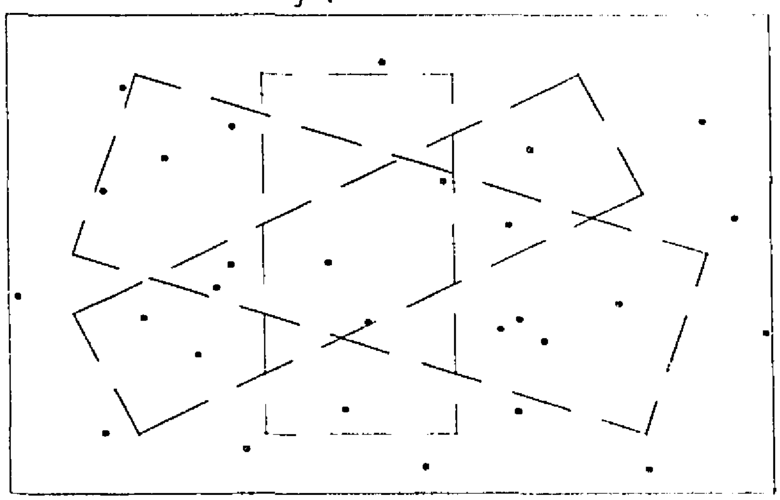

Figure 5.4-2 Idealization of a region surveyed several times.

In the context of iceberg reports, the sampled region corresponds to the region swept by SLAR or visual inspection during over-flight, or the region covered by radar for a ship crossing through the area. The estimators of Equations 5.4-1 and 5.4-2 assume that all icebergs within each surveyed region are reported. Alternatively, one could assume that for some reporting sources, such as ships, that reliability of reporting, or probability of detection P_D, decreases with distance from the observation point. Then,

$$\lambda_{observed} = \lambda_{true} \cdot \overline{P}_D \qquad (5.4\text{-}3)$$

where $\overline{P}_D$ is the average probability of detection over the region surveyed (Figure 5.4-3).

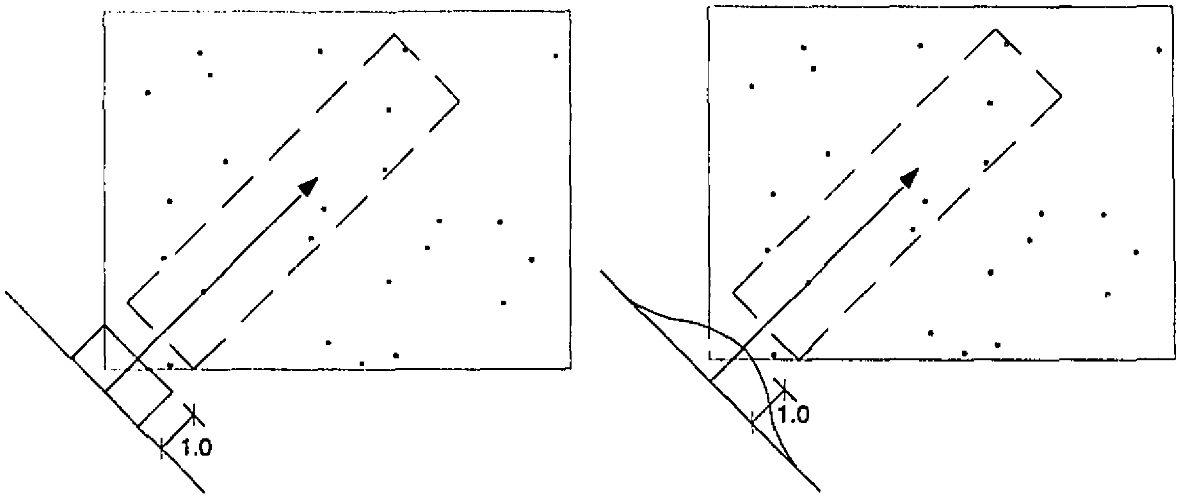

Figure 5.4-3 Idealization of the change in the probability of detection as a function of distance from the survey path: (a) probability of detection is constant up until a given distance (swath width); (b) probability of detection gradually decreases with distance from the survey path.

The estimator introduced above assumes that the boundaries of the region surveyed are known. However, in the case of the IIP database, there is no information on the flight paths of aerial surveys or on the shipping route of reporting vessels. Information on flight paths can be obtained from other reports from IIP or AES, but this information is available for only a very small fraction of the total number of icebergs reported in the database.

For these reasons, an alternative estimator which does not require prior knowledge with respect to the region surveyed has to be used. The proposed estimation is based on kernel estimation procedures and can be used to obtain estimates of the intensity function over regions where icebergs have been reported.

Given that an iceberg has been reported at a given location, it is assumed that all neighboring icebergs are reported with a probability which decreases as a function of the distance from the iceberg (Figure 5.4-4). In its simplest form, the probability of detection is assumed to be 1.0 within a given distance of the iceberg and equal to zero outside of this distance. An alternative is to assume that the probability of detection decreases monotonically with distance according to some specified function. The exact form of the probability of detection is a function of the source of the report. Under these assumptions, a local estimator of the intensity function, or density, can be formulated by using a modified version of the classic kernel density estimation procedure. An estimate of the intensity function is obtained by summing the contributions of the kernel function, or probability of detection, centred over each of the icebergs in the database (Figure 5.4-5).

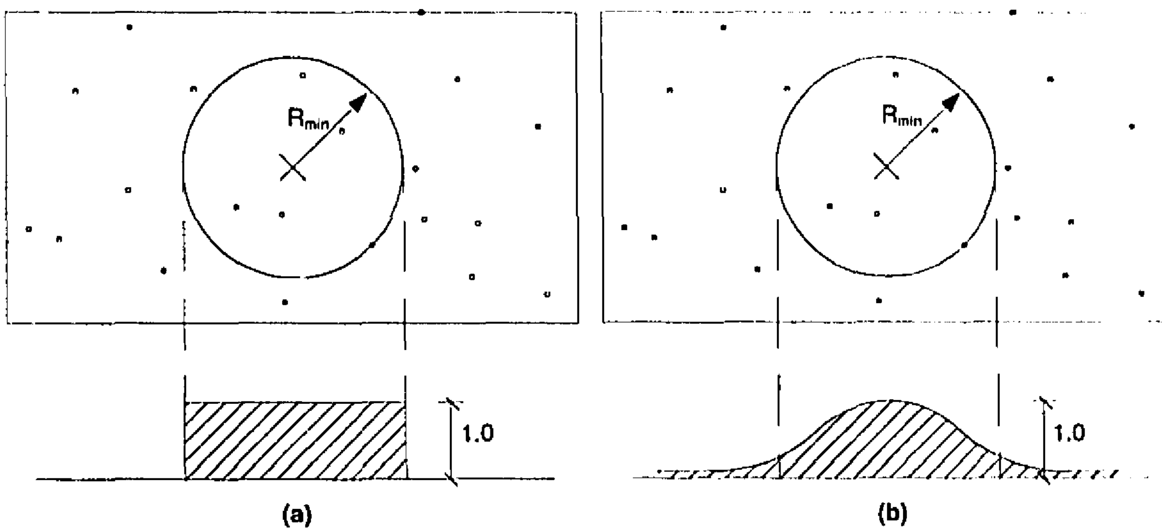

Figure 5.4-4 Idealization of probability of detection at the sighting source: (a) 100% probability that all icebergs within R_{min} will be reported; (b) the probability that an iceberg within R_{min} will be detected decreases with increasing distance from the sighting source.

An estimate of the intensity function at $\underline{x}$ is:

$$\lambda(\underline{x}) = \frac{1}{N_R} \cdot \frac{\sum I\left[\left(\underline{x} - \underline{y}\right) \leq h\right]}{\pi \cdot h^2}; \quad h \leq R_{max} \qquad (5.4\text{-}4)$$

where h is the kernel bandwidth $I[(x - y) \leq h]$ is an indicator function and is equal to 0 or 1 and N_R is the number of report-days, defined as the total number of distinct days for which iceberg are counted at location $\underline{x}$ (i.e. $I[\cdot] = 1$). It is important to account for the number of report-days as evidenced by the appearance of a high density of icebergs along preferential flight paths (Figure 5.4-2). For a circular kernel, h is characterized by the radius of the kernel, while for a square kernel, h is half the side length of the kernel.

The selection of the proper value of h in equation 5.4-4 is a function of the source reporting the iceberg, the density of icebergs and the spatial scale for the variation of the intensity function.

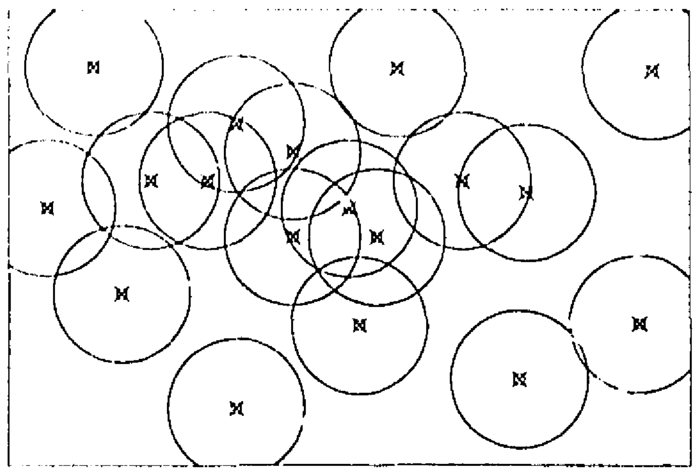

Figure 5.4-5 Idealization of kernel function centred over reports of iceberg locations.

Density estimates of icebergs, $\hat{\lambda}(\underline{x})$, were obtained for the Grand Banks using the IIP database through a modified form of the kernel estimation method (see Section 4.4). Estimates were obtained at locations defined by a grid spacing of 0.1° degrees, along both latitude and longitude between 40°N to 52°N and 39°W to 57°W.

As mentioned previously, the IIP database is a listing of icebergs from daily reports, therefore, the kernel estimator has to take into account the number of report-days at any given location. The number of reports was obtained by centering the kernel over each reported iceberg location and recording the dates of iceberg sightings at grid points falling within the kernel boundaries. Each distinct date was termed a report-day. It is assumed that the probability of detection for an iceberg within the kernel boundary is equal to 1.0. Therefore, it implies that if an iceberg is sighted by a vessel, all other icebergs within the kernel boundaries, centred over the iceberg, will also be reported. Using this procedure, both monthly and annual density estimates are obtained. To obtain annual density estimates, monthly density estimates were first calculated and then combined, giving each month equal weight:

$$\hat{\lambda}_{annual} = \sum_{i=1}^{12} w_i \cdot \hat{\lambda}_i = \sum_{i=1}^{12}\left(\frac{1}{12}\right)\cdot\hat{\lambda}_i = \frac{1}{12}\cdot\sum_{i=1}^{12}\hat{\lambda}_i \qquad (5.4\text{-}5)$$

Different kernel estimators are proposed for the estimation of the iceberg density function. These kernel estimators can be classified broadly into uniform, Normal and adaptive kernel estimation procedures. In the following sections, these procedures will be examined and will be illustrated with results for the annual average iceberg densities and for the month of May, which is the month with the most iceberg sightings. Figure 5.4-6 shows the locations of icebergs in the IIP database reported during May, from 1960 to 1993. The IIP database contains some erroneous reports, which were not omitted from the estimation of iceberg densities. However, there are few erroneous reports and their effect on estimates are negligible.

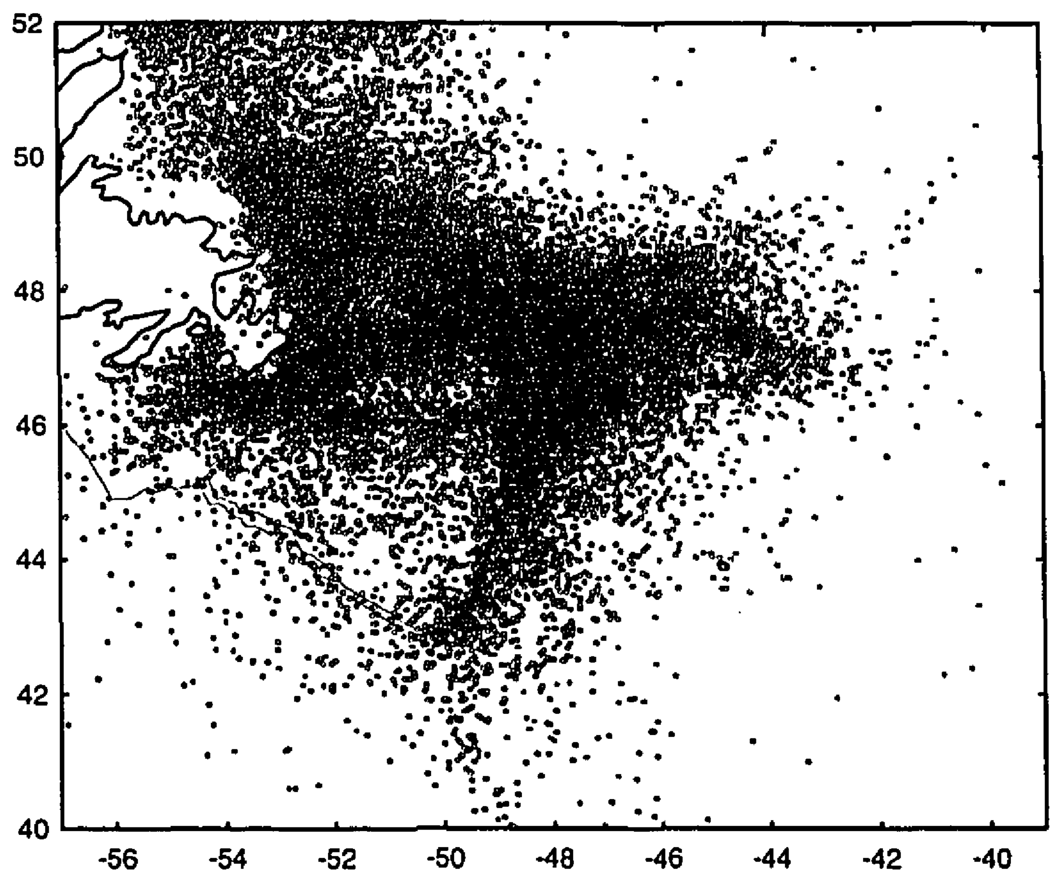

Figure 5.4-6 Plot of location of icebergs from IIP database reported during month of May (1960 to 1993). May accounts for 25589 reports or 30.47% of all the reports in the IIP database.

5.4.2 Uniform Kernel

As mentioned in Section 4.2, iceberg drift patterns can be idealized as a random line process. Each observation in the IIP database can be considered as a point on an iceberg trajectory. An estimator based on a square kernel function with a bandwidth, h, is defined as follows:

$$\lambda(\underline{x}) = \frac{1}{N_R(\underline{x})} \cdot \frac{1}{h^2} \sum_{j=1}^{N} K_S\left(\underline{x} - \underline{y}_j\right) \tag{5.4-6}$$

where

$$K_S\left(\underline{x} - \underline{y}_j\right) = 1 \quad \text{if} \begin{cases} \left|x_1 - y_{1j}\right| \le h \\ \text{or} \\ \left|x_2 - y_{2j}\right| \le h \end{cases} \tag{5.4-7}$$

$$= 0, \quad \text{otherwise}$$

where $\underline{y}_j$ is the position in longitude and latitude of iceberg j, N is the total number of icebergs and N_R is the number of report-days. In this application, a bandwidth of 50 km was chosen to correspond with the range of SLAR imagery and ship radar. As a consequence, all data was treated equally, however, the procedure could be modified to account for varying degrees of reliability and range, or as a function of the source reporting icebergs. To account for the non-uniformity of sampling over the region, the estimated densities are divided by the number of report-days.

Figure 5.4-7 shows estimates of the spatial annual average iceberg density obtained using a square kernel and the estimators of Equations 5.4-6 and 5.4-7. Similarly, Figure 5.4-8, shows the density estimates for the month of May. Figures 5.4-9 and 5.4-10 show, respectively, the corresponding counts and number of report-days used to obtain the density estimates for May. Iceberg counts and report-days are not provided for the annual average iceberg densities because these were derived from the estimates of the monthly density estimates. The results of a similar analysis, which was done using a circular kernel of constant radius, can be found in Figures 5.4-11 to 5.4-14. The results of annual average iceberg densities correspond to the mean annual density obtained using Equation 5.4-5. Both the counts and the number of report-days vary significantly as a function of location. As expected, there is a high degree of correlation between the number of report-days and the counts, however, the resulting density estimates exhibit spatial irregularities. Part of the irregularities can be attributed to the discontinuous form of the kernel function of equations 5.4-6 and 5.4-7, and part can be attributed to the statistical uncertainty of the estimates, especially for locations at the outer edge of the region where icebergs densities are low.

A disadvantage of the uniform kernel bandwidth procedure is that it can result in overestimation of the densities in regions of low iceberg densities, for example, in regions where the spatial density of icebergs is close to 1 in a circle with a 50 km radius. In such a case, the kernel should be adjusted to reflect the sparseness of the icebergs. Smoothness in the spatial variation of the estimates can be introduced by using a continuous kernel function that decreases monotonically with distance, such as the Normal distribution function, or by increasing the value of the smoothing constant h.

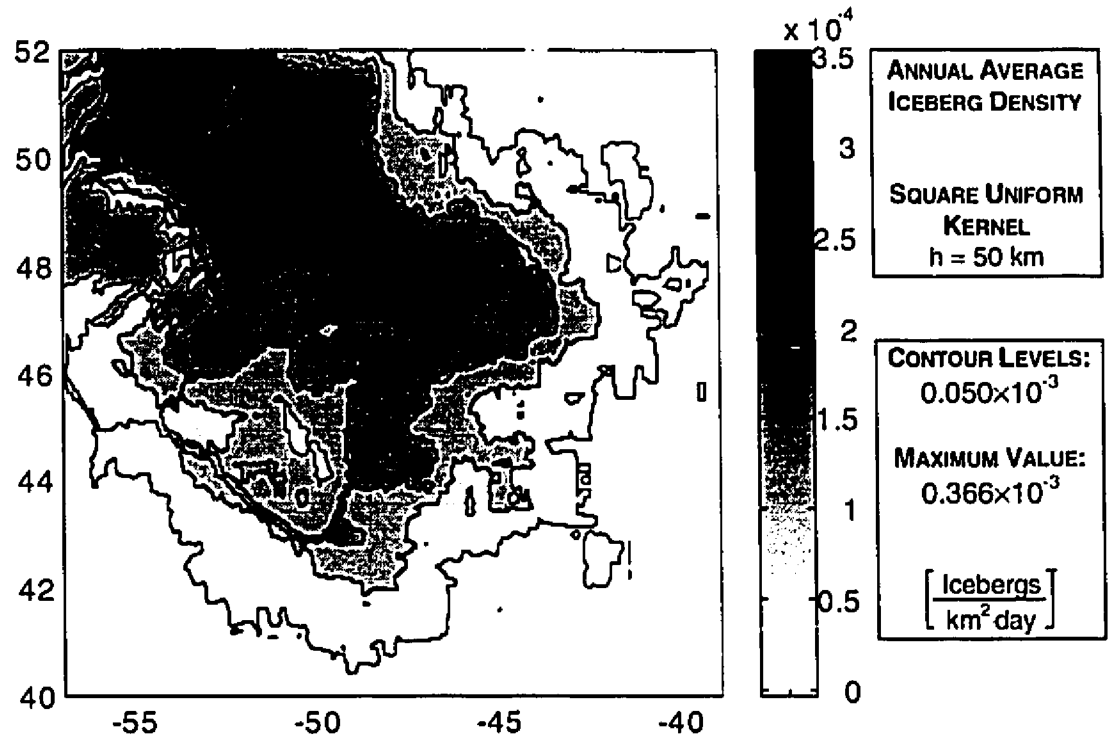

Figure 5.4-7 Annual average iceberg density, obtained using a square kernel with sides of 100 km.

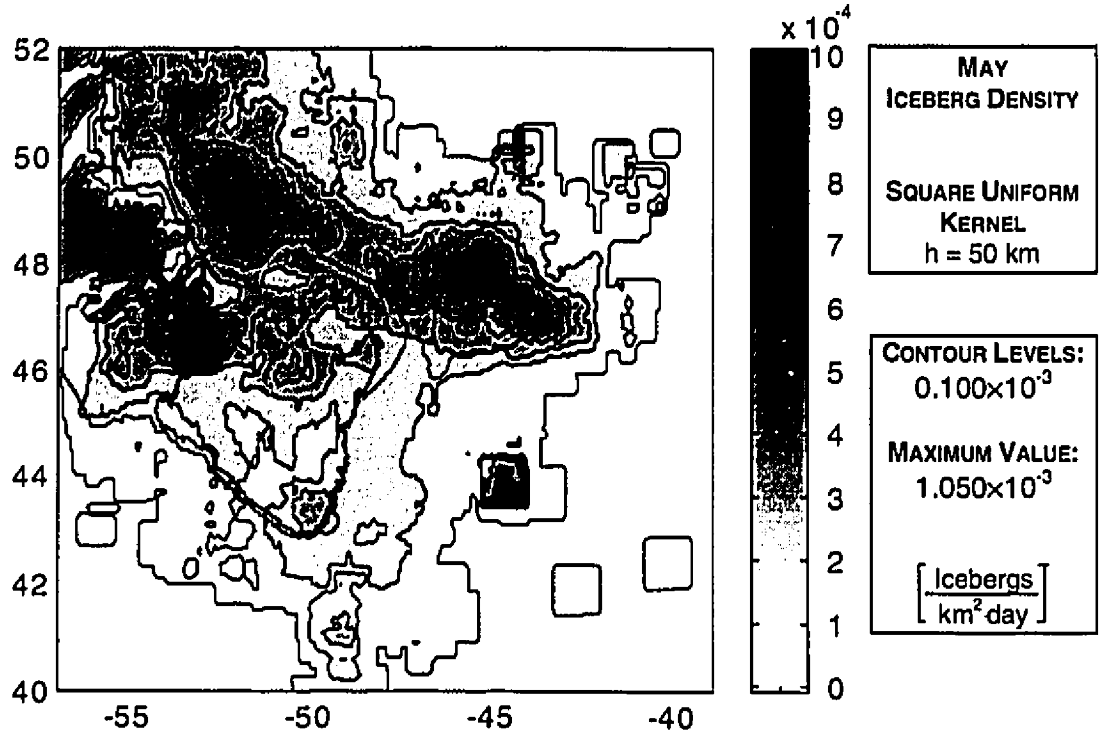

Figure 5.4-8 Iceberg density for May, obtained using a square kernel with sides of 100 km.

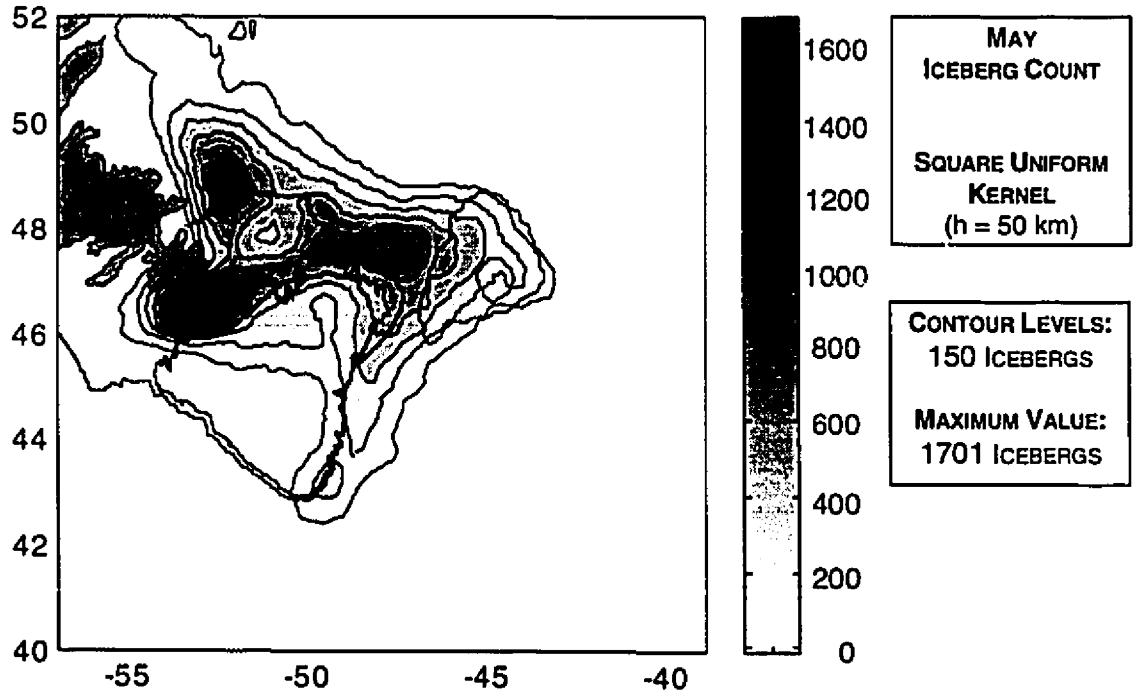

Figure 5.4-9 Iceberg count for the month of May, obtained using a square kernel with sides of 100 km.

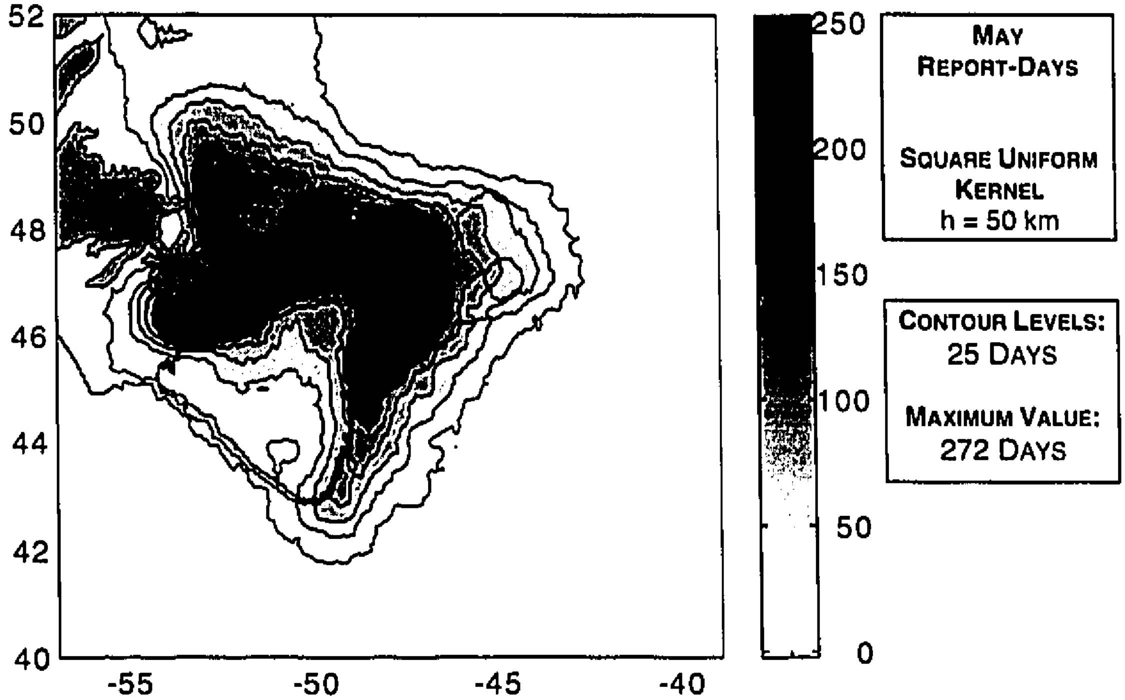

Figure 5.4-10 Count of report-days, N_R, for May, obtained using a square kernel with sides of 100 km.

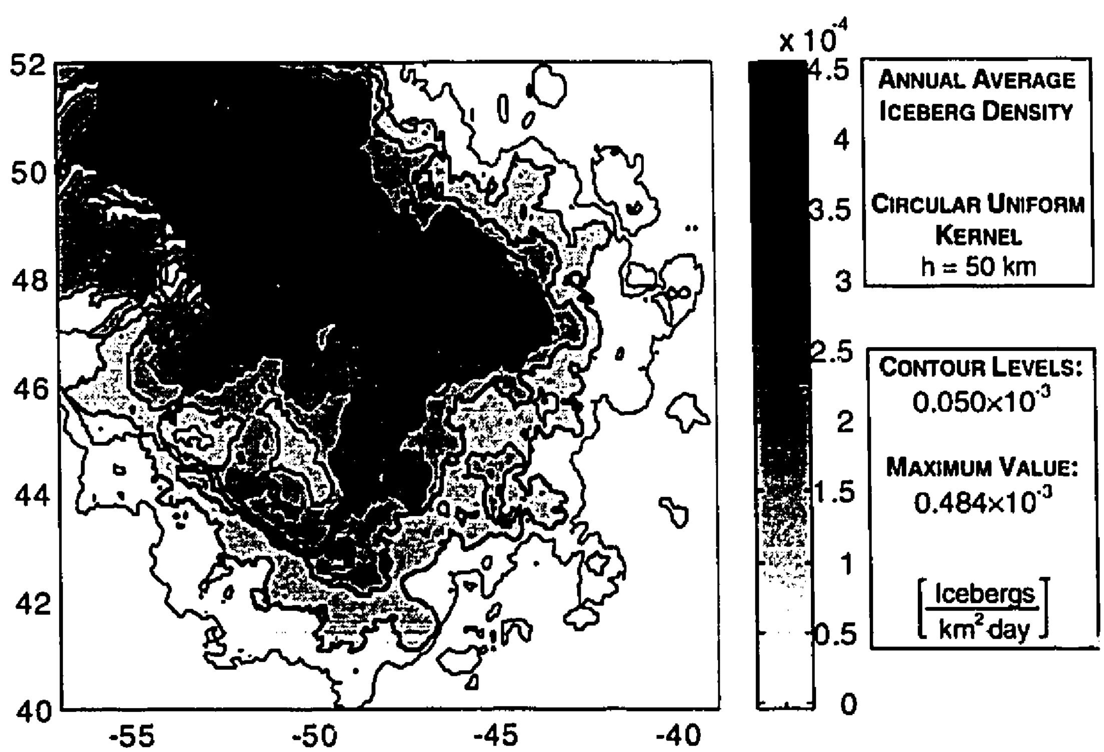

Figure 5.4-11 Annual average iceberg density obtained using a circular kernel with a radius of 50 km.

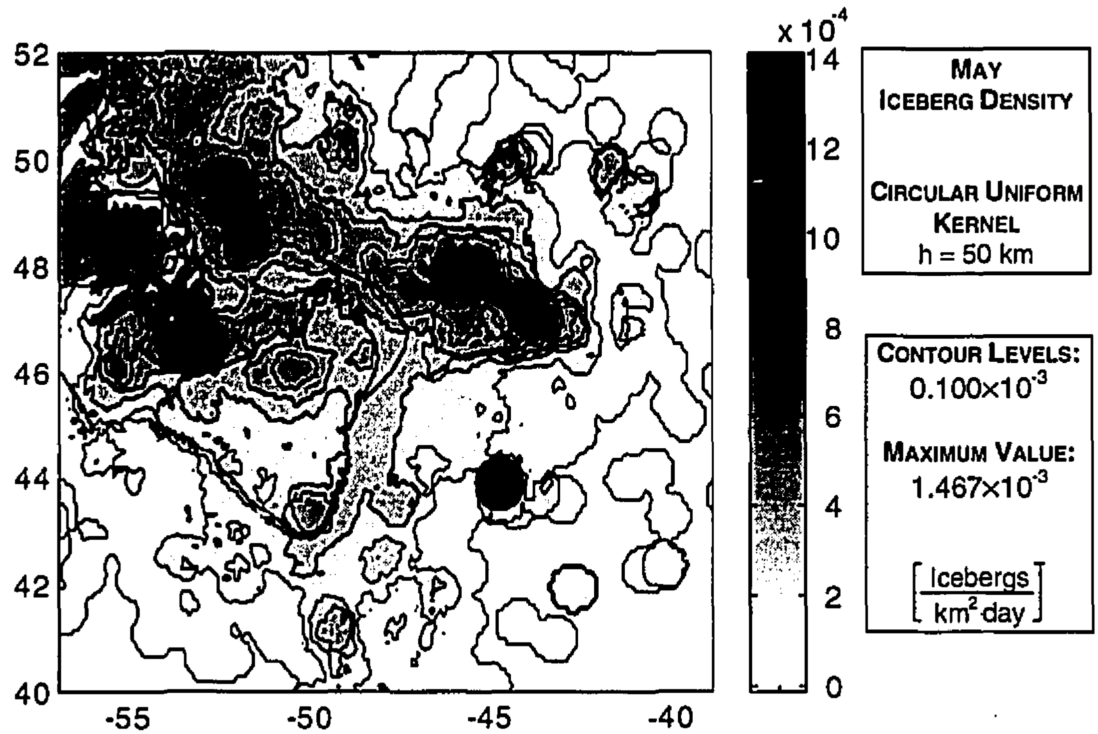

Figure 5.4-12 Iceberg density for May, obtained using a circular kernel with a radius of 50 km.

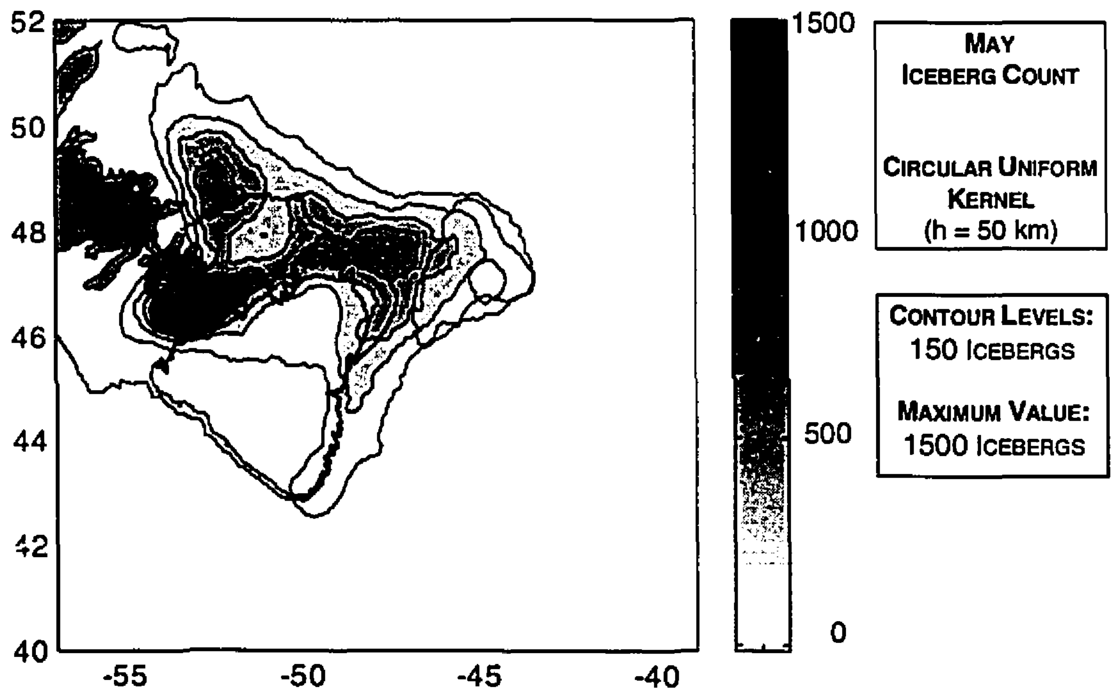

Figure 5.4-13 Iceberg count for the month of May, obtained using a circular kernel with a radius of 50 km.

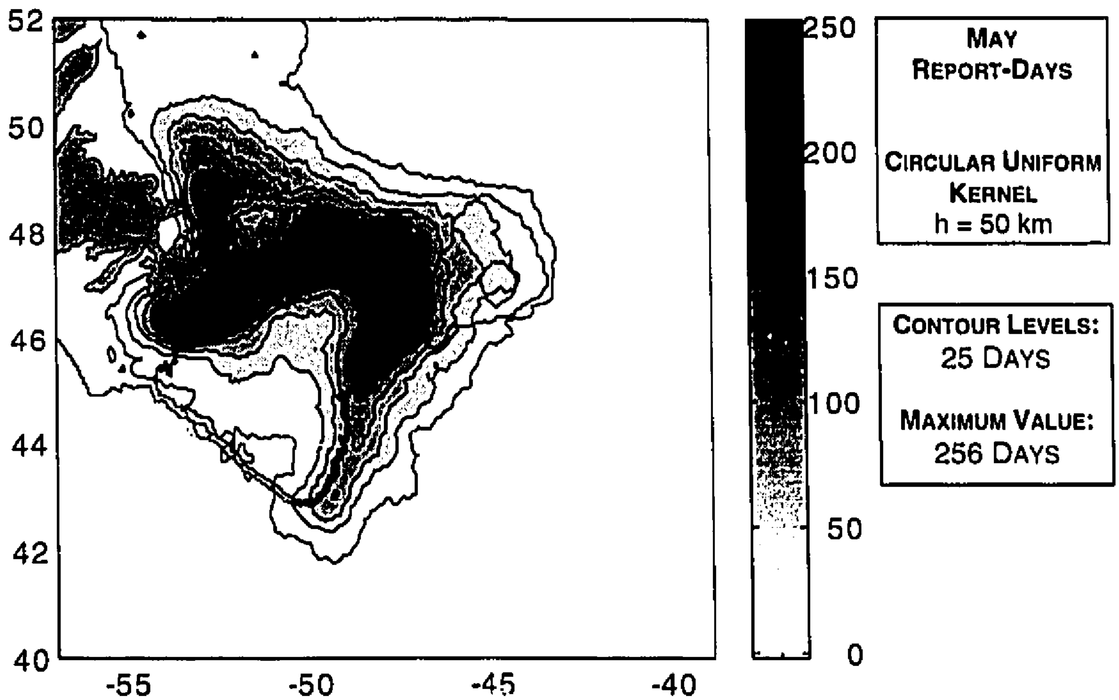

Figure 5.4-14 Count of report-days, N_R, for May, obtained using a circular kernel with a radius of 50 km.

5.4.3 Normal Kernel

For this application, an axi-symmetric Normal kernel was used with a correlation coefficient of 0 (ρ=0). The only free parameter is the standard deviation, or the kernel bandwidth, of the Normal distribution which is centred over the location of each reported iceberg. Therefore, the weight associated with a grid point a distance d from a reported iceberg is:

$$K(d) = \frac{1}{2\pi} \cdot exp\left[-\frac{1}{2}\left(\frac{d}{h}\right)^2 \right] \qquad (5.4\text{-}8)$$

the estimator of the density is as before:

$$\hat{\lambda}(\underline{x}) = \frac{1}{N_R(\underline{x})} \cdot \sum_{j=1}^{N} \frac{1}{\pi \cdot h^2} \cdot K\left(d_j = \left|\underline{x} - \underline{y}_j\right|\right) \qquad (5.4\text{-}9)$$

where $N_R(\underline{x})$ is the number of report-days at $\underline{x}$ and is estimated in the same fashion as for the uniform kernel function (Figure 5.4-17). Therefore, the value of the kernel function assigned to an iceberg observation decreases monotonically with distance, but the value associated with each new report-day remains constant. Note that for the Normal kernel, the maximum spatial extent of the kernel is equal to three times the standard deviation of the Normal distribution function ($h = 3 \cdot \sigma = 3 \times 50$ km = 150 km). The resulting estimations (Figures 5.4-15 and 5.4-16) are much smoother than with a uniform kernel but still exhibit spurious results in regions of low iceberg density. A solution to this problem is to estimate densities through an adaptive kernel procedure which is described in the next section.

Figures 5.4-15 and 5.4-16 show that the Normal kernel eliminates some of the noise at the periphery of the region, where densities are low. The spatial variation of the estimates is also much smoother. A disadvantage of this procedure is that it can result in an underestimation of iceberg densities. This is attributed to the large kernel bandwidth and the unequal weighting of report-days and iceberg reports, which makes the number of report-days relatively large in relation to the iceberg counts.

Interesting features in the spatial variation of the densities derived using the Normal kernel are that the contour lines closely follow the bathymetry, specifically around the Grand Banks. Changes in the direction of the contour lines at the periphery of the Grand Banks appear to be well correlated with the position of known eddies (Figure 2.3-1).

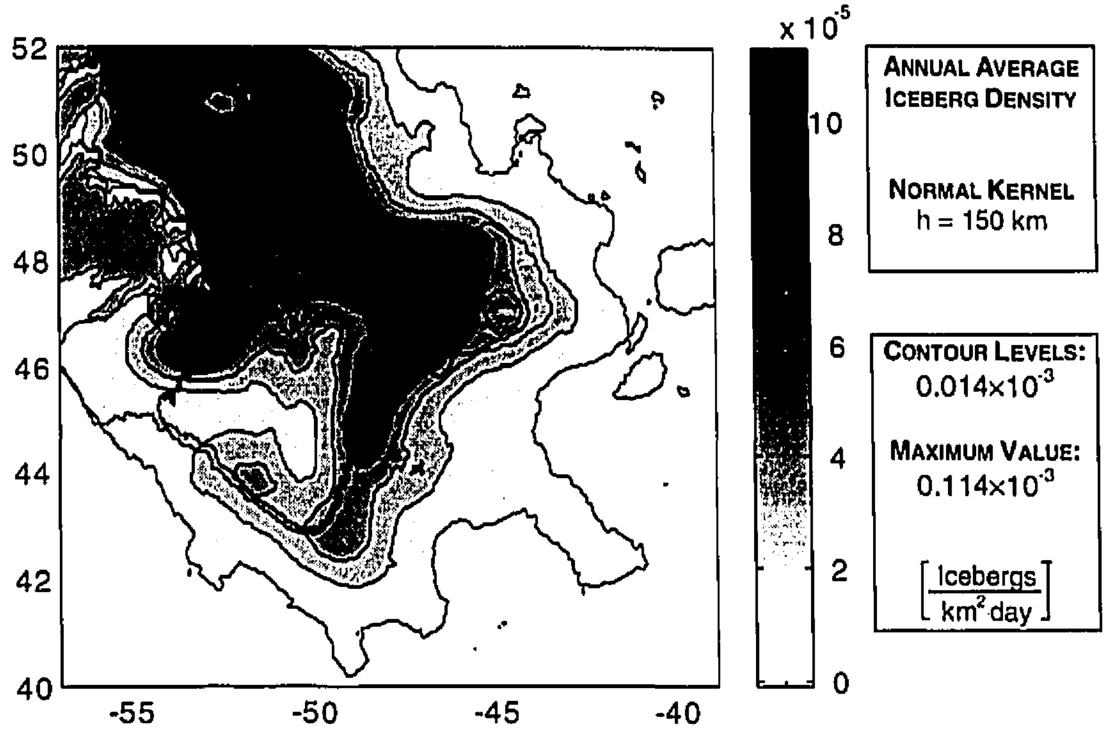

Figure 5.4-15 Average annual iceberg density, obtained using a Normal kernel with a 50km standard deviation.

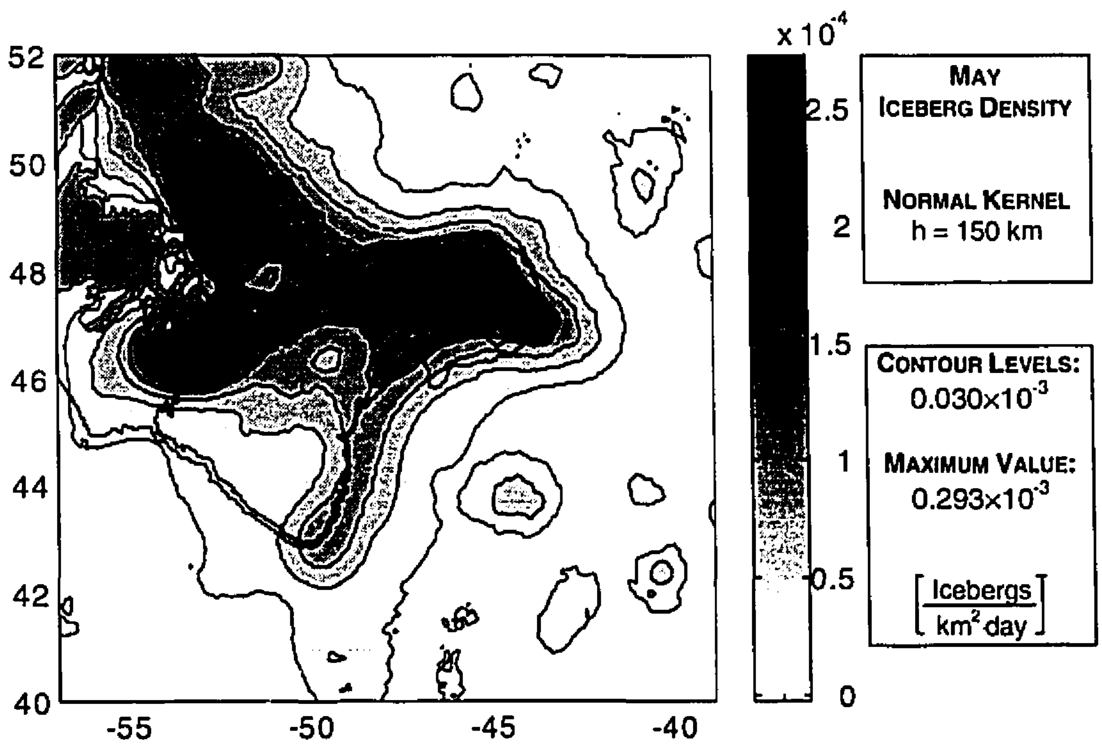

Figure 5.4-16 Iceberg density for May, obtained using a Normal kernel with a standard deviation of 50 km.

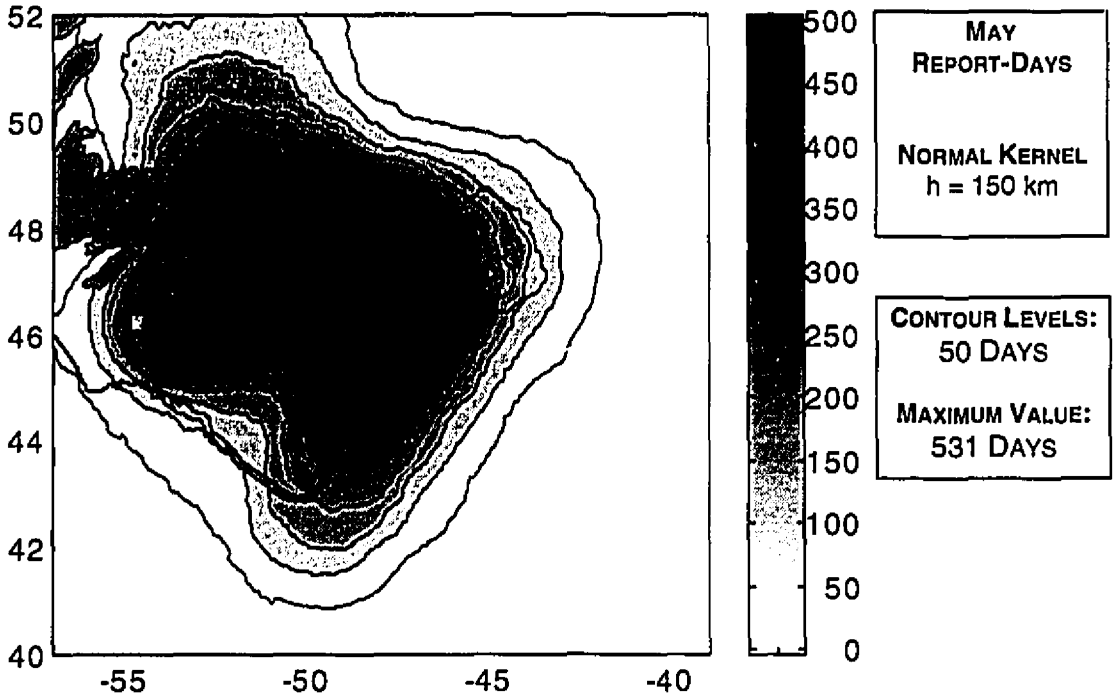

Figure 5.4-17 Count of report-days for May, obtained using a Normal kernel with a standard deviation of 50km.

5.4.4 Modified Adaptive Kernel

The estimates obtained with constant bandwidth kernels produce unexpected peaks at the outer limits of the iceberg infested region. These features are regarded as anomalies. An adaptive kernel method can be used to smooth the estimates over the outer regions while preserving statistically significant peaks in the interior region.

The idea behind the adaptive kernel is that the amount of smoothness introduced in the estimation should be inversely proportional to the number of observations. Note that the coefficient of variation of the estimator for the intensity function of a Poisson process is inversely proportional to the number of observations N in the sample:

$$V(\hat{\lambda}) = \frac{E(N/A)}{\sqrt{\mathrm{Var}(N/A)}} \approx \frac{1}{\sqrt{N}} \qquad (5.4\text{-}10)$$

where $\hat{\lambda}$ is the estimated density and A is the area of the region sampled.

In regions of high densities, the bandwidth should be kept relatively small in order to capture all significant features in the spatial variation of the rate and minimizing the bias. Conversely, the bandwidth should be much larger in the outlying regions to decrease the variance of the estimates at the expense of possibly introducing a relatively small amount of bias.

Several types of adaptive kernel function can be formulated (Silverman, 1986). The one which has been retained for this application is a variable size uniform square kernel:

$$\lambda(\underline{x}) = \frac{1}{N_R(\underline{x})} \cdot \frac{1}{h(\underline{x})^2} \cdot \sum_{j=1}^{N} K\left(\left|\underline{x} - \underline{y}_j\right|\right) \qquad (5.4\text{-}11)$$

where

$$K\left(\underline{x} - \underline{y}_j\right) = 1 \quad \text{if} \begin{cases} \left|x_1 - y_{1j}\right| \leq h(\underline{x}) \\ \text{or} \\ \left|x_2 - y_{2j}\right| \leq h(\underline{x}) \end{cases} \qquad (5.4\text{-}12)$$

$$= 0, \text{ otherwise}$$

The size of the kernel, $h(\underline{x})$, is selected such that a minimum specified number of observations N_{min} is contained within the boundaries of the kernel. This guarantees a degree of uniformity in the uncertainty associated with estimates of the density throughout the region. The choice of the square kernel instead of the circular one is strictly dictated from computational benefits.

A grid of equally spaced points at which estimates are obtained is laid out over the region. A minimum number of observations, N_{min}, is specified and the size of the kernel is determined by extending the boundaries of the kernel until the number of observations within the kernel is greater than or equal to N_{min}.

This method has the advantage of eliminating unexpected large estimates in outlying areas which occur when using a kernel with a constant bandwidth. From Eq 5.4-11, it can be shown that, for a kernel with a constant bandwidth, these peaks can be obtained when the number of report-days is low, even if the number of observations is small. In other words, the size of the region which is sampled should be proportional to the density of the observations. The variance of the estimator increases with a decrease in the number of observations, which is influenced both by the size of the sample region and the density of the icebergs. Note that the number of report-days $N_R(\underline{x})$ includes all the distinct reports for the region defined by the kernel with dimension $h(\underline{x})$ centred at $\underline{x}$.

The selection of N_{min} is based on several factors: the true density of the icebergs; the size of the resulting kernel function, and the spatial scale of the variation of the densities. N_{min} should be large enough such that the coefficient of variation associated with the estimator is small, while limiting the radius of the kernel to avoid over-smoothing statistically significant spatial variations, and limiting $h(\underline{x})$ to a range which is consistent with the assumptions associated with the detection of reported icebergs within the region defined by $h(\underline{x})$. A value of N_{min} equal to 75 icebergs appears to fulfill all of the above requirements for the present application.

The size of the kernel $h(\underline{x})$ for each month of the year is provided in Appendix D. A comparative illustration of monthly density estimates can be found in Appendix B, which is a series of monthly densities constructed using constant contour levels. These estimates are then combined using equal weighting to obtain the annual average density of Figure 5.4-18. Monthly density estimates with corresponding plots of monthly iceberg locations are found in Appendix C. The figures in Appendix C illustrate the effectiveness of the adaptive kernel at representing the local density of the iceberg population.

The sequence of monthly density estimates illustrate the seasonal trend in the variation of the iceberg population over the Grand Banks and correlate well with qualitative descriptions of the iceberg regime. In early January, most of the icebergs are grounded to the North-East of Newfoundland when the presence of ice cover near shore prevents icebergs from drifting into coastal waters. Icebergs begin drifting southward and closer to shore in February. The drift pattern of the icebergs correlate well with depth average currents which have been calculated for the East Coast (Figure 2.3-1). By March, the density of icebergs starts to be much more diffused north of the Grand Banks as the ice sheet continues retreating. Icebergs are now drifting closer to Newfoundland and begin also drifting over the Grand Banks.

In April and May, icebergs drift further South and around the Flemish Cap. Higher iceberg densities are apparent where there are currents which concentrate the icebergs. The deterioration of icebergs may also contribute to an apparent increase of the density. There is still a steady influx of icebergs from the North, however, these icebergs drift closer to the Labrador and Newfoundland coasts, where they ground more frequently due to the absence of the ice cover. Densities decrease in June as the icebergs deteriorate and melt under the combined action of warmer air and water temperatures and wave action, and as the supply of new icebergs from the North dwindles.

Figure 5.4-18 shows the estimates of the annual mean iceberg densities as the average of the monthly densities. The higher densities are highly correlated with the predominant current and eddies in the region. A significant feature is the marked contrast between the high density of icebergs in the dominant current and the low density over the Grand Banks. The adaptive kernel is successful in preserving the distinct densities for these two regions, while eliminating the spurious high density estimates at the periphery of iceberg infested waters. Similarly, Figure 5.4-19 shows the density estimates for May.

Note that the extent of the adaptive kernel is always below 50 km for the estimation of iceberg densities over the Grand Banks and in the regions of high densities (Figure 5.4-20 and Appendix D). Note also that the apparent high densities around 48°N in the IIP historical record are eliminated.

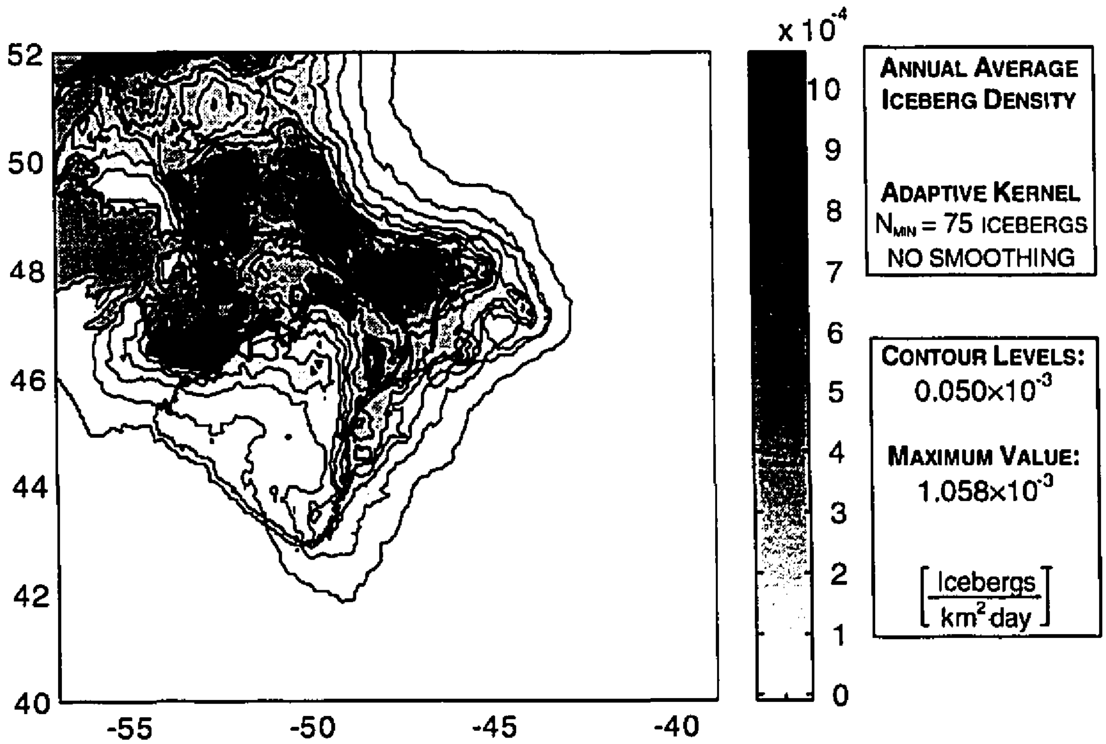

Figure 5.4-18 Annual average density estimate obtained using an adaptive kernel function.

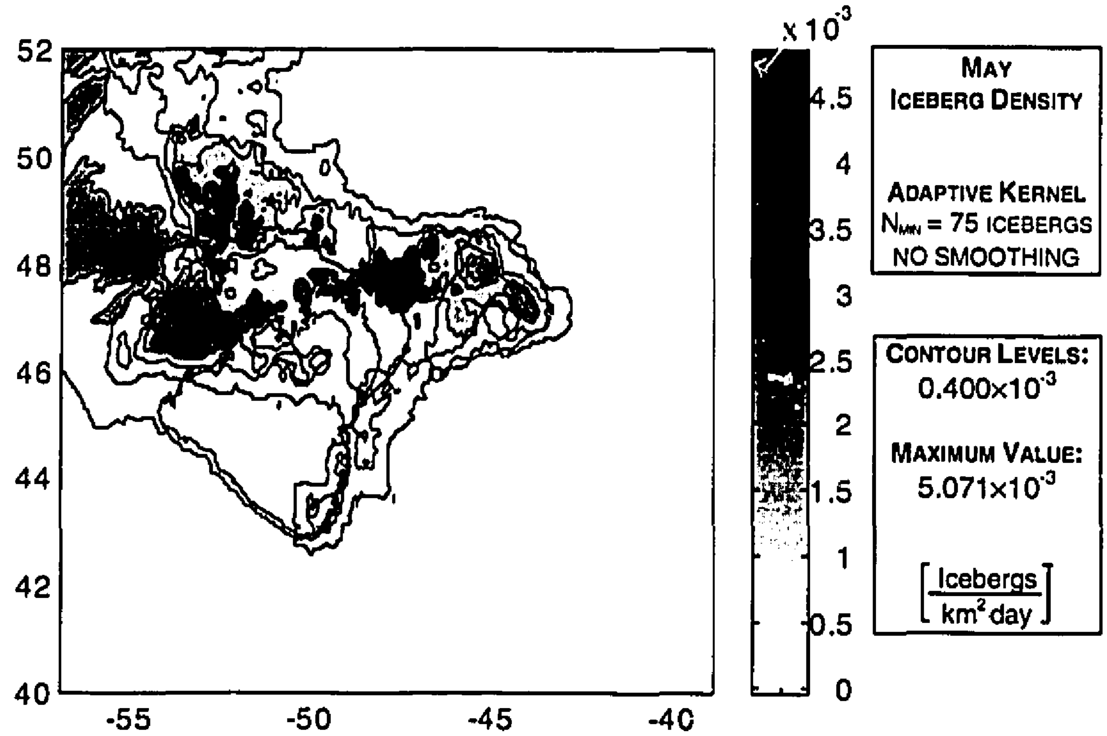

Figure 5.4-19 Iceberg density estimate for May, obtained using an adaptive kernel function.

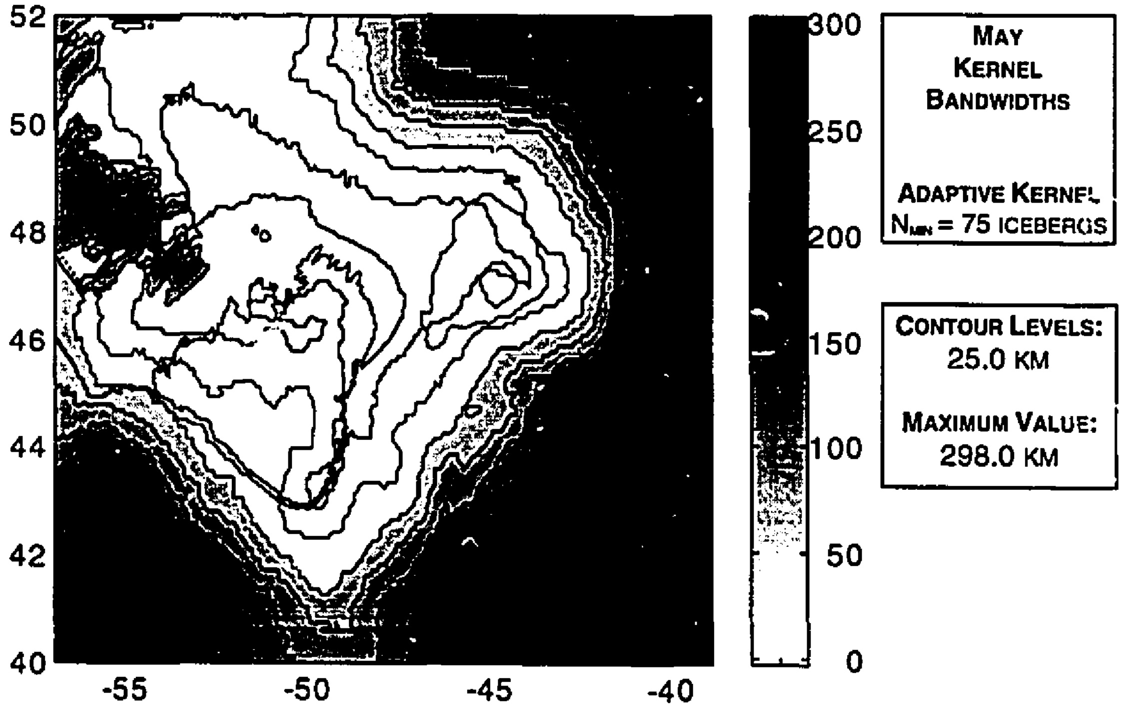

Figure 5.4-20 Adaptive kernel bandwidths for May iceberg density estimates.

The estimates of Figure 5.4-18 and 5.4-19 still contain a fair amount of irregularity associated with statistical uncertainty. A smoothing procedure was applied to these annual estimates in order to enhance their interpretability. A simple averaging procedure is defined as follows:

$$\hat{\lambda}(\underline{x},\delta)=\frac{\sum_{j=1}^{N_j}\lambda(\underline{y}_j)\cdot\sum_{j=1}^{N_j}\left\{\left|\underline{x}-\underline{y}_j\right|\leq\delta\right\}}{\sum_{j=1}^{N_j}I\left(\left|\underline{x}-\underline{y}_j\right|\leq\delta\right)-N_0} \qquad (5.4\text{-}13)$$

where δ is the smoothing parameter and N_0 is equal to the number of observations of zero density. Although the nature of the adaptive kernel prevents observations of zero density, these were made available to flag land.

Figures 5.4-21 to 5.4-23 show a sequence of estimates for increasing values of δ for the annual average density estimate. Similarly, Figures 5.4-24 and 5.4-25 are a series of density estimates for the month of May obtained using increasing values of δ. The averaging procedure removes the irregularities of the estimates without affecting the overall spatial trend in the variation of the densities. The contour lines are smoother without affecting their overall position. Only the largest local peaks are eliminated, but these represent a very small fraction of the total area.

Figure 5.4-27 shows ratios of the original to smoothed values of the annual average iceberg densities, while Figure 5.4-28 provides the same analysis using the density estimates of May. These indicate that the spatial trend is preserved, while eliminating isolated peaks in the estimates. Note also that after one smoothing procedure (δ = 1), the ratio of the original versus the smoothed value is less than 20% for both the annual average density estimates and the density estimates for May. This is within the range expected for the coefficient of variation of the estimates for the present sample size of $N_{num} \geq 75$ icebergs. The ratio of smoothed to unsmoothed values continues to decrease for increasing values of δ, however, these affect only a very small portion of the sample. Further, peak values generally occur near land, where the estimation of iceberg densities is not as important as over the Grand Banks.

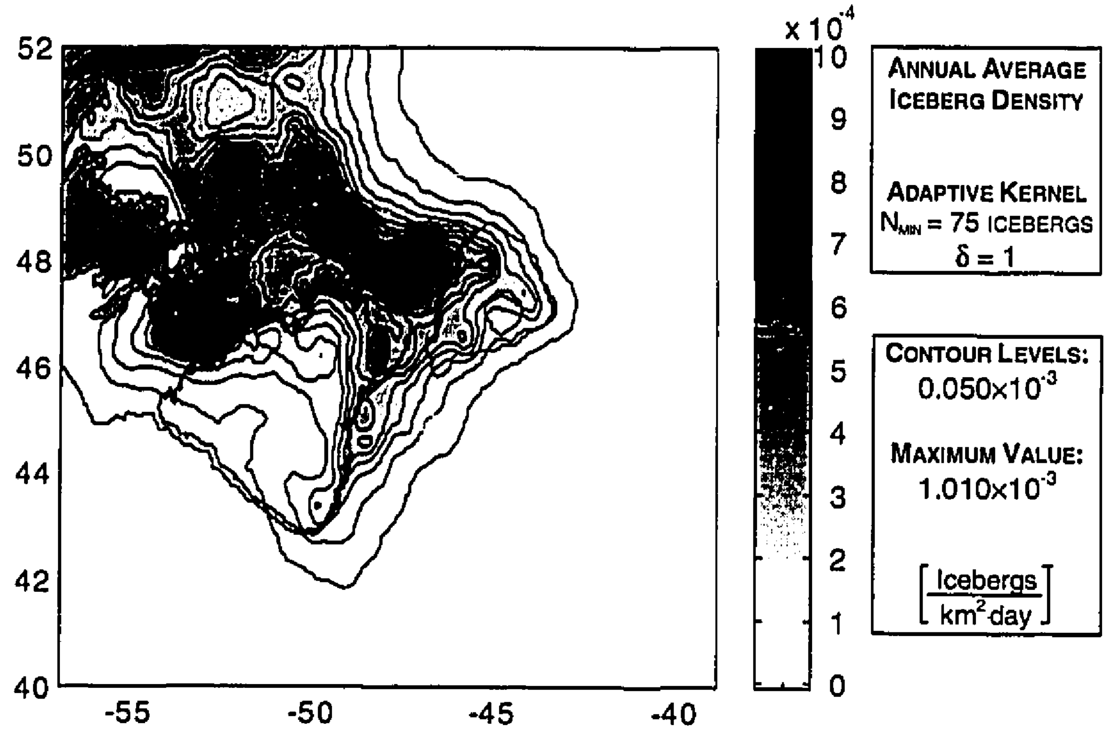

Figure 5.4-21 Annual average density estimate using an adaptive kernel function and a smoothing factor of 1.

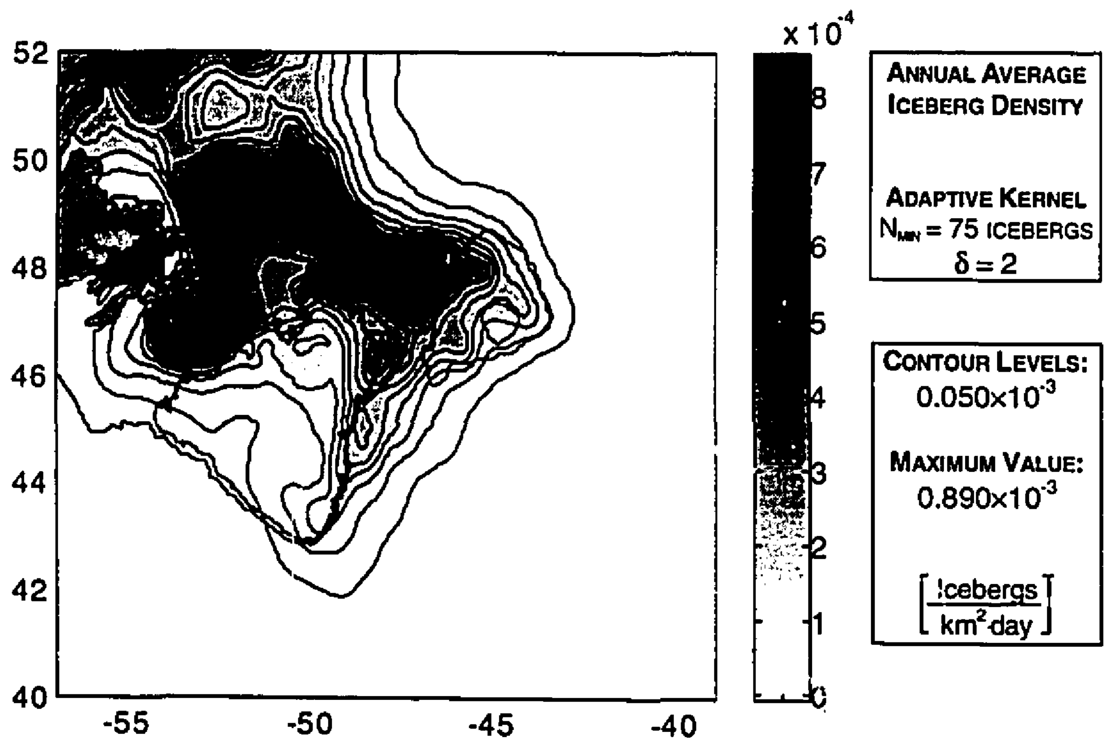

Figure 5.4-22 Annual average density, obtained using an adaptive kernel function and a smoothing factor of 2.

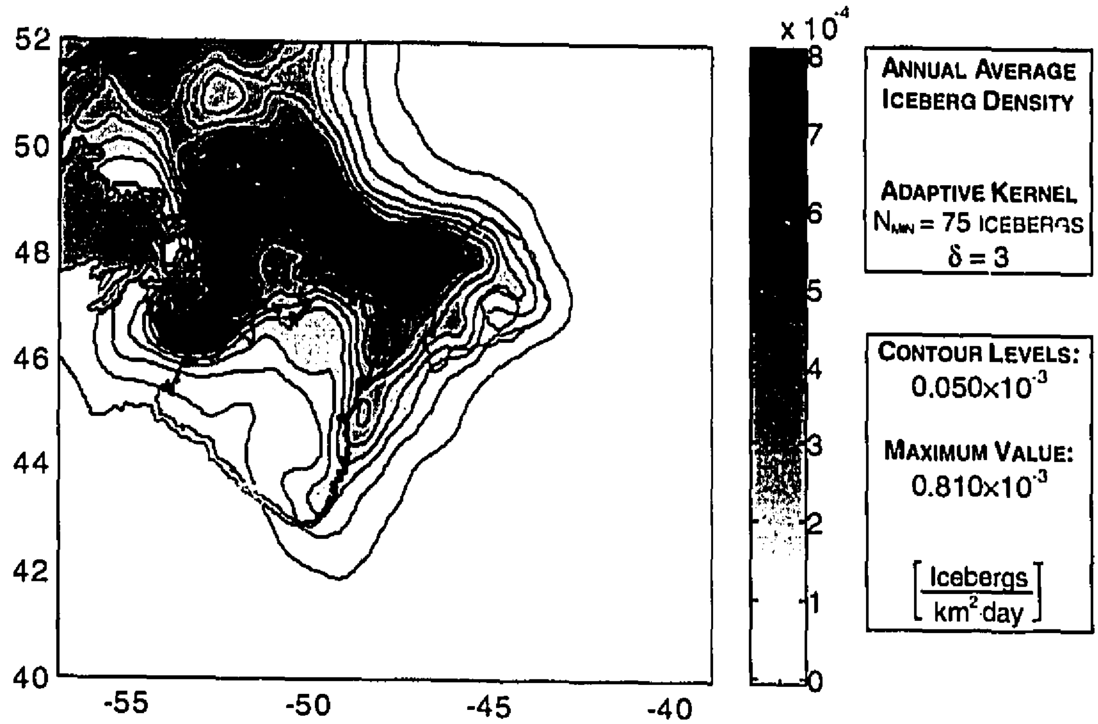

Figure 5.4-23 Annual average density, obtained using an adaptive kernel function and a smoothing factor of 3.

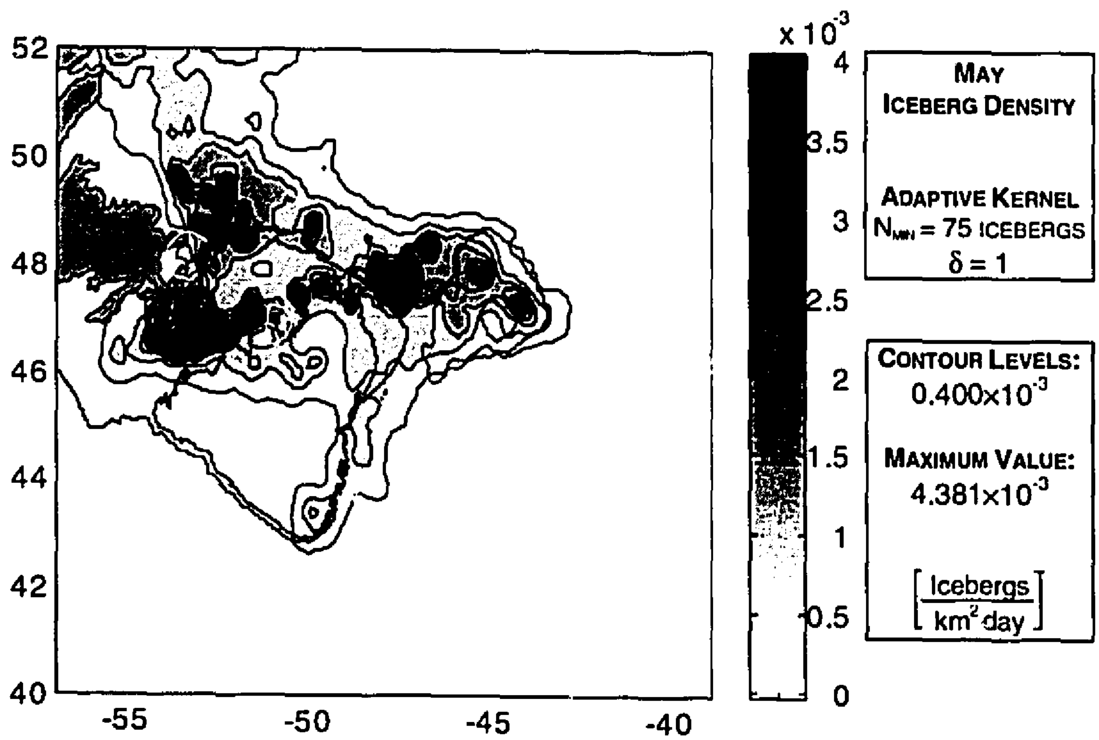

Figure 5.4-24 Iceberg density for May, obtained using an adaptive kernel function and a smoothing factor of 1.

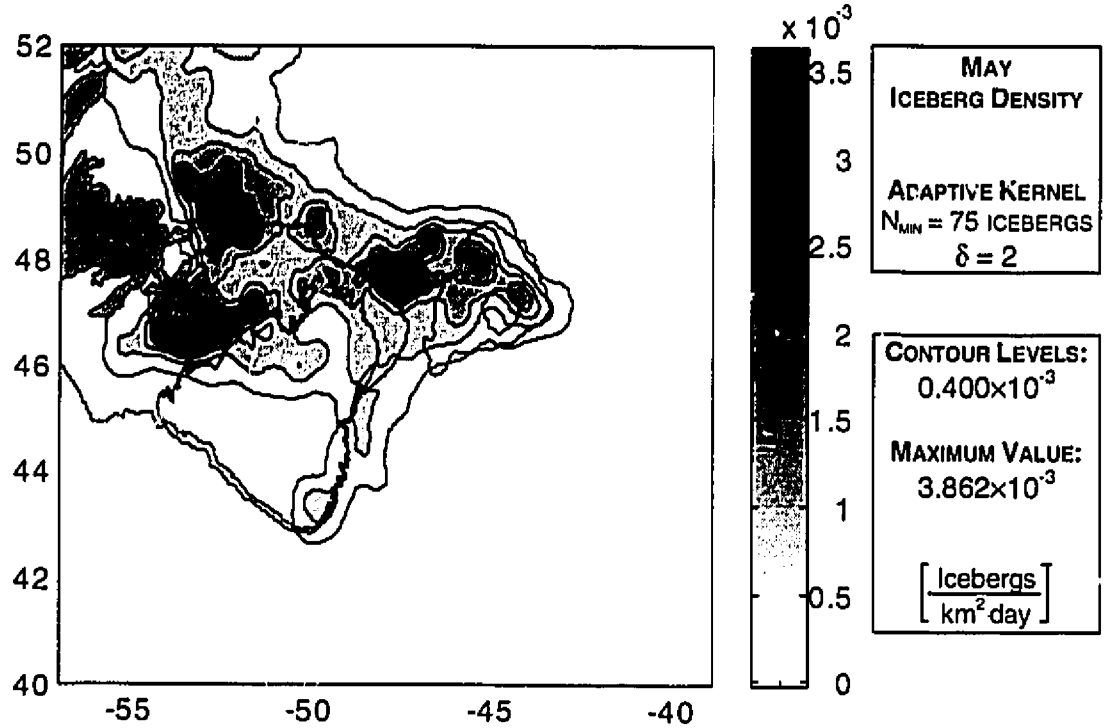

Figure 5.4-25 Iceberg density for May, obtained using an adaptive kernel function and a smoothing factor of 2.

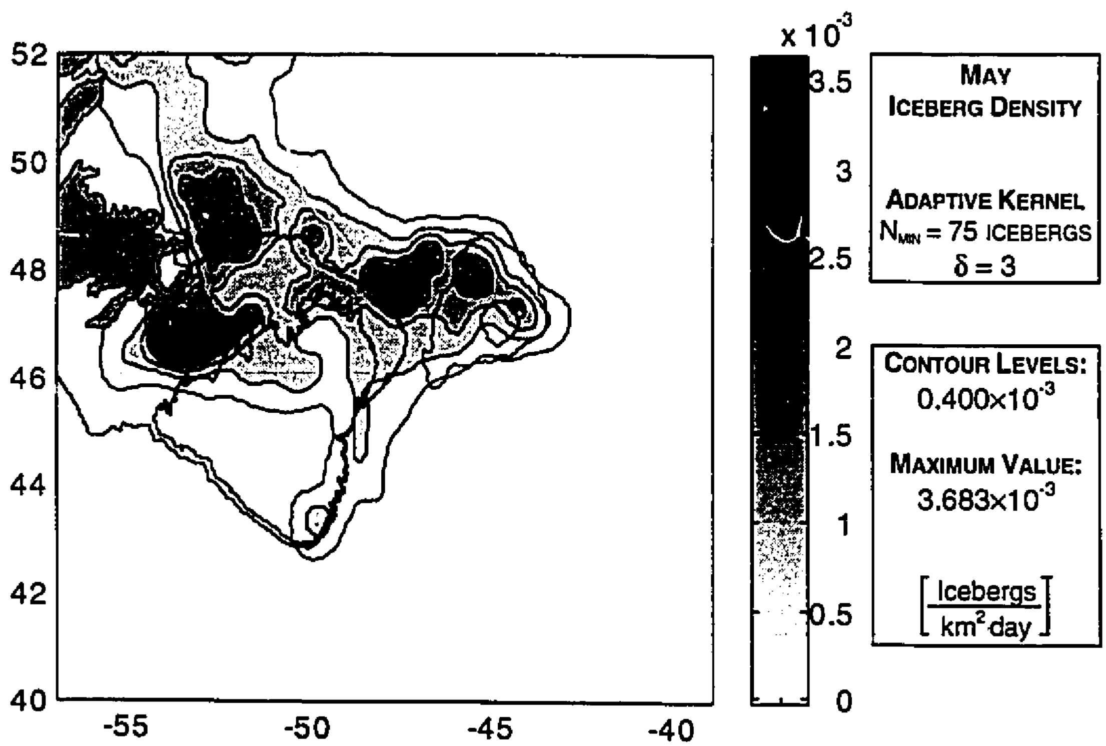

Figure 5.4-26 Iceberg density for May, obtained using an adaptive kernel function and a smoothing factor of 3.

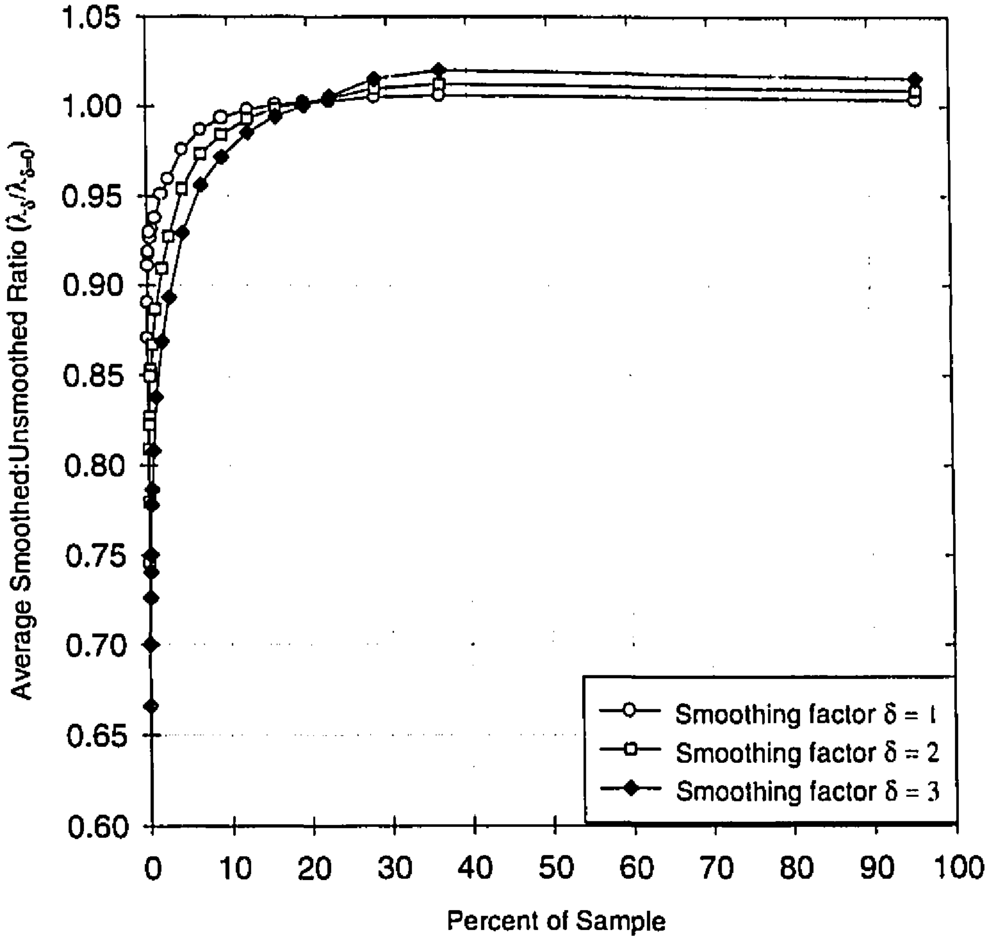

Figure 5.4-27 Ratios of smoothed to unsmoothed annual average iceberg density estimates.

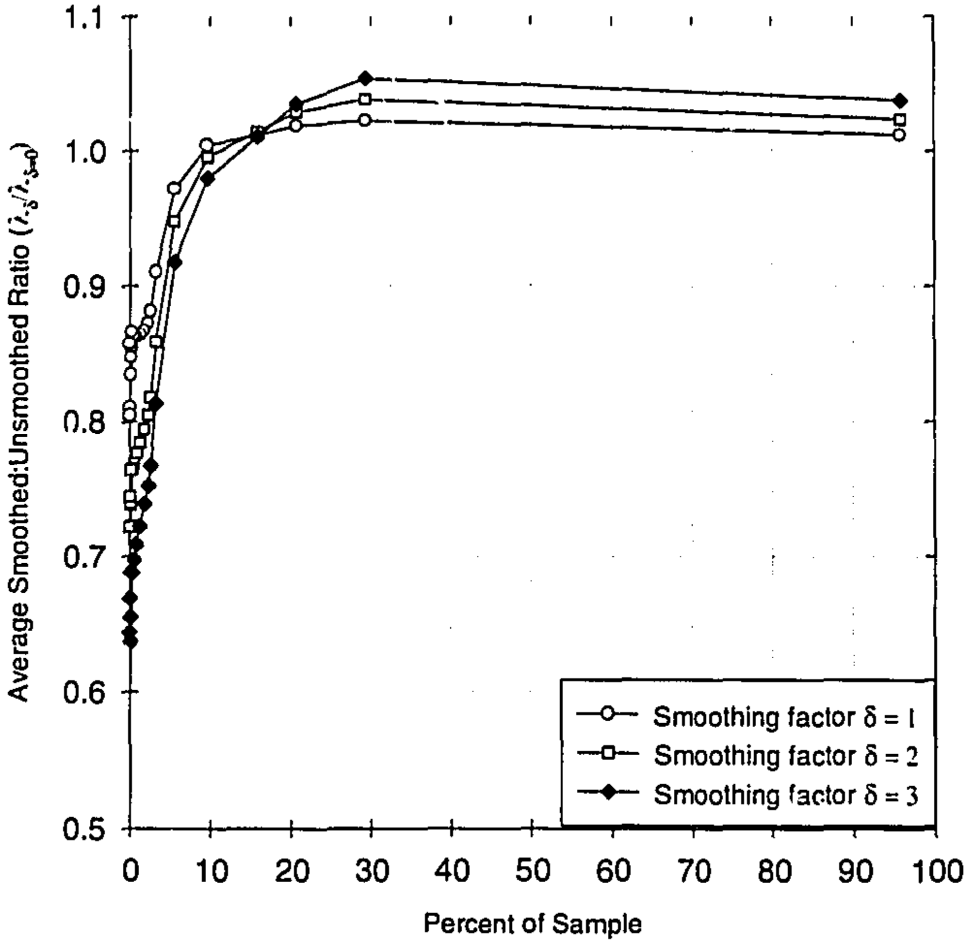

Figure 5.4-28 Ratios of smoothed to unsmoothed density estimates for May.

6. Summary and Conclusions

This thesis has examined several methods for estimating iceberg densities over the Grand Banks of Newfoundland. Three kernel density estimation procedures were used to analyze the IIP database: a uniform kernel, a Normal kernel and an adaptive kernel. The resulting estimates correspond well with given iceberg patterns, regional bathymetry and with local currents. Overall, the proposed methods of estimating iceberg densities have proved successful at obtaining credible results using available data. The proposed kernel procedures may easily be adapted to emphasize certain types of data more effectively, for example by growlers and bergy bits from the database.

The IIP database is the most extensive historical record of iceberg occurrences currently available. It contains over 30 years of data for the entire Grand Banks region. The broad spatial and temporal extent of the IIP database provides useful information for the long term density patterns of icebergs. However, the results of the kernel analysis suggest that more information is still required before reliable estimates can be produced. The IIP database, however, does not represent an ideal sample. IIP only surveys small portions of the region, and typically, with prior knowledge of iceberg locations. In contrast, icebergs reported by other sources, such as AES and ships, appear to be more uniformly distributed spatially. Also, these regions are generally at the periphery of the iceberg corridor. The method by which icebergs are reported in the database has evolved with changes in technology. It is difficult to presume that all sources report the size and location of icebergs with equal reliability and that iceberg reports made before the use of SLAR are as accurate as reports made using this technology. As such, the IIP database provides a combination of reporting sources of varying reliability. Ideally, reports by different sources would be analyzed independently and weighted according to the level of confidence of each. However, this is not feasible at present since the majority of the data in the IIP database would be excluded from the analysis, resulting in incomplete sub-sets. With the use of smaller, more accurate data sets, such as the Husky Oil data sets, estimates obtained from the IIP database could be calibrated to increase their accuracy.

The Husky Oil database comprises three data sets characterizing iceberg drift and size in the northern region of the Grand Banks. It contains detailed information concerning icebergs entering this region, including numerous measured iceberg dimensions. The data sets were compiled as icebergs were monitored during exploratory drilling operations. Icebergs drifting within the range of the drilling rigs were monitored frequently, providing useful information on iceberg drift patterns. The Husky Oil database, however, is too limited in time and space to derive relevant estimates of iceberg densities. However, this database, as with the IIP database, contains qualitative size descriptors of reported icebergs, which can prove to be useful in determining scouring rates. The Husky Oil qualitative size descriptors, coupled with a probability size distribution derived from the iceberg measurements in the Husky Oil database, can be used to calibrate the IIP size descriptors by examining reported icebergs in the same region. Once accurate iceberg size distributions are available, the IIP database can be re-analyzed, but only using sizable icebergs. This would produce iceberg density estimates of icebergs likely to cause scouring.

Iceberg density estimates were derived using the entire IIP database. As such, each report was treated as being equally reliable. Three types of kernel estimators were used to derive estimates from the IIP database. These were the constant kernel, the Normal kernel and the adaptive kernel. Each of these methods has particular benefits and limitations, although they were all subjected to the limitations of the database.

The uniform kernel involved assigning a fixed value to each iceberg observation. Two uniform kernels with different shapes were examined: the square kernel and the circular kernel. Both kernels produced similar results. Irregularities at the periphery of the iceberg region was observed in both, and the shape of the irregularities reflected the shape of the kernel employed. The uniform kernel involved the least amount of computational effort and was therefore very quick to run. However, the uniform kernel did not account for the local iceberg density. This method is prone to large uncertainties in regions with sparse data, such as at the periphery of the iceberg region. The estimates are improved by using a Normal distribution for the kernel function.

The Normal kernel assigns weights to observations which decrease monotonically with distance. It also minimizes the effect of isolated observations.. However, although values assigned to iceberg observations decreased with distance, the value assigned to each distinct report-day, which was used to normalize densities, remained a constant. As well, the Normal kernel encompasses an area three times larger than the constant kernel. These two factors produce results which under-estimate true densities. The Normal kernel, however, was very effective at retaining the morphology of the spatial distribution of the iceberg population and at minimizing spurious effects at the limits of the iceberg infested region.

Finally, an adaptive kernel which accounts for the regional iceberg density by varying the size of the kernel was investigated. Since smoothing increases with the size of the kernel, a kernel that increases in size in regions with sparse data is ideal. The adaptive kernel effectively eliminates spurious estimates and preserves important features in the spatial density of icebergs. Although the results obtained using the adaptive kernel were not as smooth as those obtained using the Normal kernel, the range of the estimates was more realistic. Smoothness was introduced into the estimates of the adaptive kernel through a simple averaging procedure. This procedure decreased the magnitude of isolated large densities, however, this affected very few data points, while the general shape and magnitude of the original estimated densities was retained. One disadvantage of the adaptive kernel procedure is that it can be computationally intensive.

6.1 Recommended Future Research

Density estimates relevant for scouring hazard analysis may also be obtained by repeating the above procedure with a limited form of the IIP database by excluding bergy bits and growlers. Such an analysis would result in the density estimates of icebergs with scouring potential and avoid issues with respect to the completeness of the data sets.

This thesis presents a method for estimating iceberg densities in the Grand Banks for the purpose of estimating scouring rates. Future work will require coupling these results with estimates of size distributions and drift patterns of icebergs.

The uncertainty and possible biases that could be associated with the proposed estimation procedure need to be further investigated through simulation but go beyond the scope of the present thesis. Preliminary results from simulations indicate that the bias is typically low (~5%) and can be controlled by increasing the size of the kernel function. Further investigations should include sensitivity analysis on the minimum number of observations in the definition of the adaptive kernel.

7. References

Anderson, I. (1993), "Appendix D -- International Ice Patrol's Iceberg Sighting Database 1960-1991", Bulletin #79, Report of the International Ice Patrol in the North Atlantic, Season of 1993, CG-188-48, U.S. Coast Guards.

Banke, E. (1989), "Recent Iceberg Groundings and Scours on the Grand Banks of Newfoundland", Atlantic Geosciences Centre, Bedford Institute of Oceanography, Dartmouth, Nova Scotia.

Barber, G.M. (1988), "Elementary Statistics for Geographers", Guilford Press, New York.

Been K., Palmer, A. and Comfort, G. (1990), "Analysis of Subscour Stresses and Probability of Ice Scour - Induced Damage for Buried Submarine Pipelines: Volume II. Deterministic Model of Ice-Soil-Pipe Interaction", contract report submitted by Fleet Technology Ltd. and Canadian Seabed Research Ltd. to the Canada Oil and Gas Lands Administration.

Blenkarn, K.A., and Knapp A.E. (1969), "Ice Conditions on the Grand Banks", CIM Special **vol.10**, Ice Seminar, pp.61-72.

Boots, B. and Getis, A. (1978), "Models of Spatial Processes", Cambridge University Press, London.

Boots, B. and Getis, A. (1988), "Point Pattern Analysis", SAGE Publications, Newbury Park, California.

Clark, J., Landva, J., Collins, W.T. and Barrie, J.V. (1986), "The Geotechnical Aspect of Seabed Pits in the Grand Banks Area", Third Annual Conference on Marine Geotechnical Engineering at Memorial University, June 11-13.

Clark, J., El-Tahan, M. and Khan, R. (1990), "Icebergs - Where They Are and Where They Are Going?", C-Core, Memorial University of Newfoundland, St John's, Nfld, *presented at* Bringint It to Market, XVI FairmontWorkshop, April 29 - May 2, 1990.

Comfort, G. and Been K. (1990), "Analysis of Subscour Stresses and Probability of Ice Scour - Induced Damage for Buried Submarine Pipelines: Summary Report", contract report submitted by Fleet Technology Ltd. and Canadian Seabed Research Ltd. to the Canada Oil and Gas Lands Administration.

Cressie, N. (1993), "Statistics for Spatial Data", Revised Edition, John Wiley & Sons, Inc, New York.

Crocker, G. (1994), "Estimating Iceberg Populations on the Grand Banks", Centre for Cold Ocean Resources Engineering (C-Core) Memorial University of Newfoundland, St John's, Newfoundland.

Crocker, G., Fuglem M. and Olsen, C. (1995), "Environment and Routes", *Canadian Offshore Design for Ice Environments*, First Annual Report, **Volume I**, Ocean Engineering Research Centre, Memorial University of Newfoundland, St. John's, NF.

Dinsmore, R.P. (1972) "Ice and It's Drift into the North Atlantic Ocean", International Commission for the Northwest Atlantic Fisheries, Special Publication no.8, pp.89-127.

Evans-Hamilton (1975), "Probability Study of Iceberg Collision During Restrictive Towing Conditions on the Northern Grand Banks, Phase I and Phase II", Report submitted to Mobil Oil Canada Ltd.

Garrett, C., Middleton, J.F., Majaess, F. and Hazen, M. (1985), "Analysis and Prediction of Iceberg Trajectories", Department of Oceanography, Dalhousie University, Halifax, Nova Scotia.

Gaskill H., Nicks, L. and Ross, D. (1985), "A Non-Deterministic Model of Populations of Iceberg Scour Depths", *Cold Regions Science and Technology*, **11** (1985), pp.107-122, Elsevier Science Publishers B.V., Amsterdam.

Härdle, Wolfgand (1990), "Applied Nonparametric Regression", Cambridge University Press, New York.

Harris, I.McK. (1974), "Iceberg Marks on the Labrador Shelf" in *Offshore Geology of Eastern Canada*, ed. B.R. Pelletier, Geological Survey of Canada, Paper 74-30, pp.97-101.

Harris, I.McK. and Jollymore, P.G. (1974), "Iceberg Furrow Marks on the Continental Shelf Northeast of Belle Isle, Newfoundland", *Canadian Journal of Earth Sciences*, **v. 11**, pp.43-52.

Lewis, C.F.M, Parrott, D.R., d'Apollonia, S.J., Gaskill, H.S. and Barrie, J.V. (1988), "Methods of Estimating Iceberg Scouring Rates on the Grand Banks of Newfoundland", *Port and Ocean Engineering Under Arctic Conditions*, **Volume III**, Geophysical Institute, University of Alaska, Fairbanks, Alaska.

Lewis, C.F.M. and Keen, M.J. (1990), "Constraints to Development", *Chapter 14 in Geology of the Continental Margin of Eastern Canada*, M.J. Keen and G.L. Williams (ed.), Geological Survey of Canada.

Marko, J.R. (1982) "The Environment Of Eastern Lancaster Sound and Northern Baffin Bay", Indian and Northern Affairs Canada Environmental Studies No.26.

Marko, J.R., Fissel, D.B., and Birch, J.R. (1986), "Physical Approaches to Iceberg Severity Prediction", Environment Sciences Research Program Project Report 038.

Marko, J.R., Fissel, D.B., and Miller, J.D. (1987), "Iceberg Movement Prediction Off the Canadian East Coast", *Natural and Man-Made Hazards*, M.J. El-Sabh and T.S Murty, (ed.), D. Reidel Publishing, 419-446.

Marko, J.R., Fissel, D.B., Wadhams, P., Kelly, P.M. and Brown, R.D. (1994), "Iceberg Severity off Eastern North America: Its Relationship to Sea Ice Variability and Climate Change", *American Meteorological Society*, September 1994.

Miles, R.E. (1964), "Random Polygons Determined by Random Lines in a Plane", *Proc. Natl. Academic Science.*, **Vol. 52**, pp.901-907 and 1157-1160.

NORDCO (1980), "Iceberg / Sea Ice Climatology Study - Grand Banks of Newfoundland", *Submitted to Mobil Oil Limited by NORDCO Limited*, File Ref 141-79, March 9 1980.

Pelletier, B.R. and Shearer, J.M. (1972), "Sea Bottom Scouring in the Beaufort Sea of the Arctic Ocean", Section 8, 24th International Geological Congress, Montreal, pp.251-261.

Pereira, C.P.G., Woodworth-Lynas, C.M.T., Barrie, J.V. (1988), "Iceberg Scour Investigations and Sedimentology of the Southeast Baffin Island Continental Shelf", ARTIC, **Vol. 41**, No. 43, September, pp.221-230.

Ripley, B.D.(1981), "Spatial Statistics", John Wiley & Sons, Inc, New York.

Scott, D.W. (1992), "Multivariate Density Estimation", John Wiley & Sons, Inc, New York.

Serra, J. (1982), "Image Analysis and Mathematical Morphology", Academic Press, London.

Silverman, B.W. (1986), "Density Estimation for Statistics and Data Analysis", Chapman and Hall, London.

Simms, A.E. (1993), "GIS, EDA and Inductive Modelling: A Methodology for the Regional Analysis of the 'East Coast Scour Database", Department of Geography, University of Calgary, Calgary, Alberta.

Upton, G. and Fingleton, B. (1985), "Spatial Data Analysis by Example, Volume 1", John Wiley & Sons, Inc, New York.

Veneziano, D (1980), "Random Processes", Department of Civil Engineering, Massachusetts Institute of Technology, Cambridge, MA.

Wadhams, P. (1983), "The Prediction of Extreme Keel Depths from Sea Ice Profiles", *Cold Regions Science and Technology*, **6** (1983), 257 - 266.

Appendix A

The following table was constructed using the IIP database. It is a summary of the number of distinct icebergs reported, the number of resights of previously reported icebergs, the average velocity of resighted icebergs and the number of reported groundings for each year of the IIP database. The average velocity of resighted icebergs is rather high in the early years of the IIP database, where few resights are reported. However, in more recent years, the average velocity of resighted icebergs approaches an average of 15 km/day to 20 km/day, which is within the correct range of drifting icebergs.

Year	Number of Reported Icebergs	Number of Icebergs Reported as Resights	Average Velocity of Resights (km/day)	Number of Groundings
1960	2870	0	0.000	0
1961	2858	0	0.000	1
1962	3418	2	12.41	1
1963	774	0	0.000	0
1964	5279	0	0.000	0
1965	1431	3	154.11	0
1966	1283	0	0.000	0
1967	4140	6	17.88	0
1968	3608	8	160.97	0
1969	2257	2	0.000	0
1970	2021	3	21.68	0
1971	1099	0	0.000	0
1972	7676	19	10.97	5
1973	4727	14	72.42	1
1974	6164	49	34.30	2
1975	848	40	17.12	1
1976	1451	55	16.03	1
1977	1044	32	33.01	3
1978	1733	25	23.80	7
1979	548	108	11.84	4
1980	197	65	14.84	1
1981	180	25	22.04	0
1982	817	170	15.63	5
1983	1977	630	22.79	24
1984	2745	1214	25.99	8
1985	2175	2151	25.57	79
1986	513	272	23.174	1
1987	954	945	24.14	10
1988	1102	1072	17.98	12
1989	1157	1819	21.99	10
1990	1129	1563	20.36	9
1991	1599	1354	20.56	17
1992	1722	840	22.94	1
1993	4322	3628	16.75	2
Total	76118	16114	21.57	205

Table A-1 Velocities of resighted icebergs in the IIP database.

Appendix B: Annual Average and Monthly Iceberg Density Estimates

The following figures show the annual average iceberg densities (Figures B-1 and B-2) and the monthly iceberg densities (Figures B-3 to B22) over the Grand Banks obtained with the adaptive kernel. Monthly iceberg density estimates are plotted using constant contour levels of 0.4×10^{-3} icebergs/km^2/day. This illustrates the relative significance of each monthly estimate to the annual average estimate.

The following figures provide the original density estimates and the corresponding density estimate, which was smoothed using Eq. 5.4-12 and a given smoothing parameter δ. Note that although the maximum values of the smoothed estimates are less than those for the corresponding unsmoothed estimates, the contours of the smoothed estimates retain the shape and magnitude of the unsmoothed estimates. The maximum values of the density estimates represent a very small fraction of the region, generally close to shore.

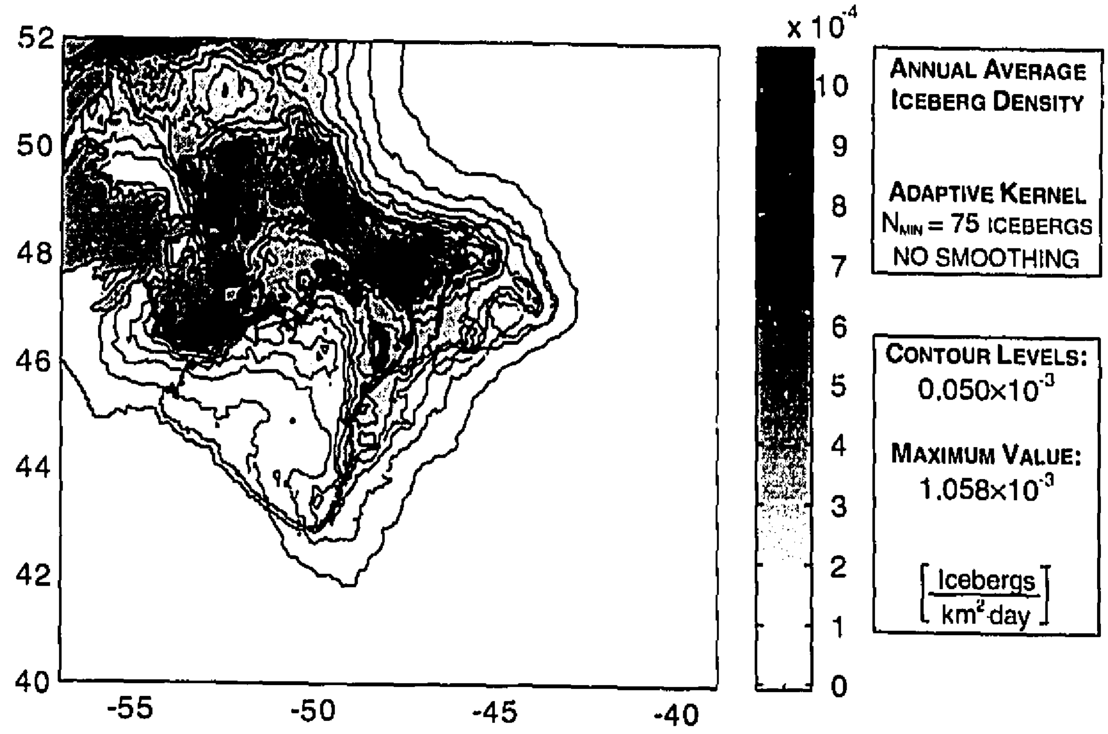

Figure B-1 Annual average iceberg densities (δ=0). Maximum density of 1.058×10^{-3} icebergs/km^2/day.

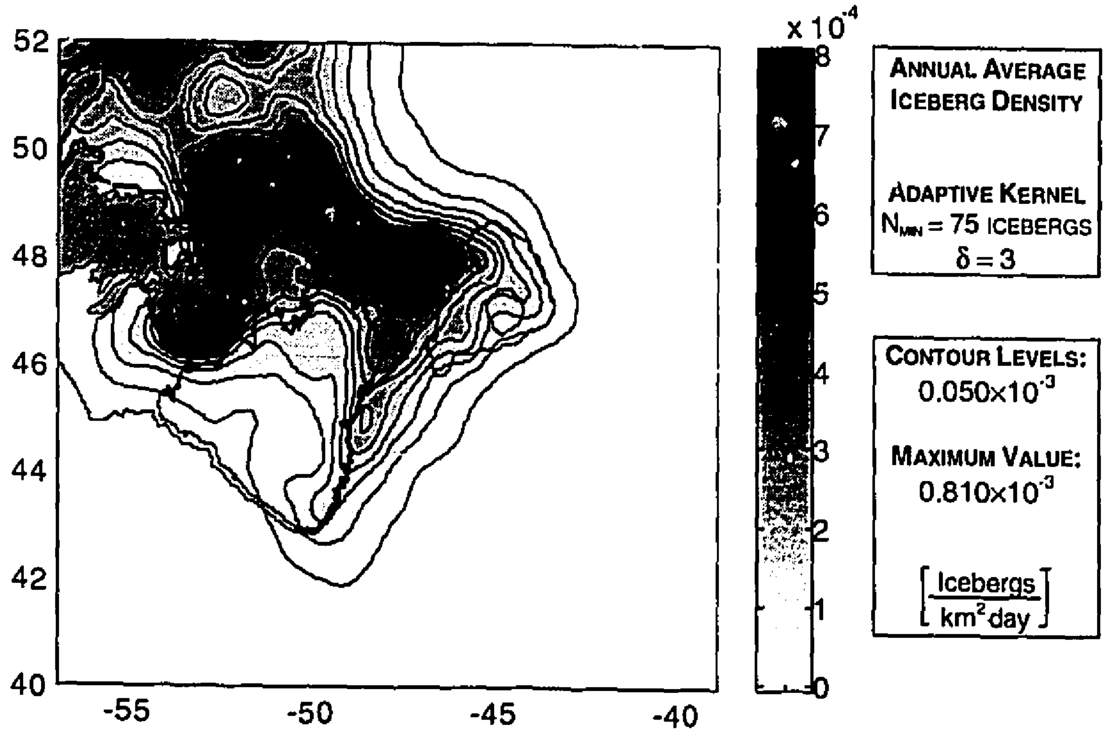

Figure B-2 Annual average iceberg densities (δ=3). Maximum density of 0.810×10^{-3} icebergs/km^2/day..

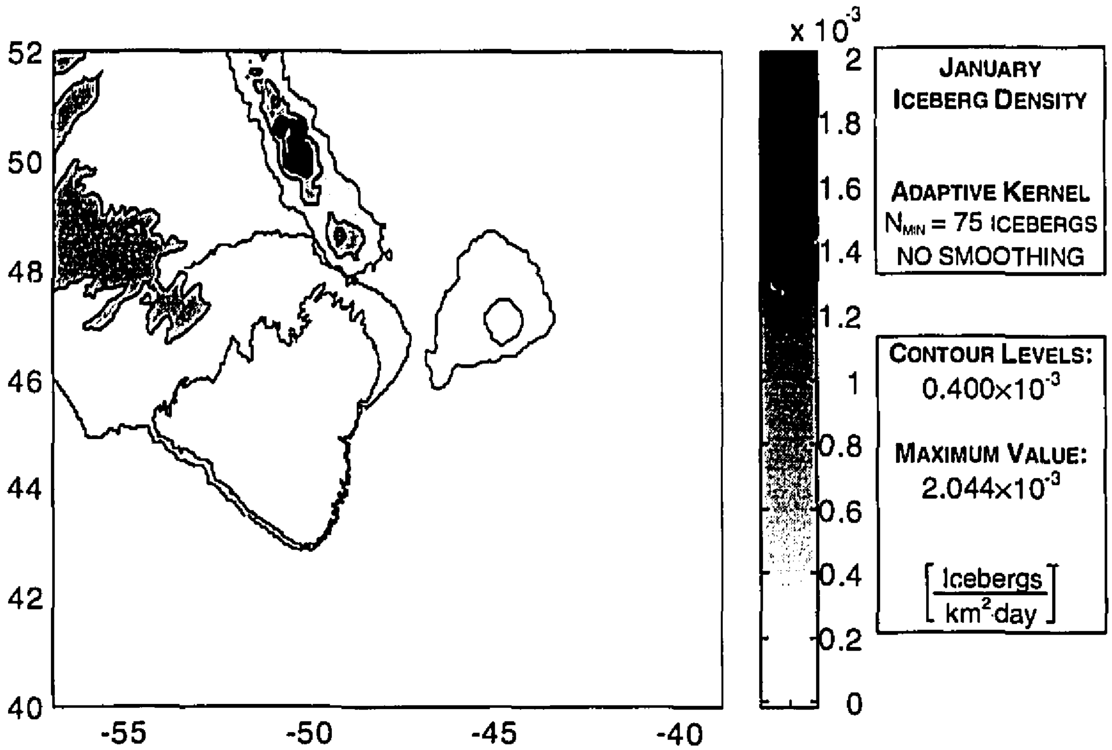

Figure B-3 Iceberg densities for January (δ=0). Maximum density of 2.044×10^{-3} icebergs/km^2/day.

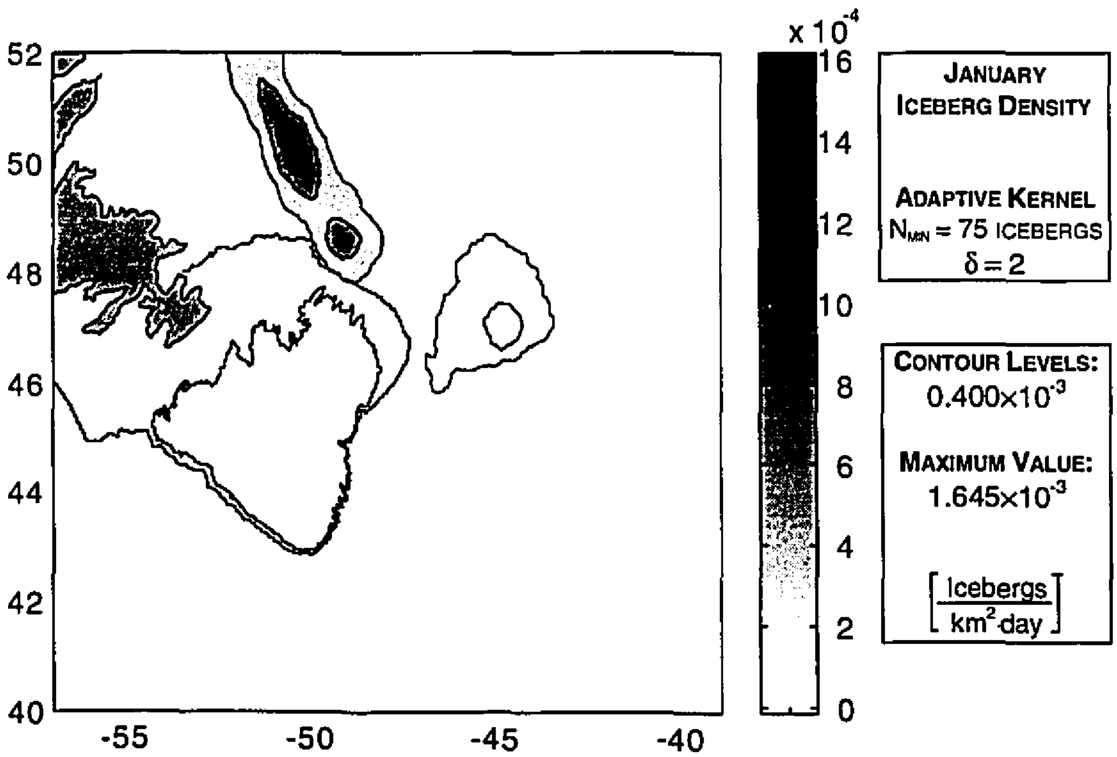

Figure B-4 Iceberg densities for January (δ=2). Maximum density of 1.645×10^{-3} icebergs/km^2/day.

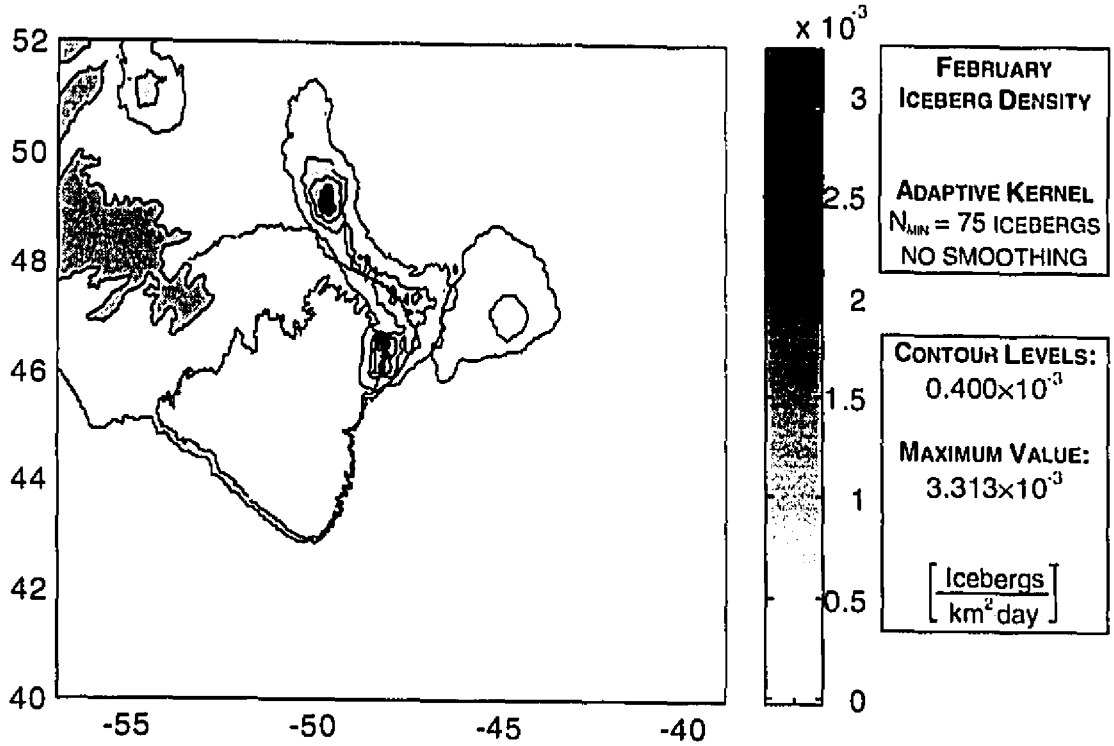

Figure B-5 Iceberg densities for February (δ=0). Maximum density of 3.313×10^{-3} icebergs/km^2/day.

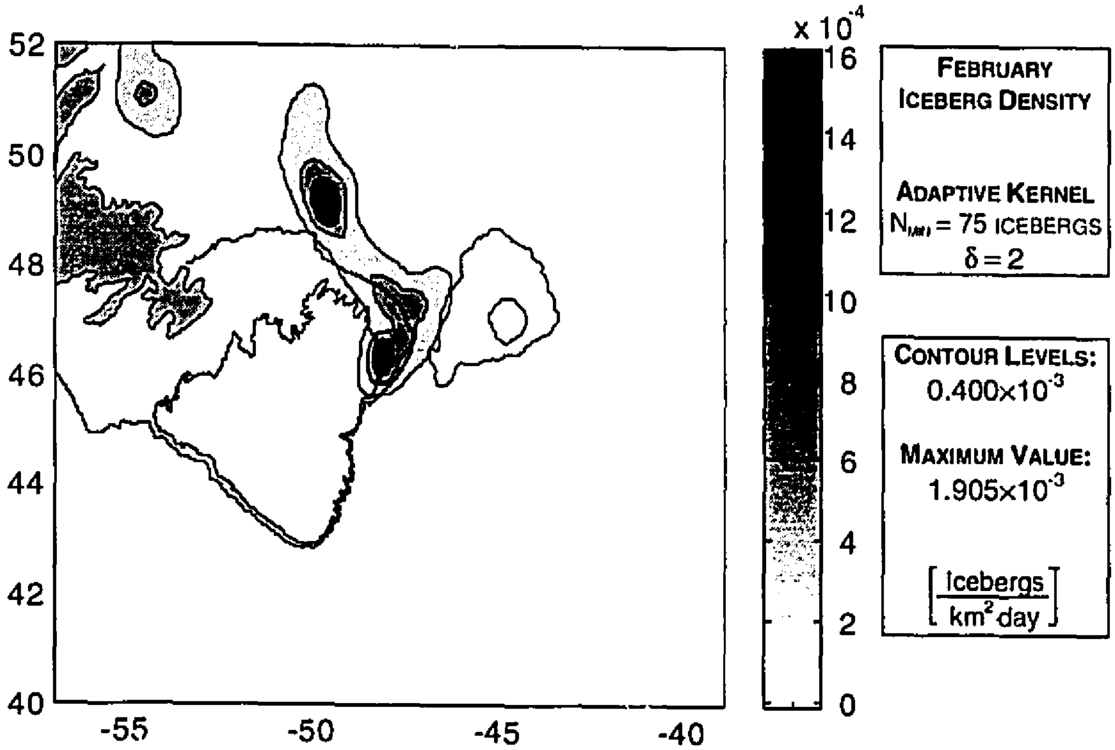

Figure B-6 Iceberg densities for February (δ=2). Maximum density of 1.905×10^{-3} icebergs/km^2/day.

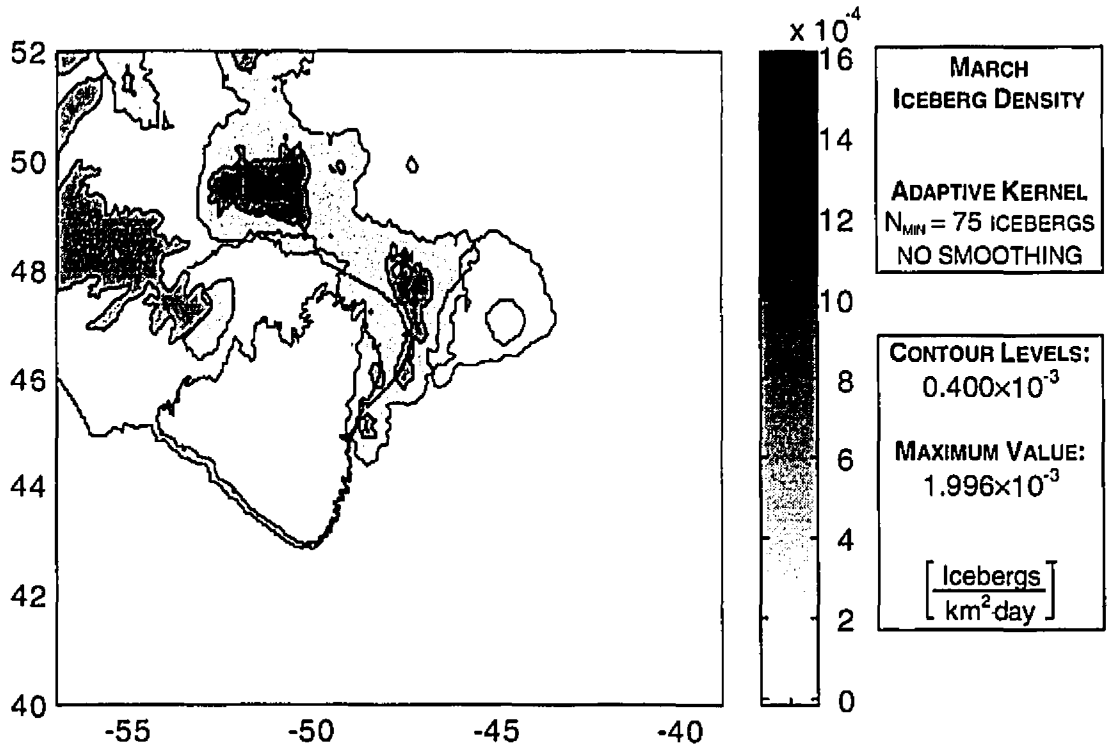

Figure B-7 Iceberg densities for March (δ=0). Maximum density of 1.996×10^{-3} icebergs/km^2/day.

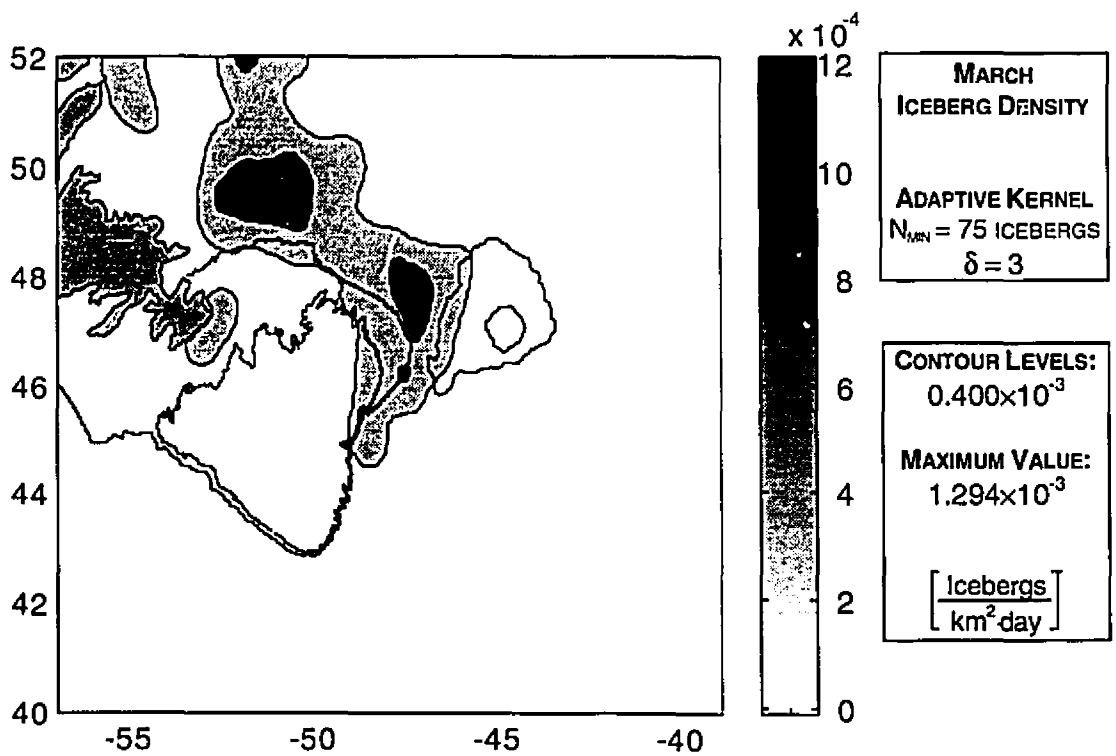

Figure B-8 Iceberg densities for March (δ=3). Maximum density of 1.294×10^{-3} icebergs/km^2/day.

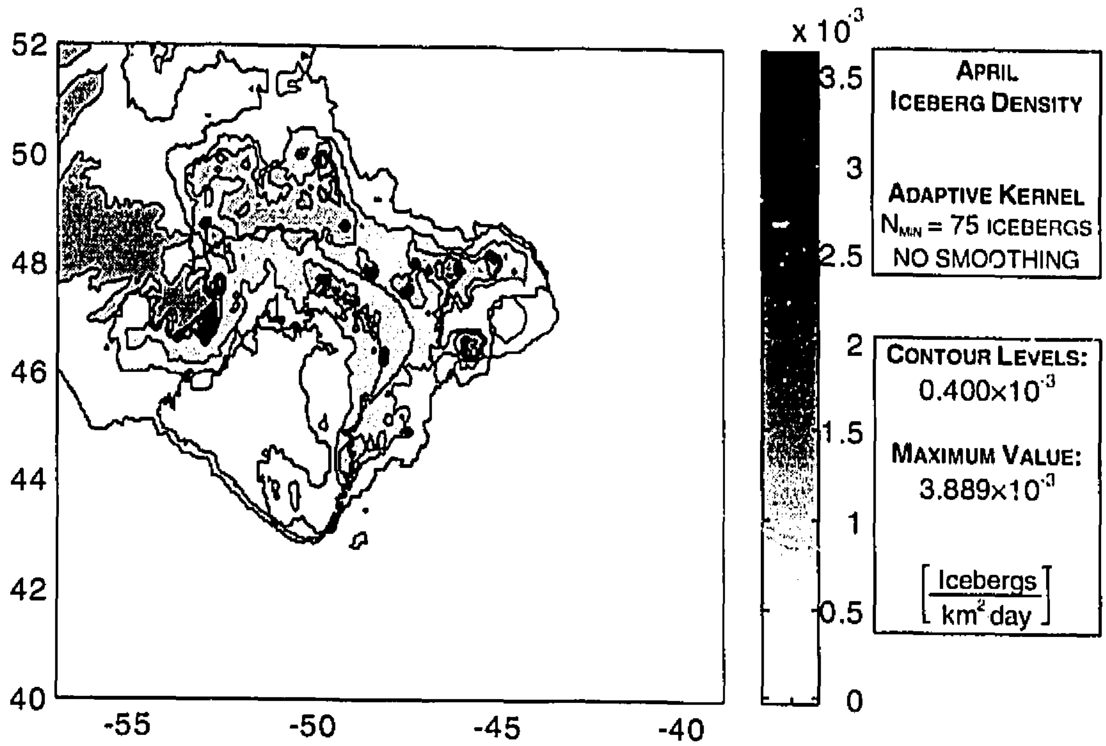

Figure B-9 Iceberg densities for April (δ=0). Maximum density of 3.889×10^{-3} icebergs/km^2/day.

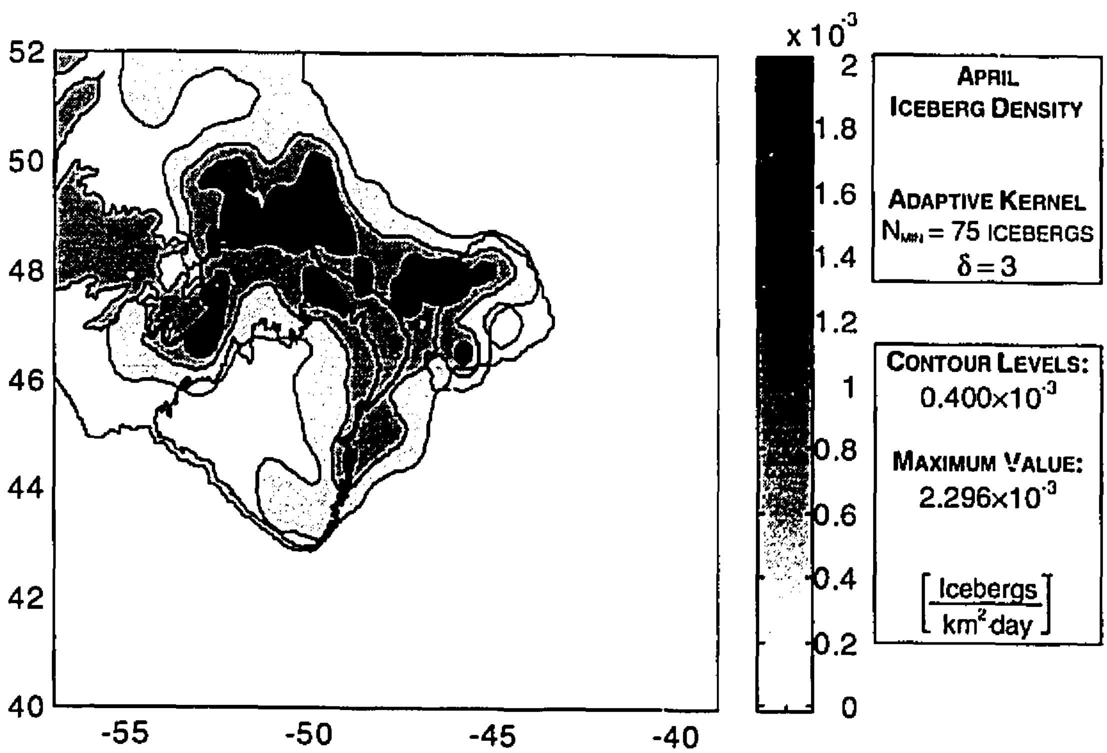

Figure B-10 Iceberg densities for April (δ=3). Maximum density of 2.296×10^{-3} icebergs/km^2/day.

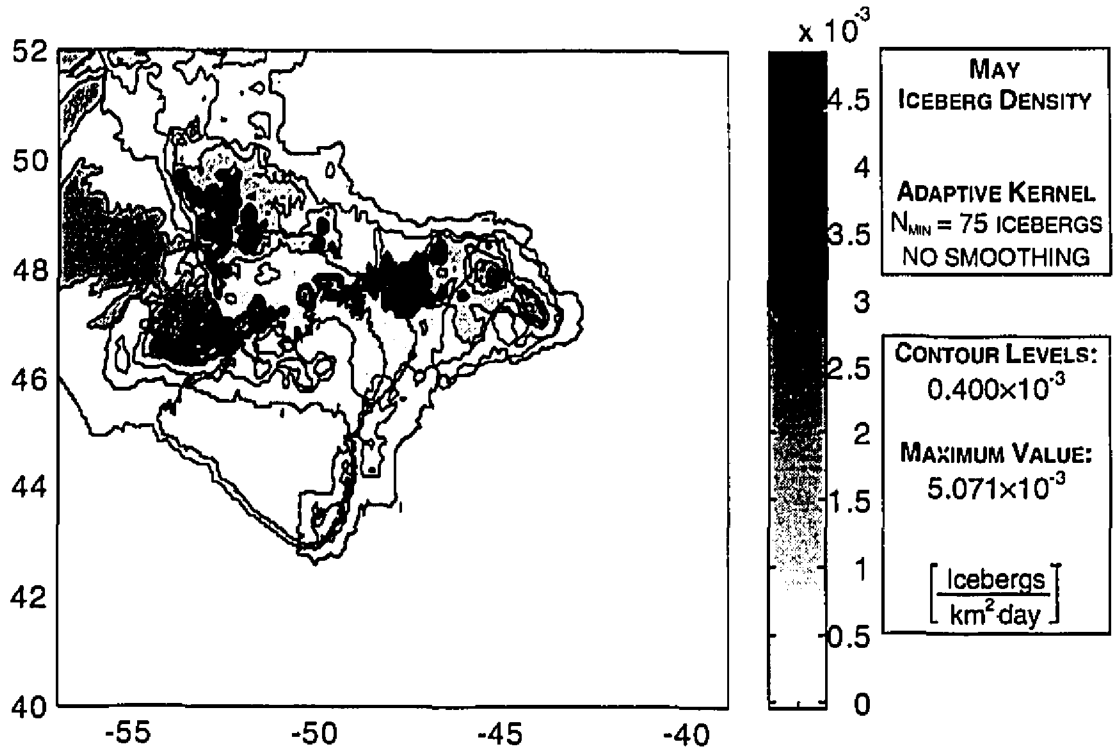

Figure B-11 Iceberg densities for May (δ=0). Maximum density of 5.071×10^{-3} icebergs/km^2/day.

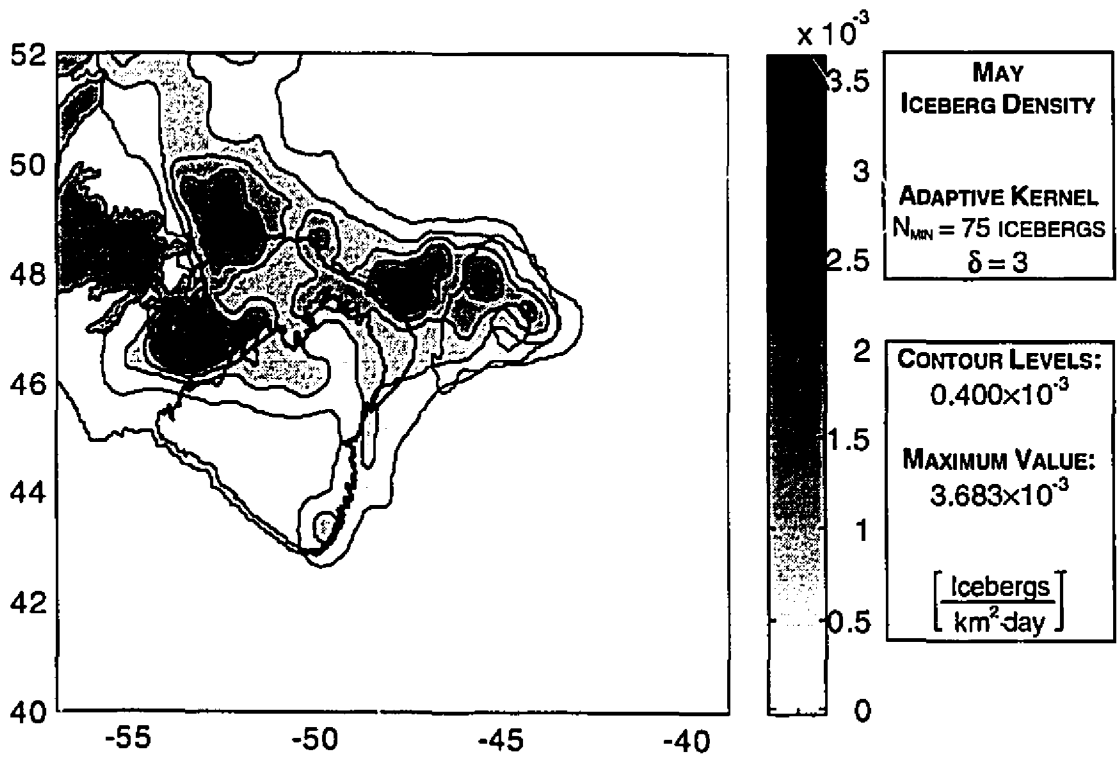

Figure B-12 Iceberg densities for May (δ=3). Maximum density of 3.683×10^{-3} icebergs/km^2/day.

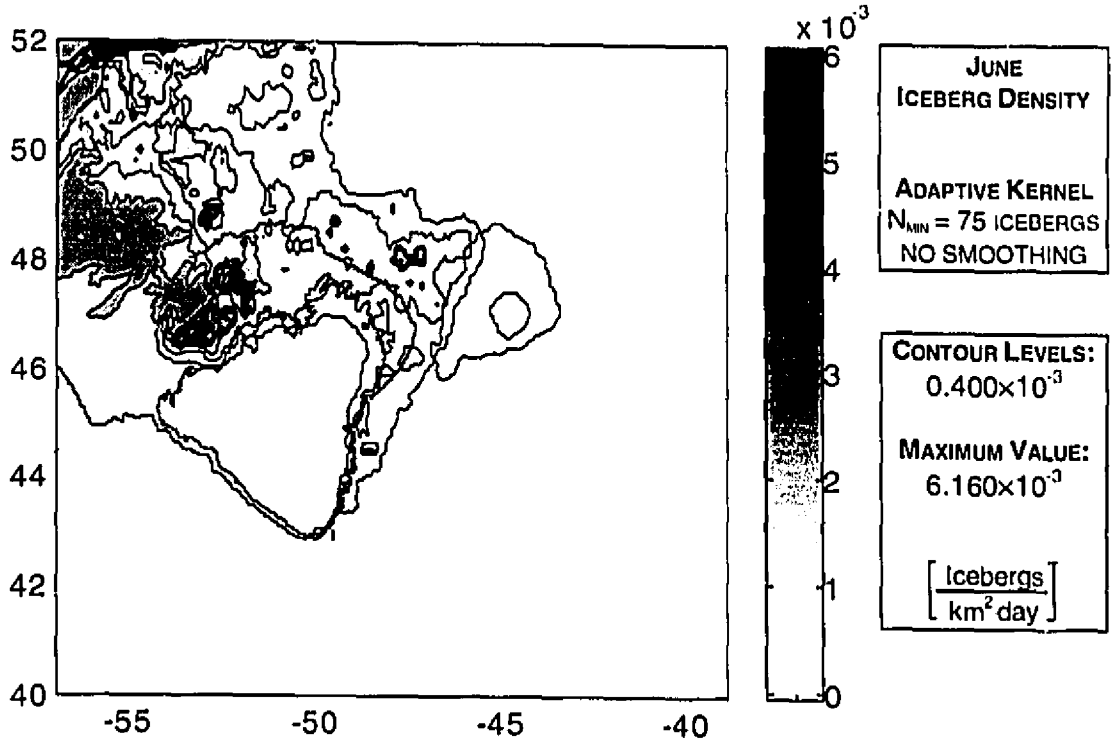

Figure B-13 Iceberg densities for June (δ=0). Maximum density of 6.160×10^{-3} icebergs/km^2/day.

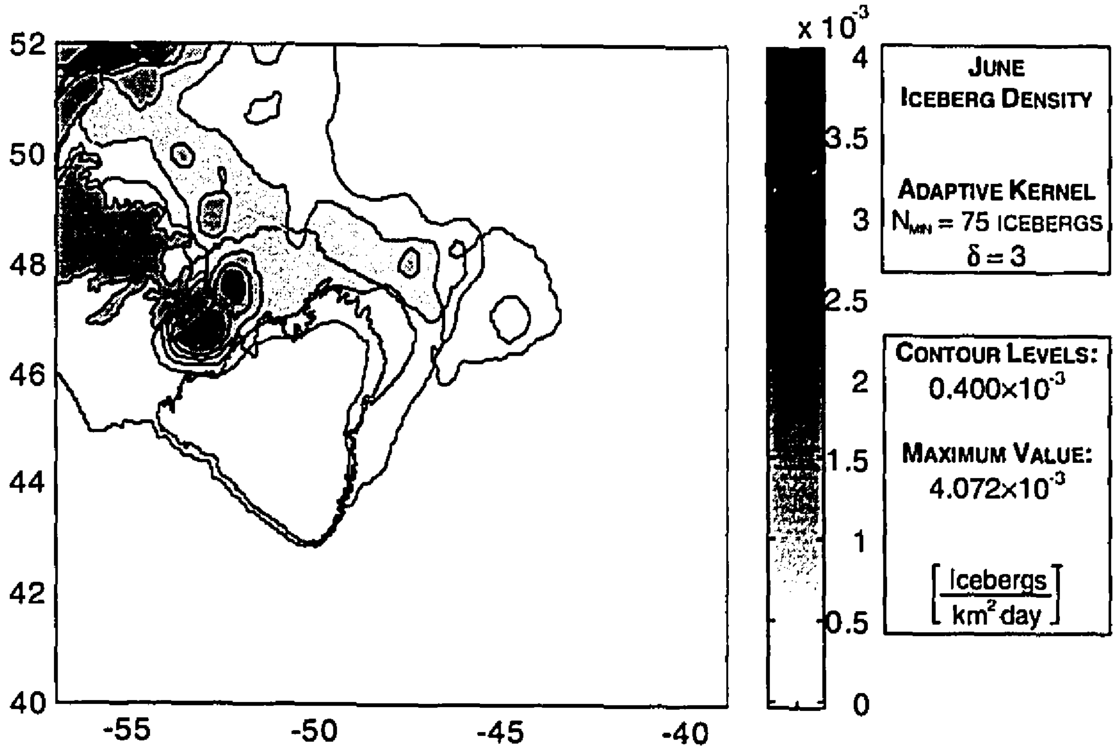

Figure B-14 Iceberg densities for June (δ=3). Maximum density of 4.072×10^{-3} icebergs/km^2/day.

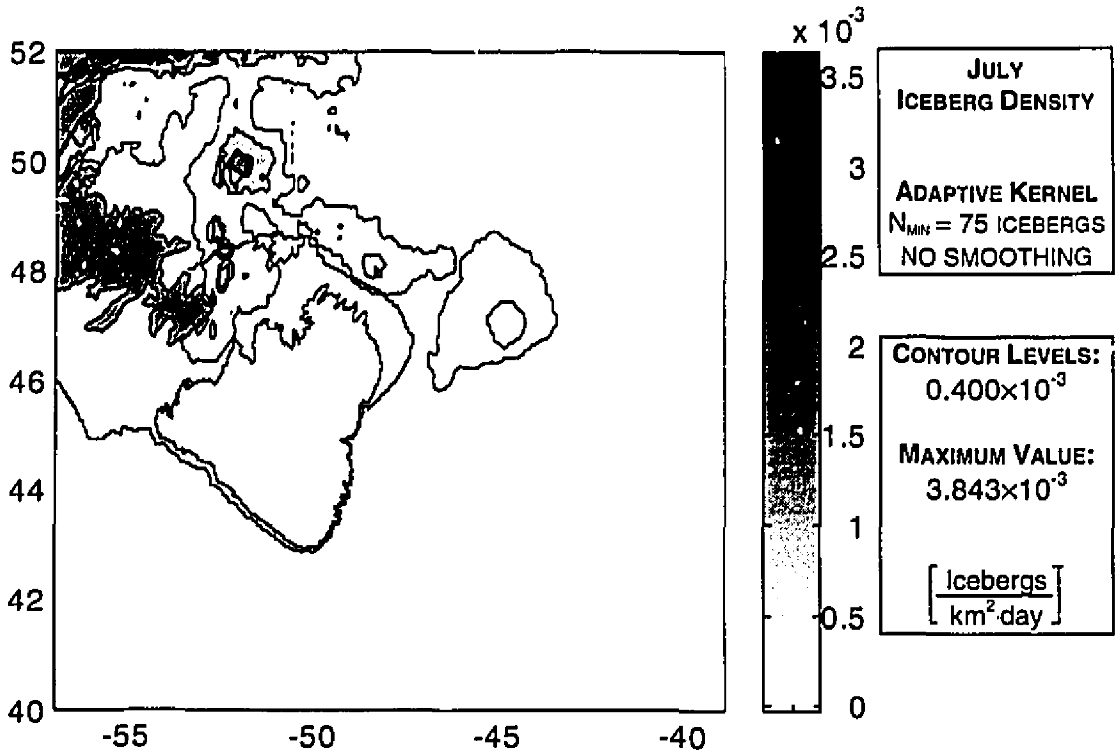

Figure B-15 Iceberg densities for July ($\delta=0$). Maximum density of 3.843×10^{-3} icebergs/km^2/day.

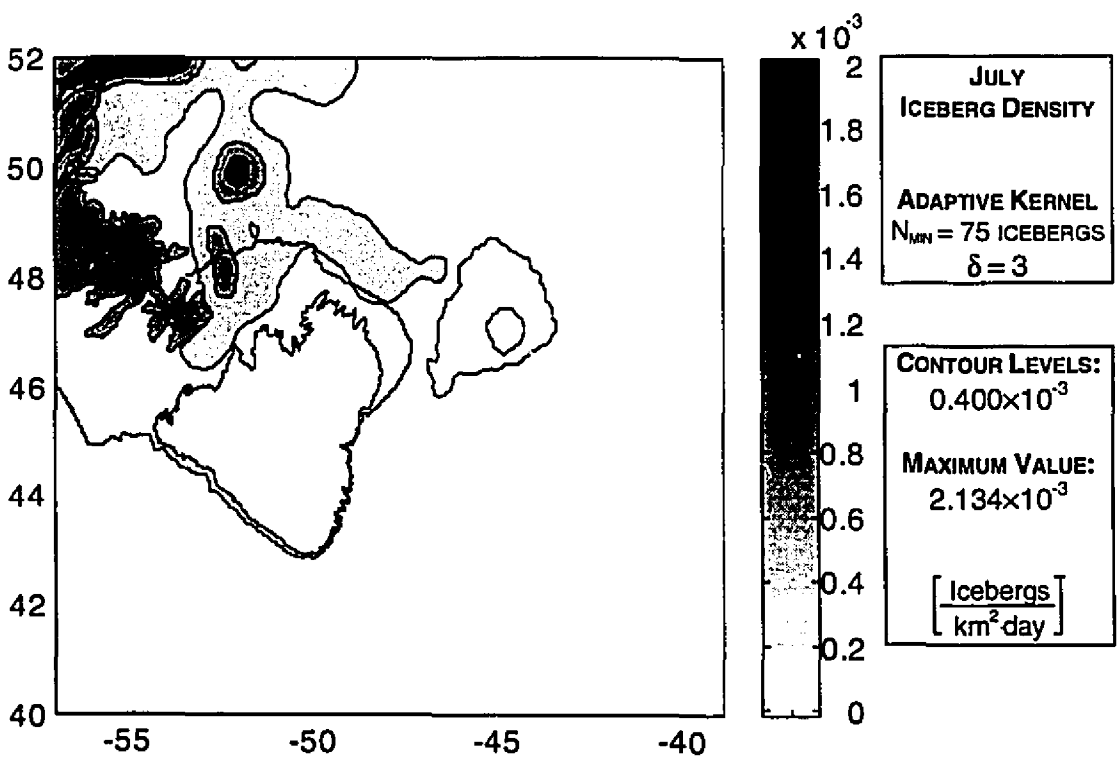

Figure B-16 Iceberg densities for July ($\delta=3$). Maximum density of 2.134×10^{-3} icebergs/km^2/day.

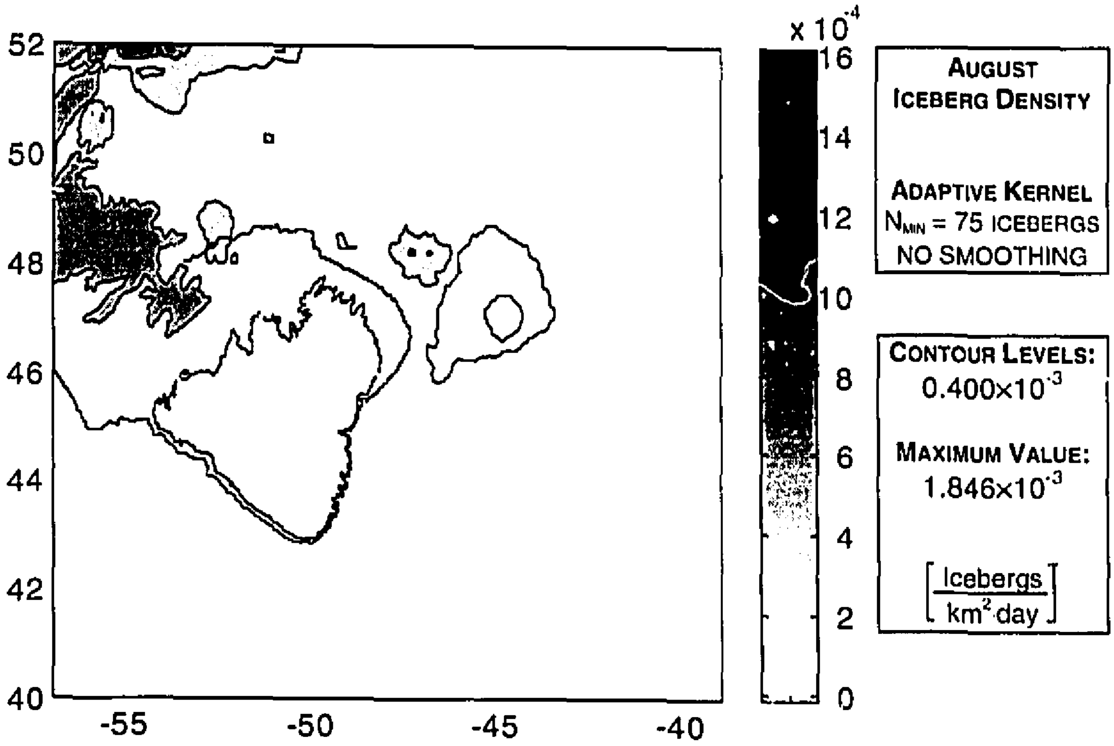

Figure B-17 Iceberg densities for August (δ=0). Maximum density of 1.846×10^{-3} icebergs/km^2/day.

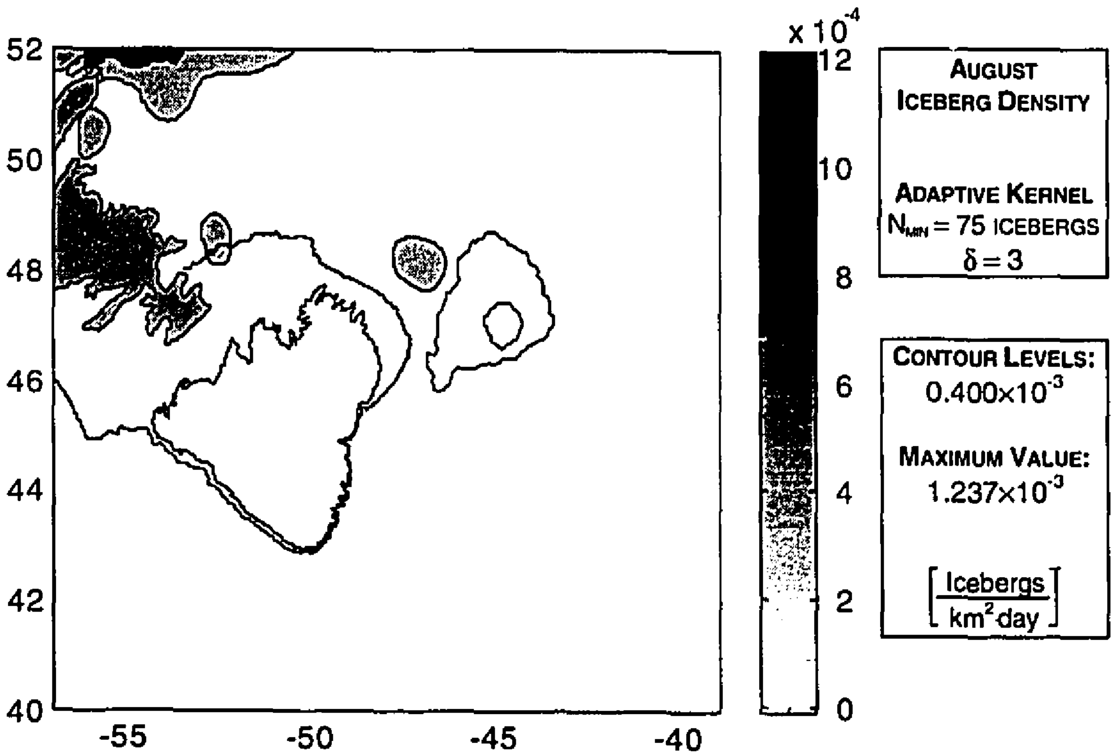

Figure B-18 Iceberg densities for August (δ=3). Maximum density of 1.237×10^{-3} icebergs/km^2/day.

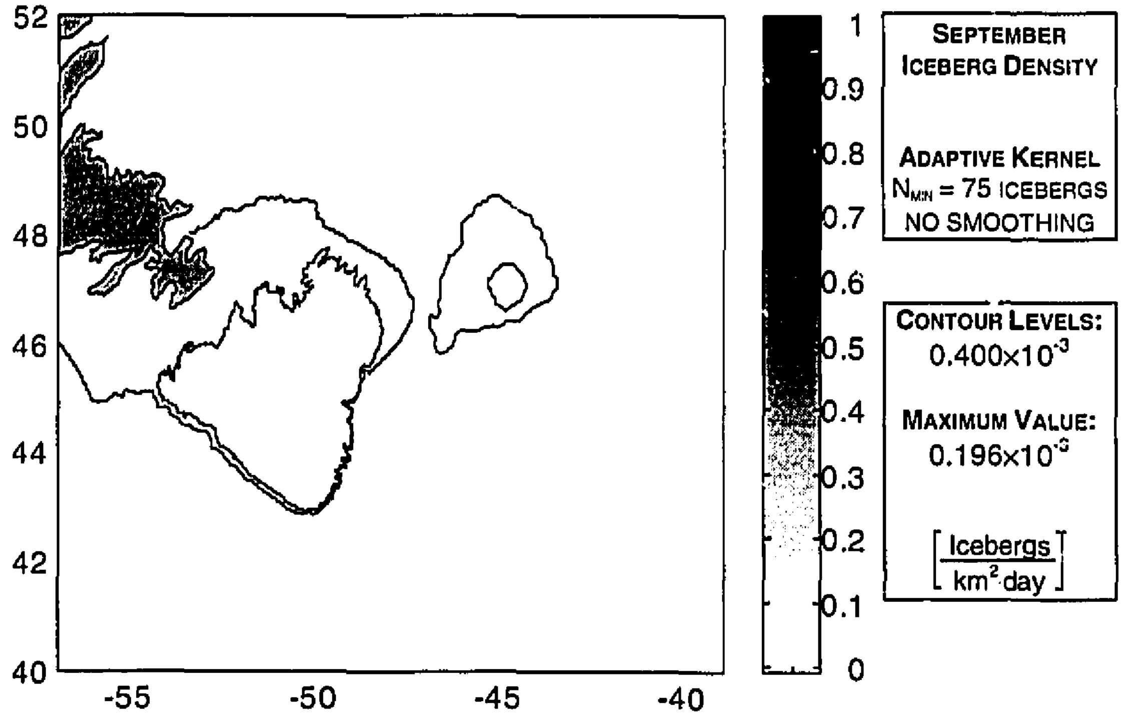

Figure B-19 Iceberg densities for September. Results are negligible (See Figures C-17 and C-18).

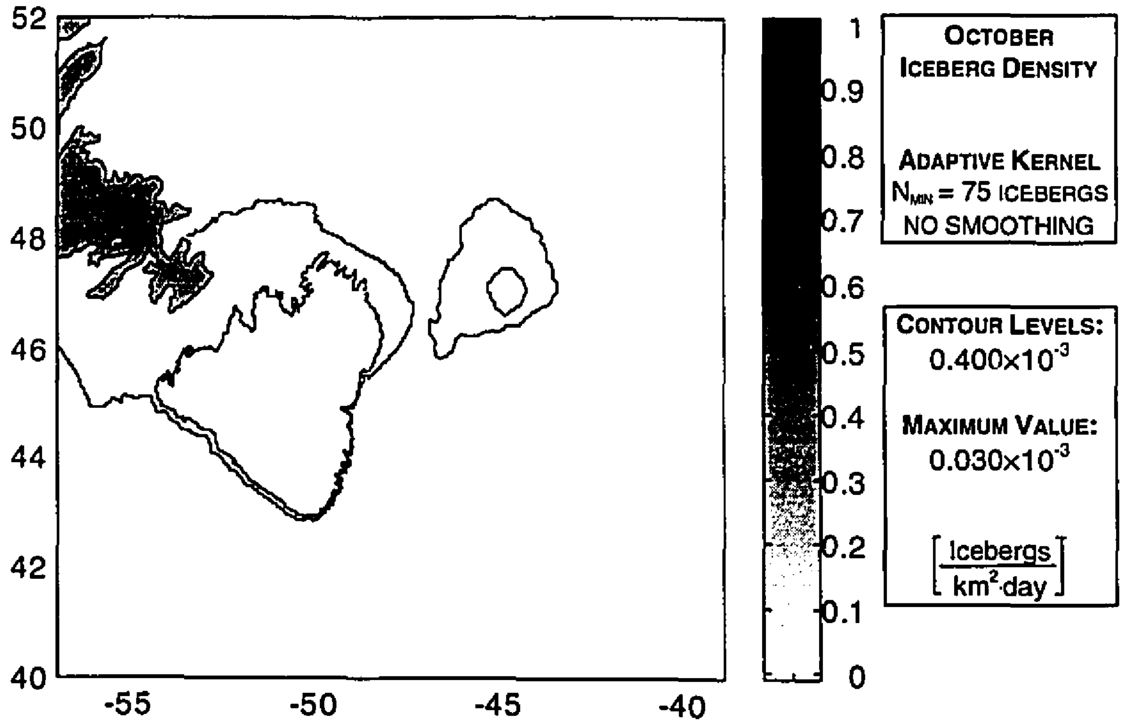

Figure B-20 Iceberg densities for October. Results are negligible (see Figures C-19 and C-20).

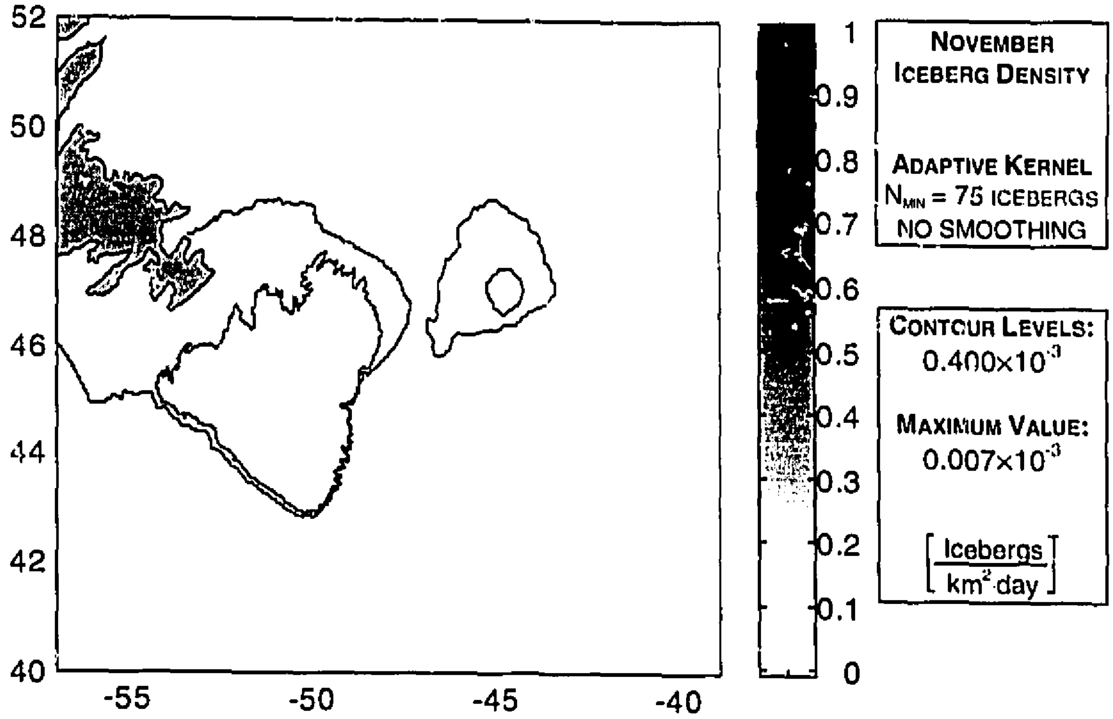

Figure B-21 Iceberg densities for November. Results are negligible (see Figures C-21 and C-22).

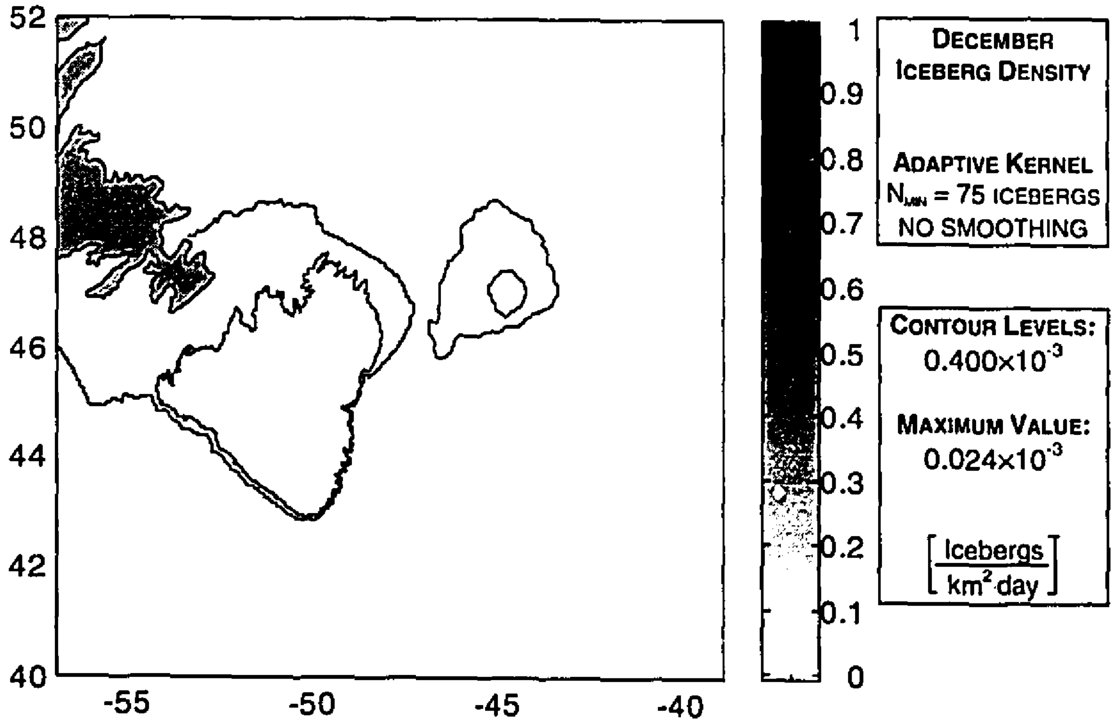

Figure B-22 Iceberg densities for December. Results are negligible (see Figures C-23 and C-24).

Appendix C

The following figures display monthly iceberg locations and estimates of iceberg densities, obtained using the adaptive kernel. Iceberg locations are as provided in the IIP database and as used in calculating estimates of iceberg densities. The IIP database contains some erroneous reports which were not omitted from the calculations (Figures C-9 and C-11). However, these are few and have a negligible effect on density estimations.

Estimates of iceberg densities are smoothed and with contours levels specific to each month to illustrate the effectiveness of the adaptive kernel in representing the density of the iceberg population.

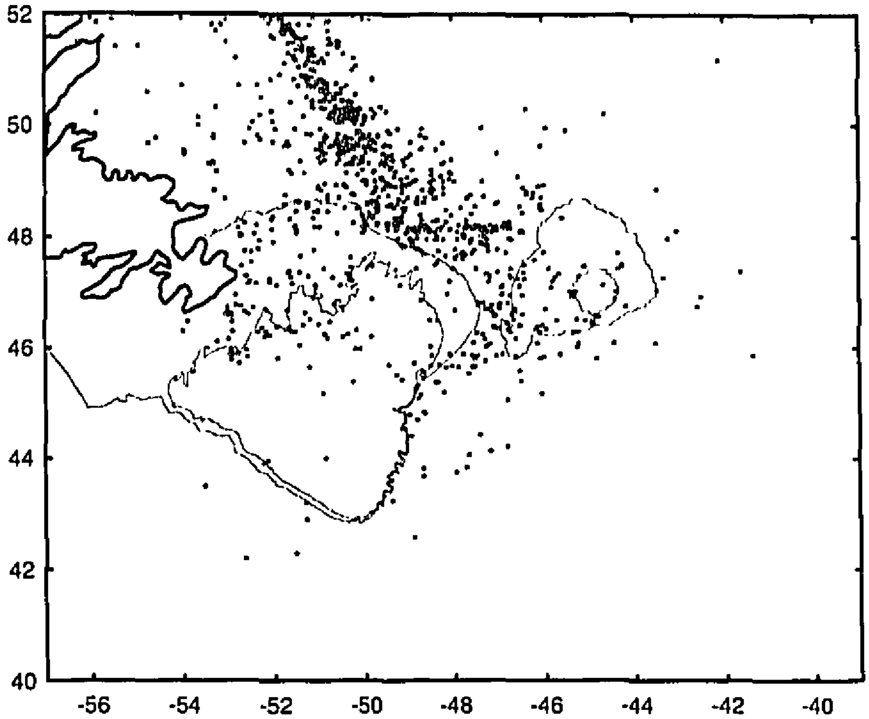

Figure C-1 IIP iceberg locations for January (1960-1993). 1067 iceberg reports (1.27% of total).

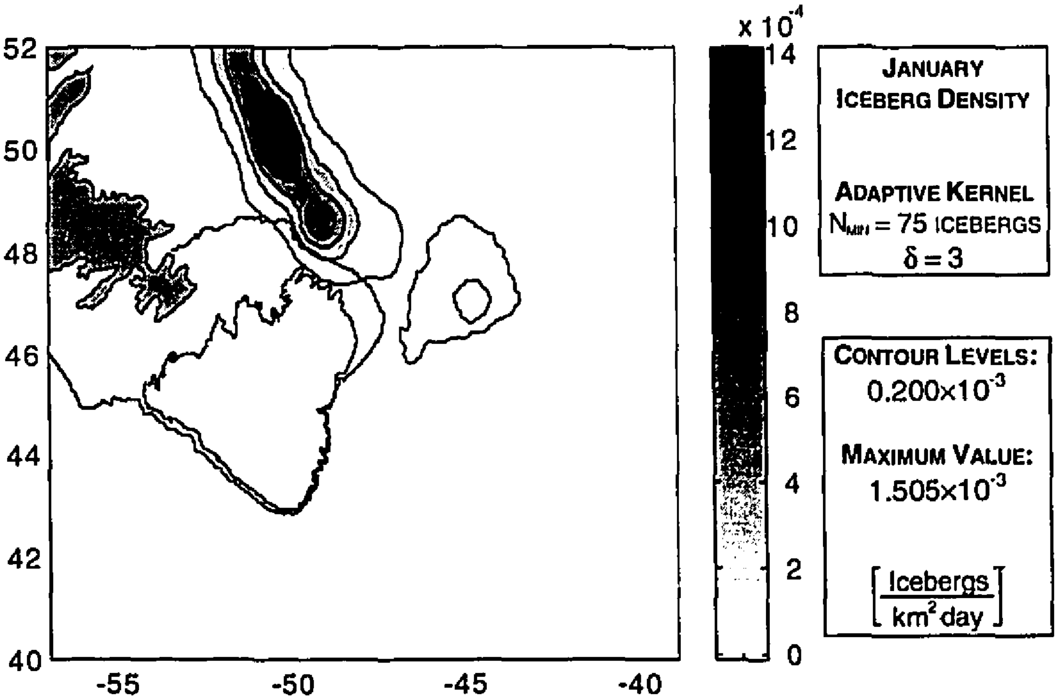

Figure C-2 Iceberg densities for January (δ=3). Contour levels of 0.20×10^{-3} icebergs/km^2/day;

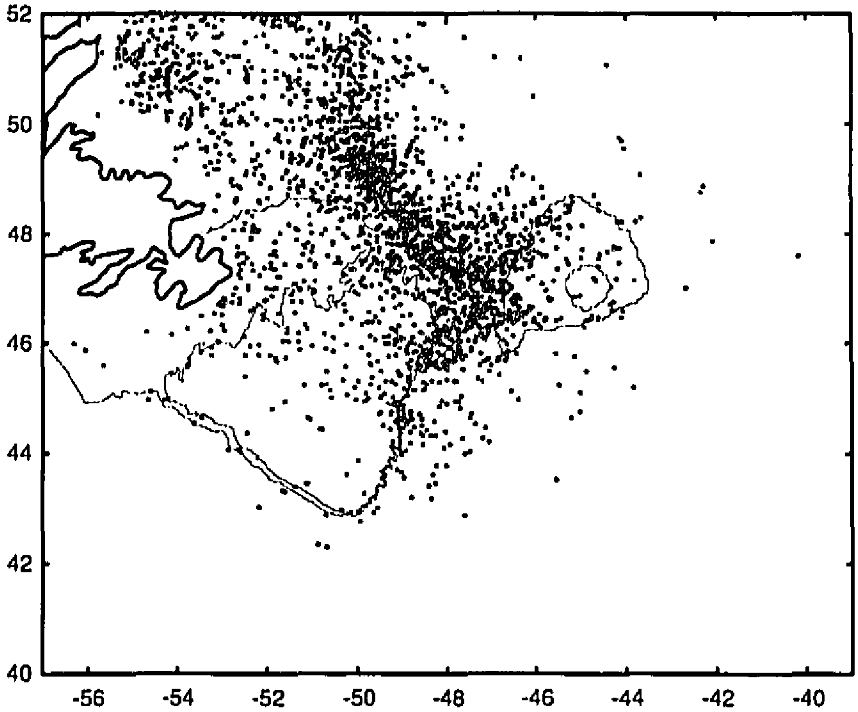

Figure C-3 IIP iceberg locations for February (1960-1993), 2784 iceberg reports (3.32% of total).

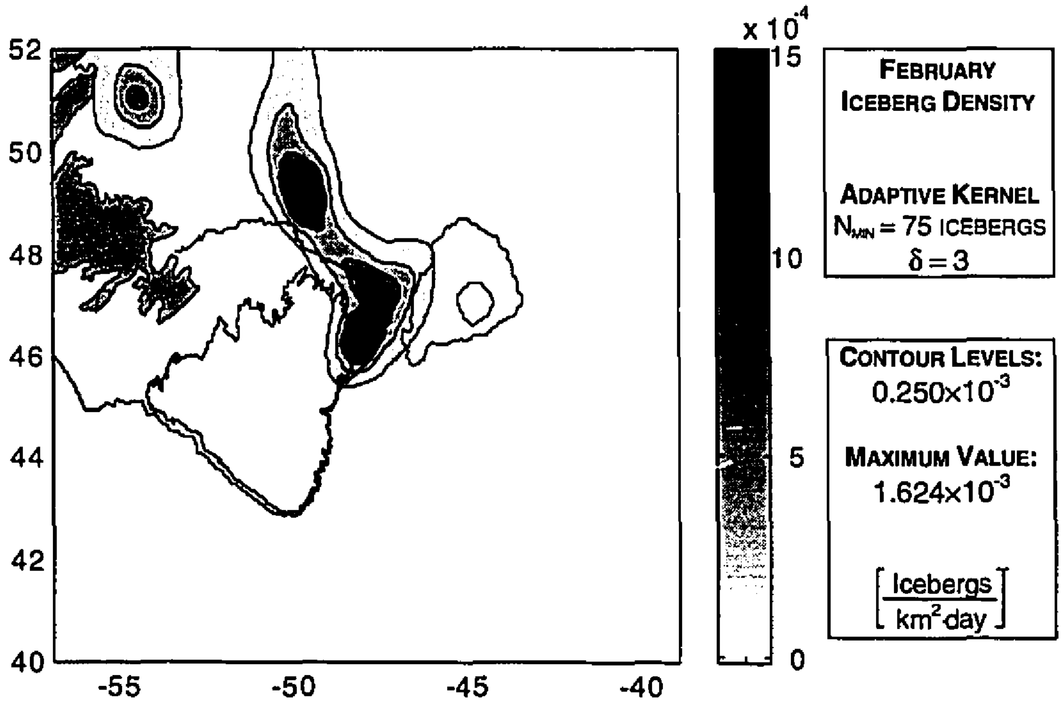

Figure C-4 Iceberg densities for February (δ=3); Contour levels of 0.25×10^{-3} icebergs/km^2/day.

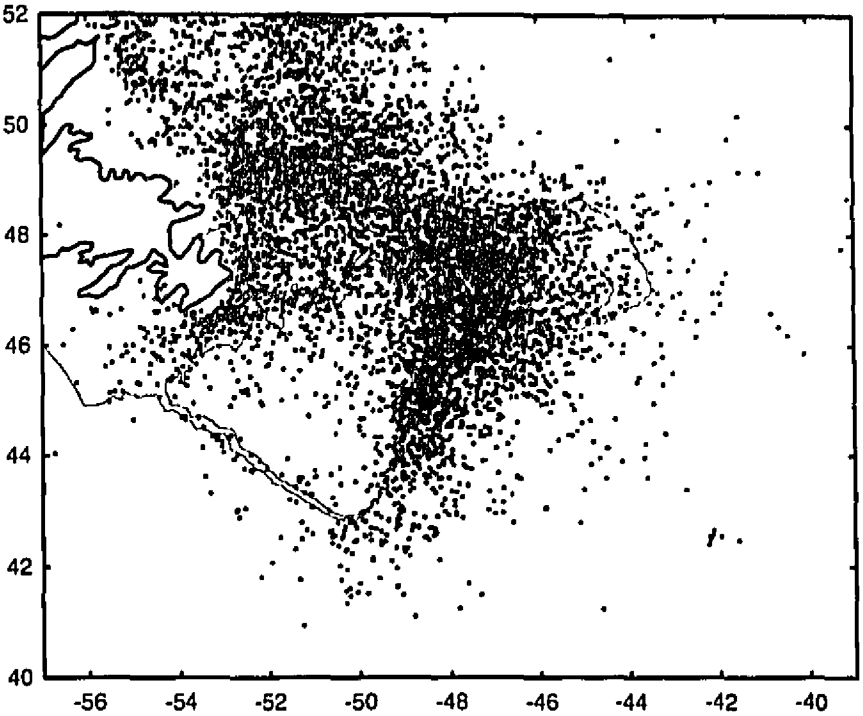

Figure C-5 IIP iceberg locations for March (1960-1993), 7270 iceberg reports (8.66% of total).

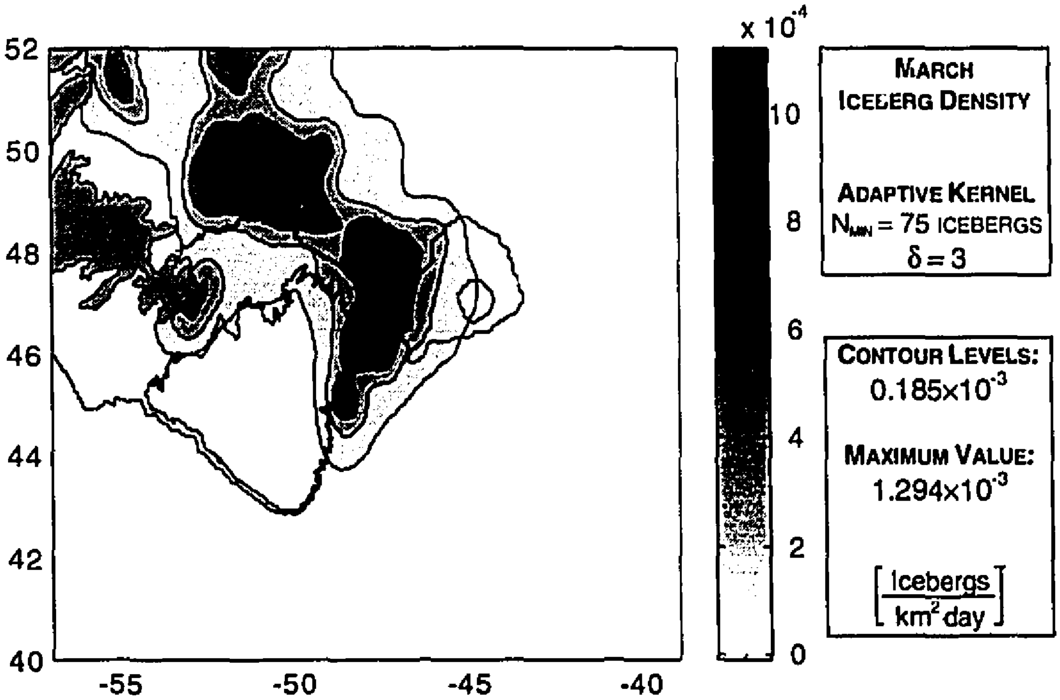

Figure C-6 Iceberg densities for March (δ=3). Contour levels of 0.185×10^{-3} icebergs/km^2/day.

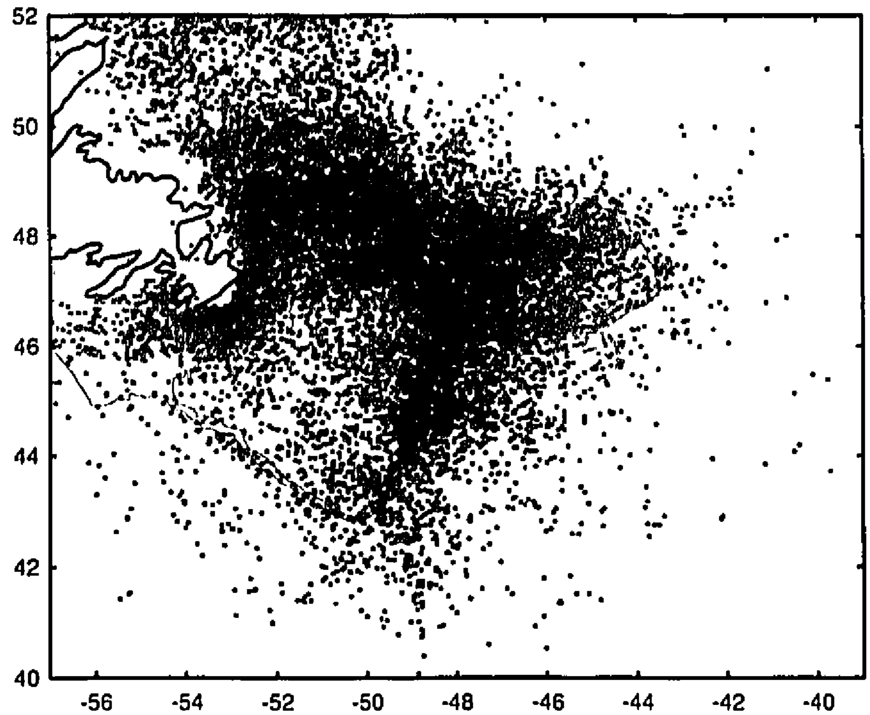

Figure C-7 IIP iceberg locations for April (1960-1993), 17797 iceberg reports (21.19% of total).

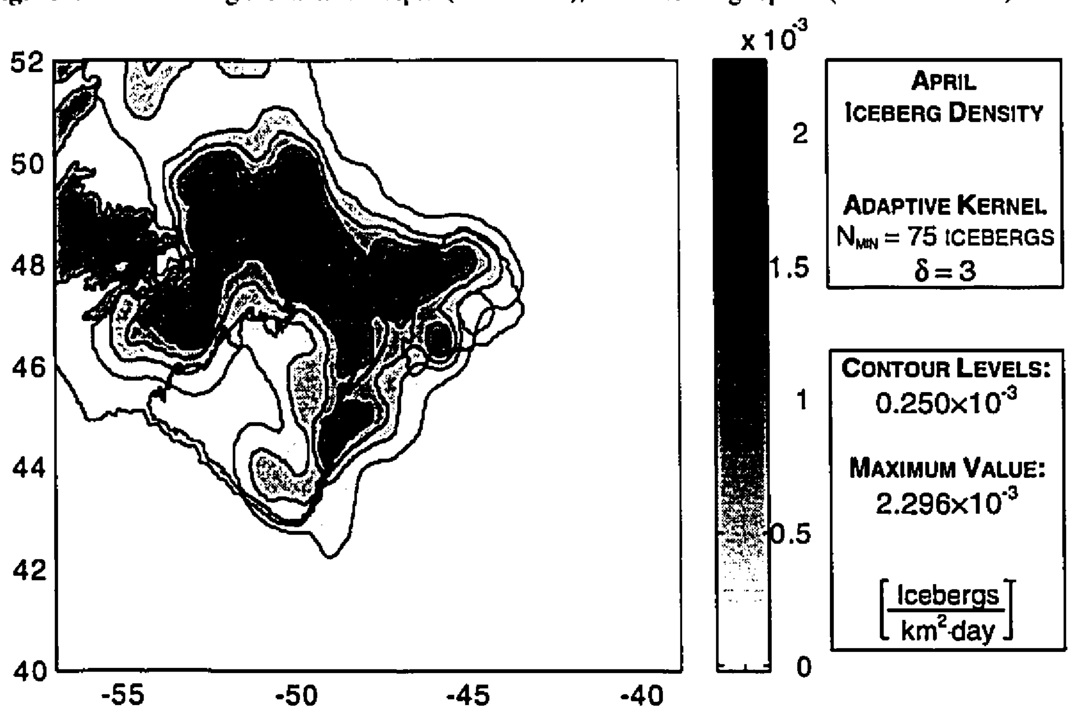

Figure C-8 Iceberg densities for April (δ=3). Contour levels of 0.25×10^{-3} icebergs/km^2/day

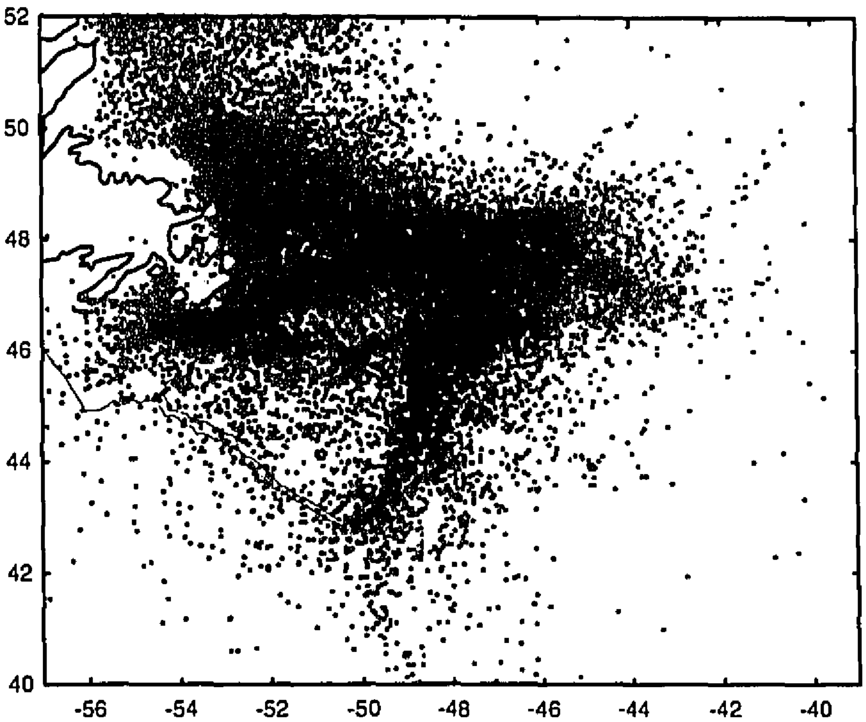

Figure C-9 IIP iceberg locations for May (1960-1993), 25589 iceberg reports (30.47% of total).

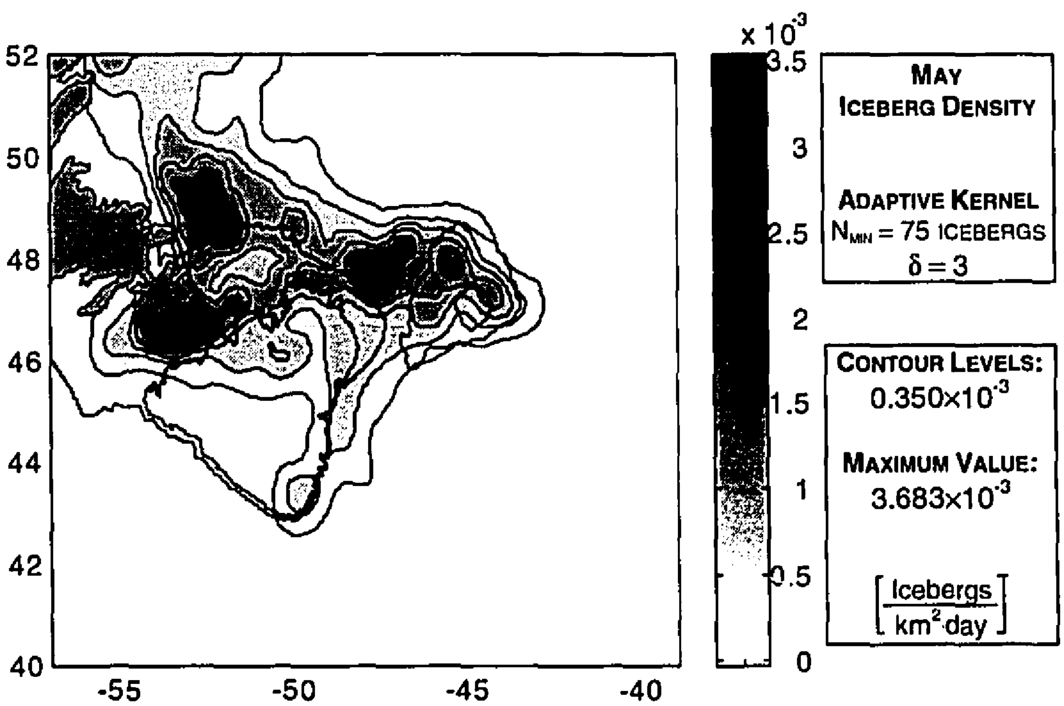

Figure C-10 Iceberg densities for May (δ=3). Contour levels of 0.35×10^{-3} icebergs/km^2/day.

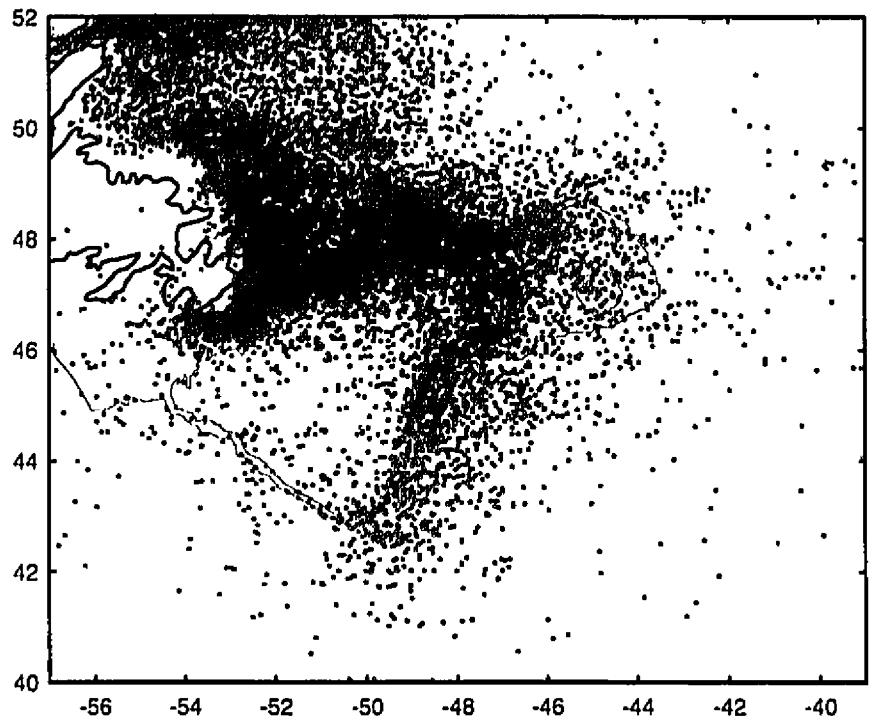

Figure C-11 IIP iceberg locations for June (1960-1993), 17923 iceberg reports (21.34% of total).

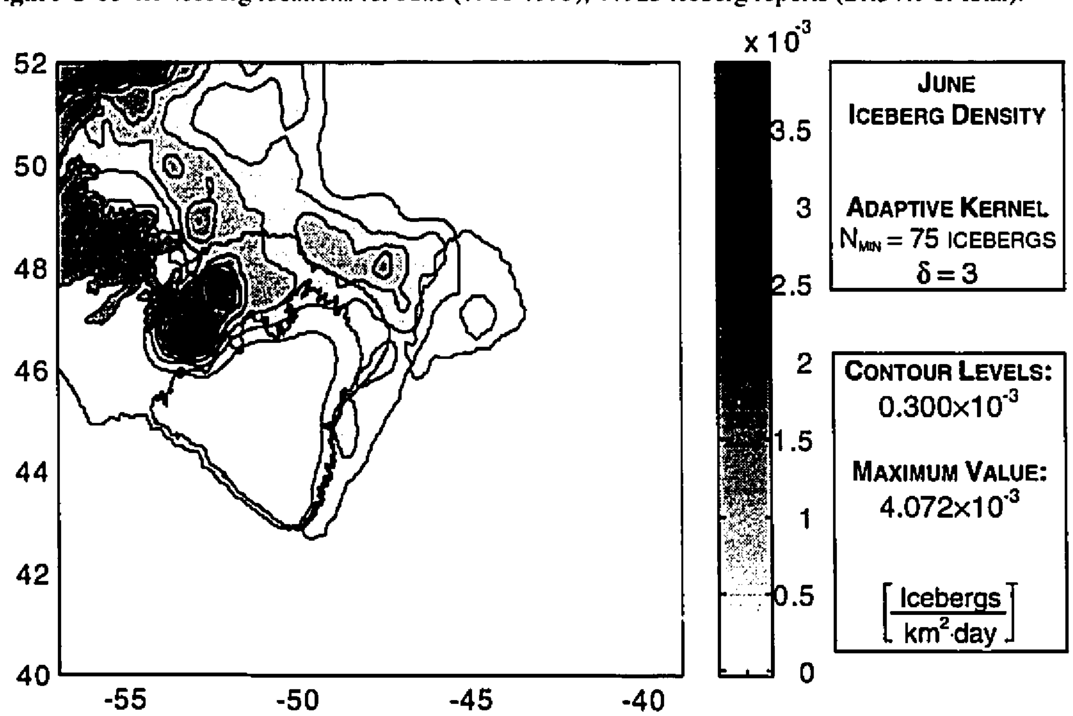

Figure C-12 Iceberg densities for June (δ=3). Contour levels of 0.30×10^{-3} icebergs/km^2/day.

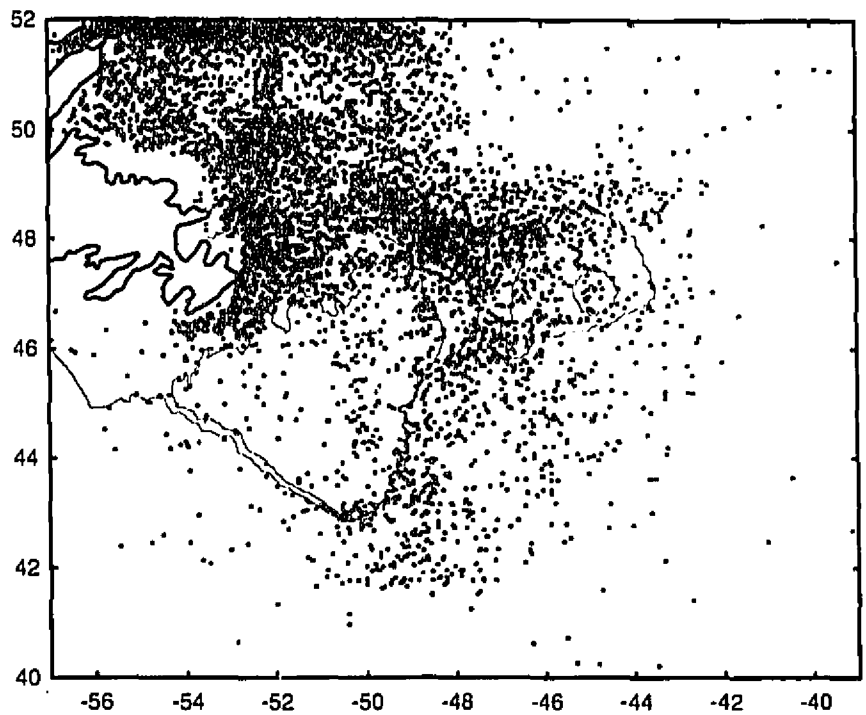

Figure C-13 IIP iceberg locations for July (1960-1993), 7836 iceberg reports (9.33% of total).

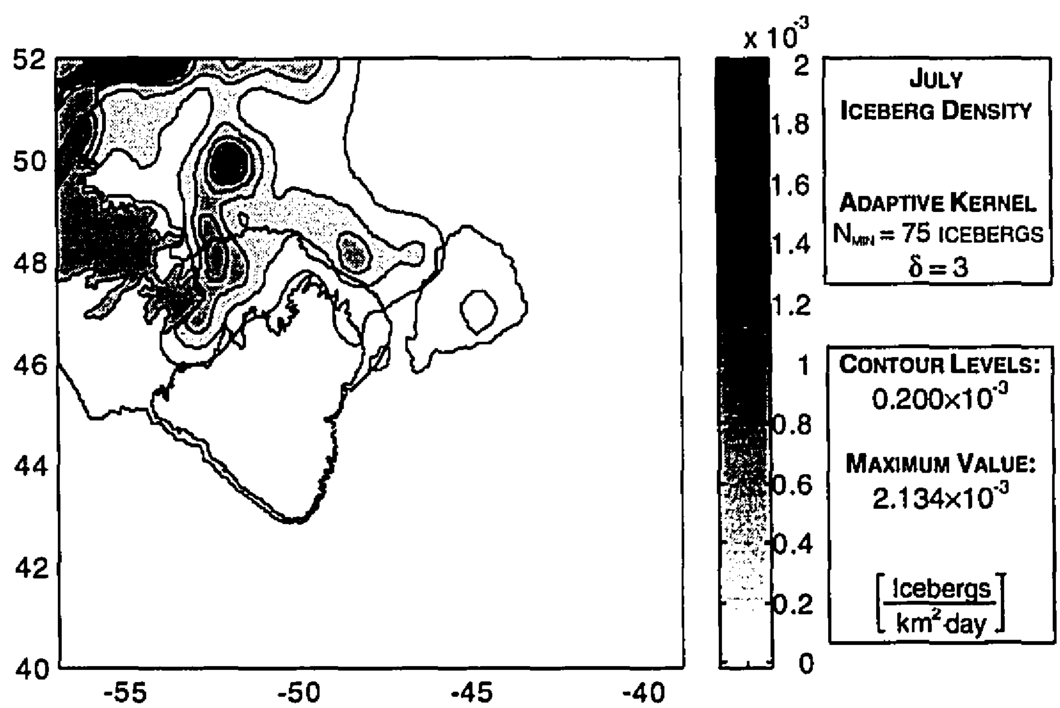

Figure C-14 Iceberg densities for July (δ=3). Contour levels of 0.20×10^{-3} icebergs/km^2/day.

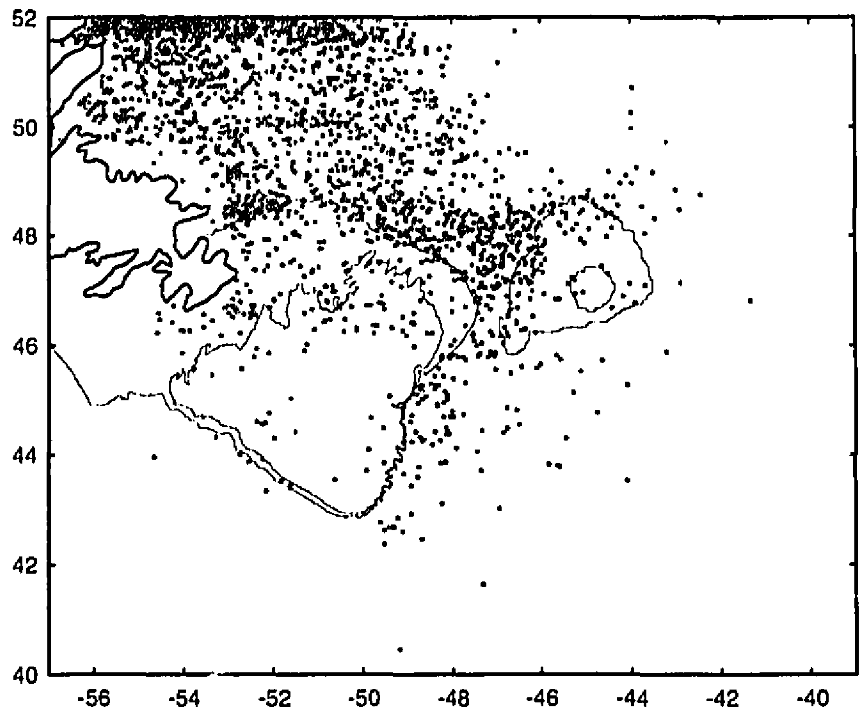

Figure C-15 IIP iceberg locations for August (1960-1993), 3020 iceberg reports (3.60% of total).

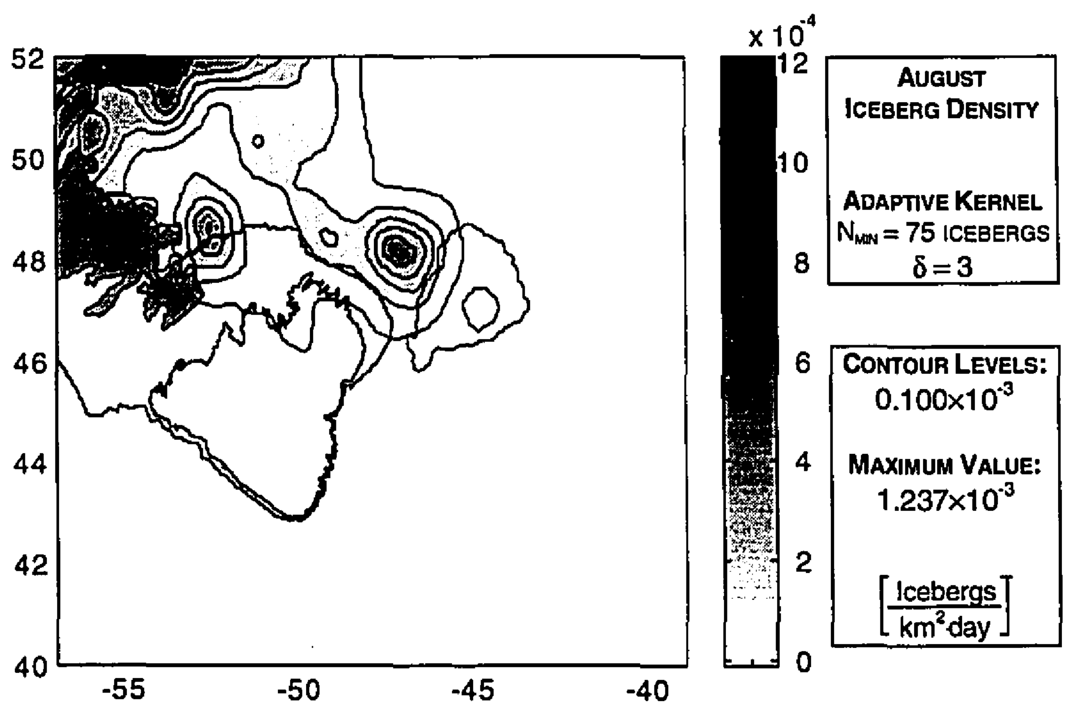

Figure C-16 Iceberg densities for August (δ=3). Contour levels of 0.10×10^{-3} icebergs/km^2/day.

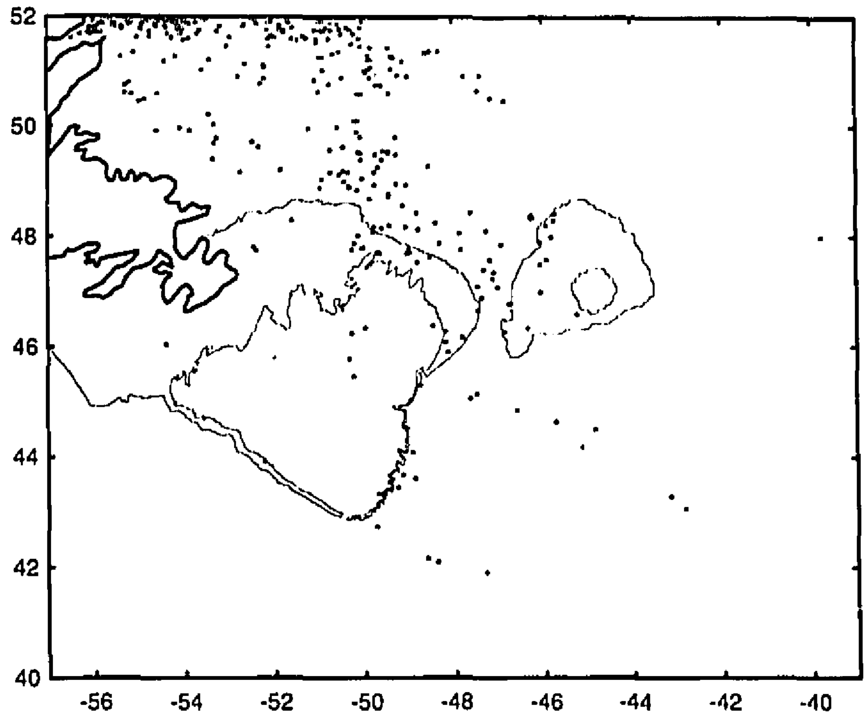

Figure C-17 IIP iceberg locations for September (1960-1993), 403 iceberg reports (0.48% of total).

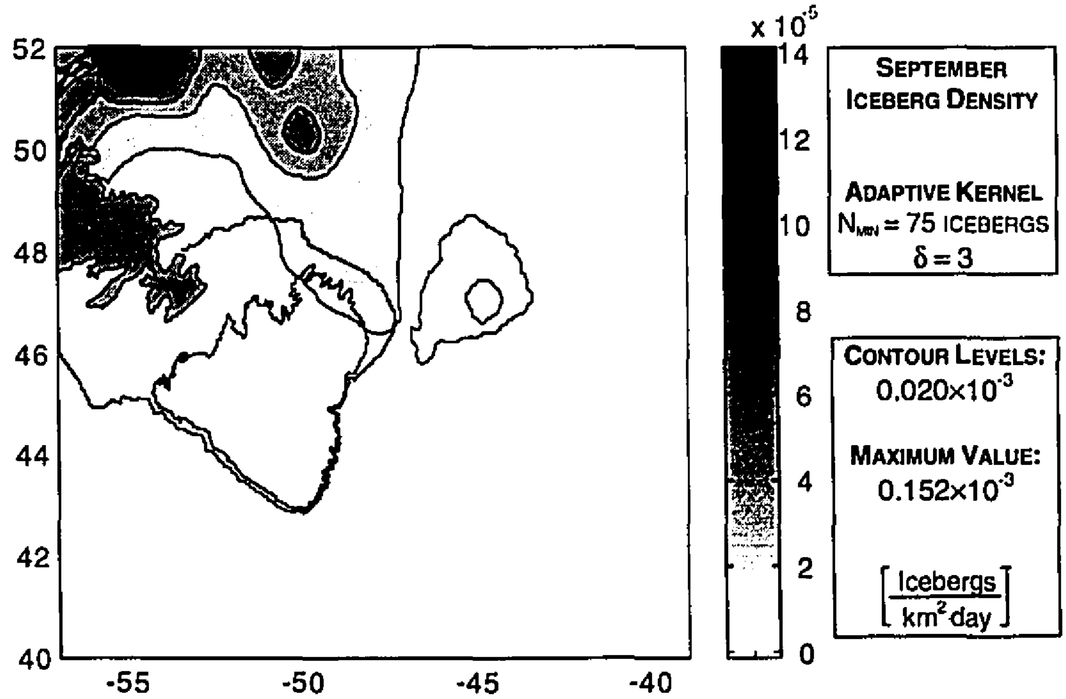

Figure C-18 Iceberg densities for September (δ=3). Contour levels of 0.02×10^{-3} icebergs/km^2/day.

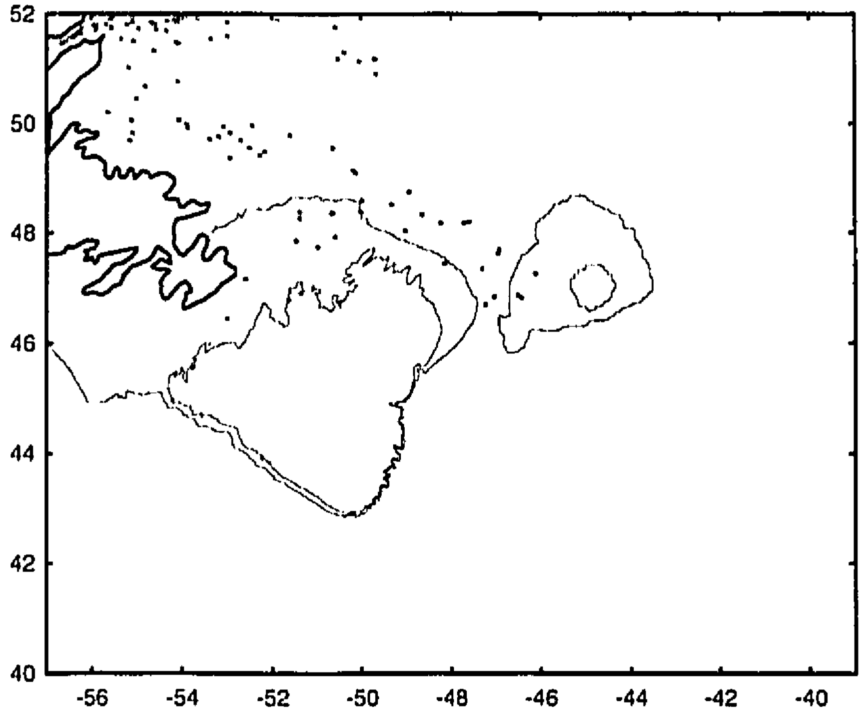

Figure C-19 IIP iceberg locations for October (1960-1993), 121 iceberg reports (0.14% of total).

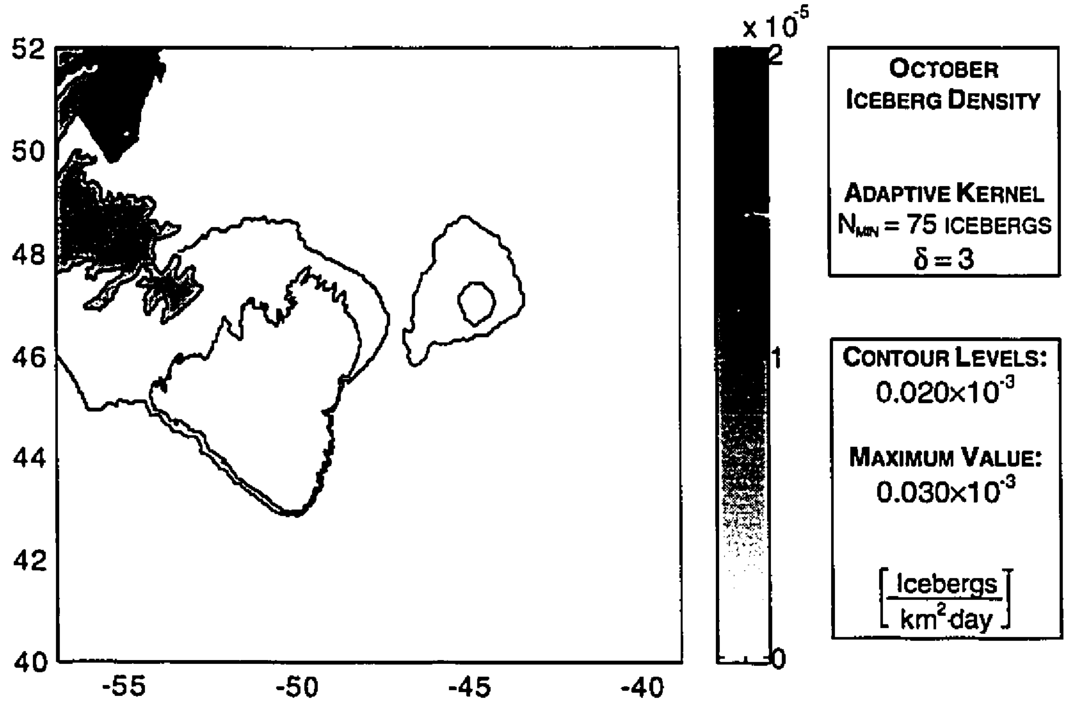

Figure C-20 Iceberg densities for October (δ=0). Contour levels of 0.02×10^{-3} icebergs/km^2/day.

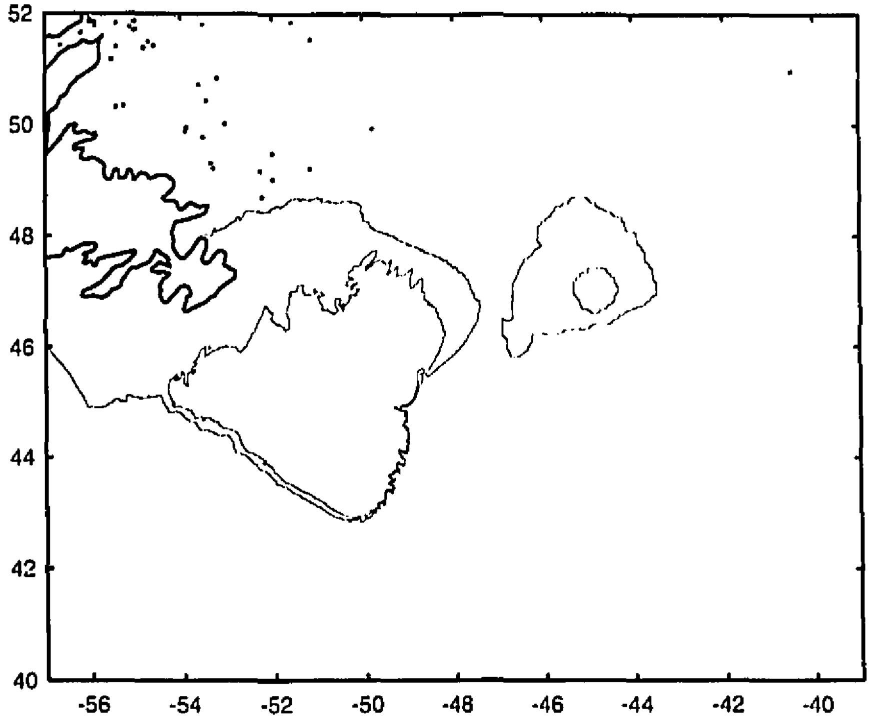

Figure C-21 IIP iceberg locations for November (1960-1993), 43 iceberg reports (0.05% of total).

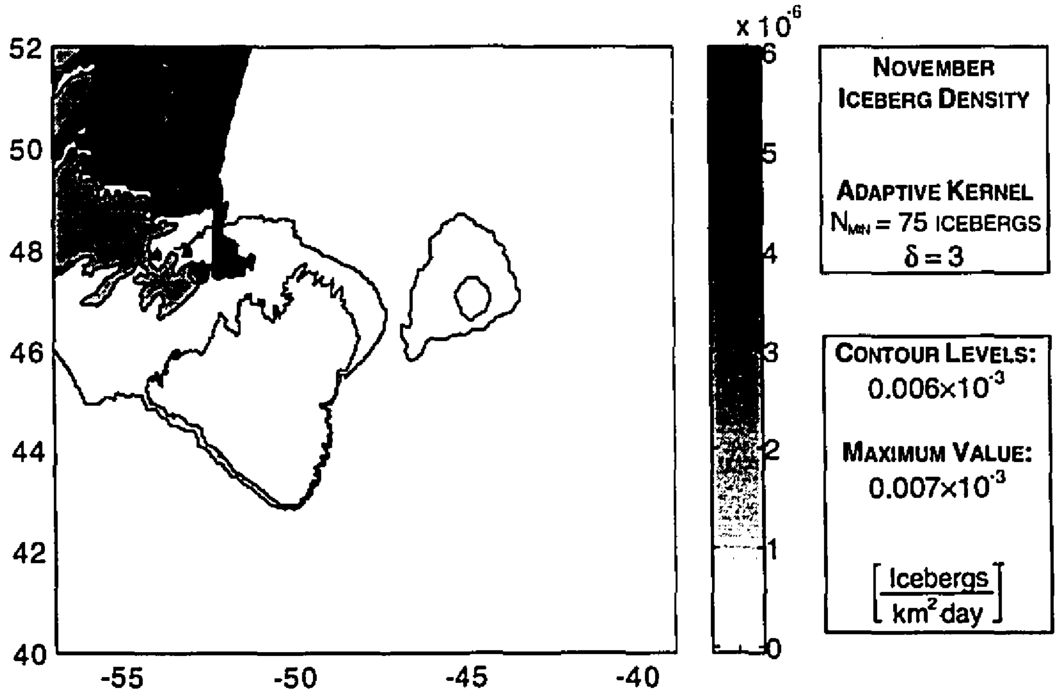

Figure C-22 Iceberg densities for November (δ=0). Contour levels of 0.006×10^{-3} icebergs/km²/day.

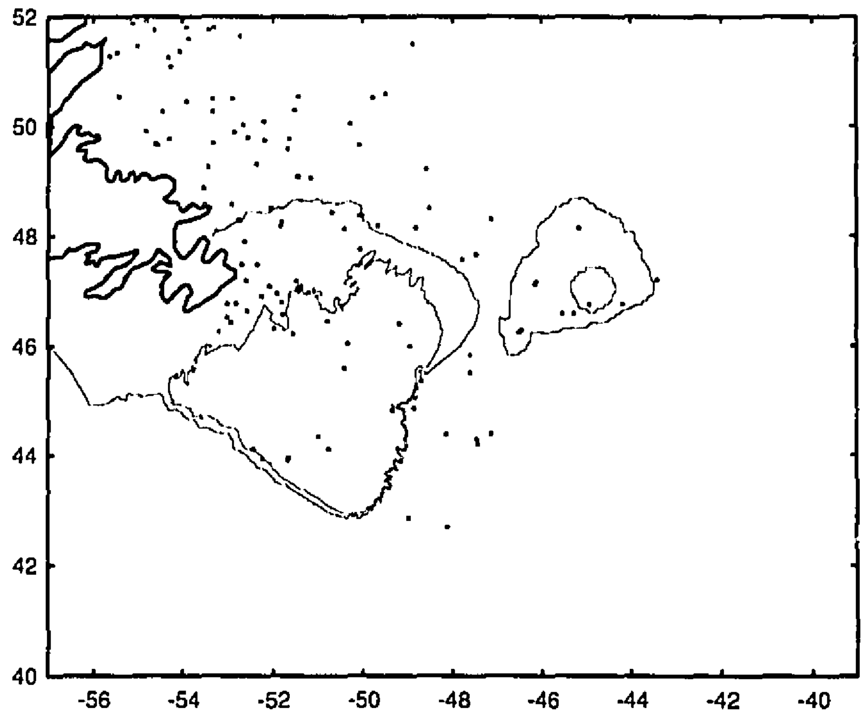

Figure C-23 IIP iceberg locations for December (1960-1993), 121 iceberg reports (0.14% of total).

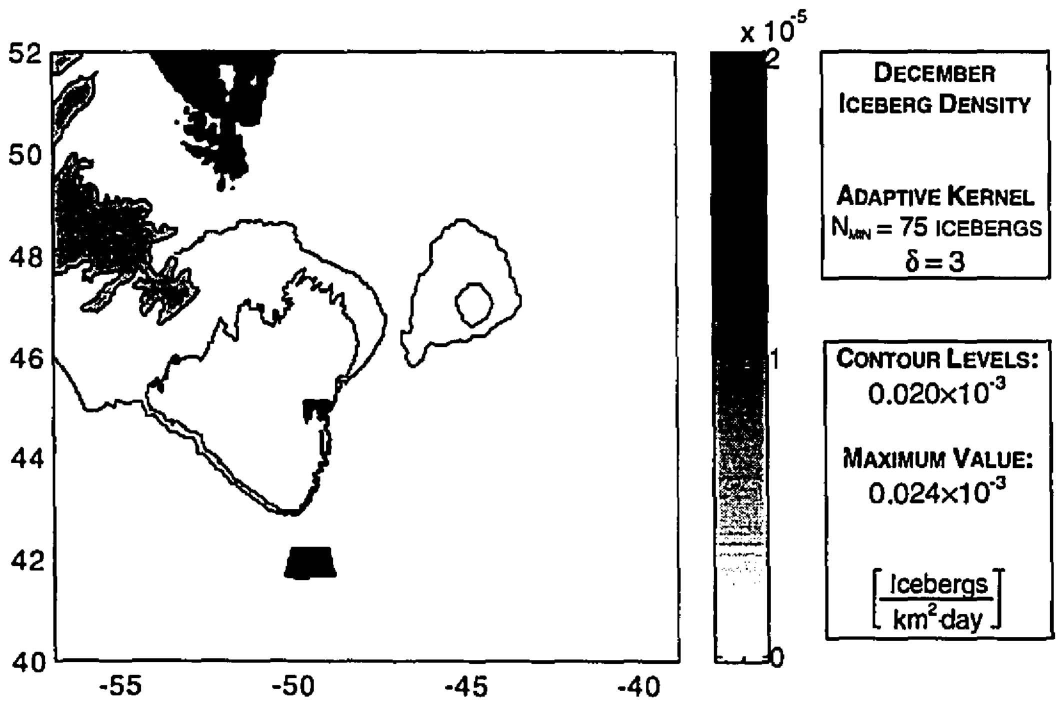

Figure C-24 Iceberg densities for December (δ=0). Contour levels of 0.02×10^{-3} icebergs/km^2/day.

Appendix D

Figures D-1 through D-12 illustrate how the adaptive kernel bandwidth varies for each monthly iceberg densities. In regions of high iceberg densities, kernel bandwidths remain below 50 km.

Some erraticity in the following figures is present at the periphery of the iceberg region. This is caused by the discontinuous nature of the square kernel (Eqs 5.4-10 and 5.4-12) which was also, for computational reasons, limited to 245 km (h_{max}). If, at a given location, the minimum number of icebergs N_{min} was not obtained within a kernel of bandwidth h_{max} the estimation proceeds to the following grid point. This constraint was used to avoid lengthy calculations where iceberg densities are negligible, such as the periphery of the iceberg region and in months where iceberg counts are very low (i.e. September through December).

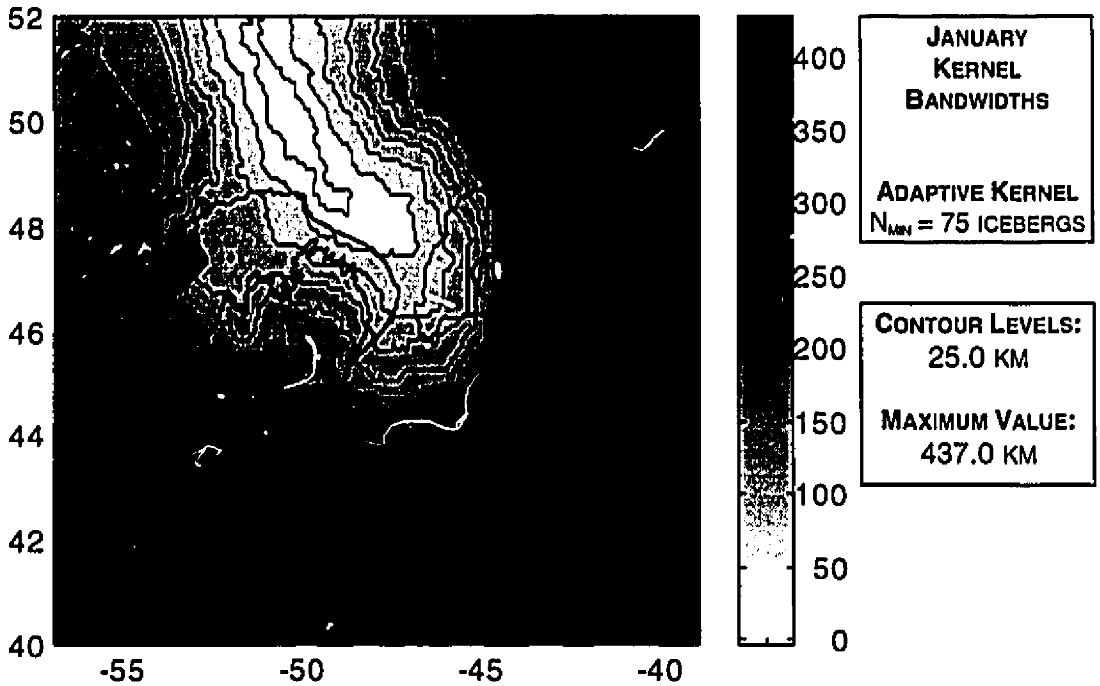

Figure D-1 Regional variation in adaptive kernel bandwidths in estimating iceberg density for January.

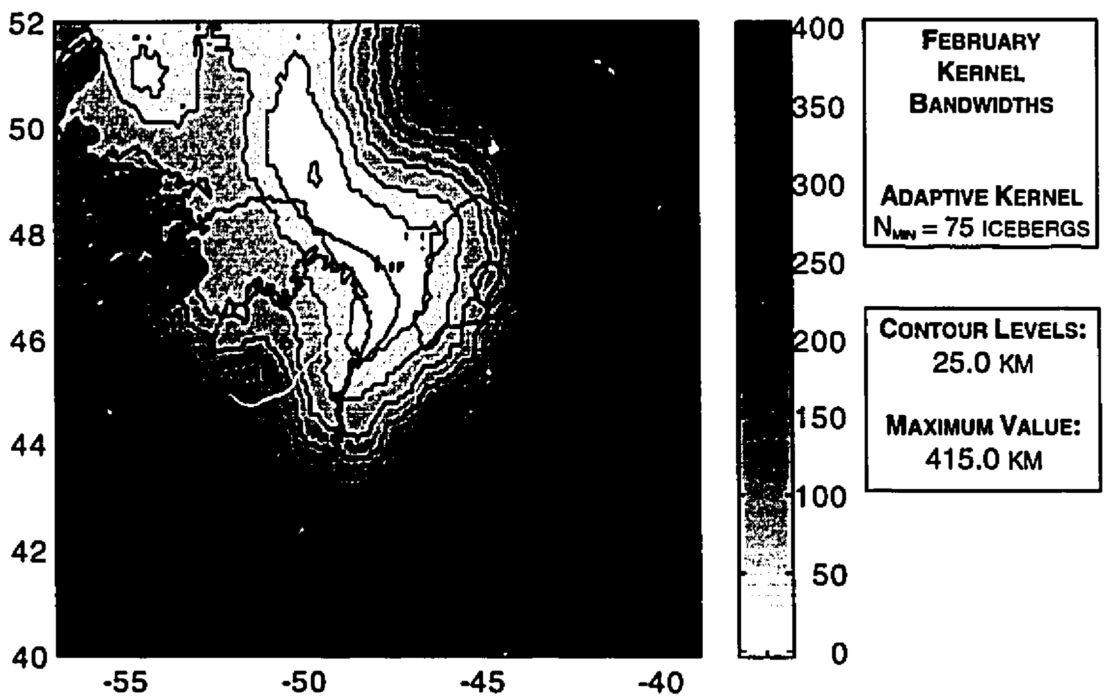

Figure D-2 Regional variation in adaptive kernel bandwidths in estimating iceberg density for February.

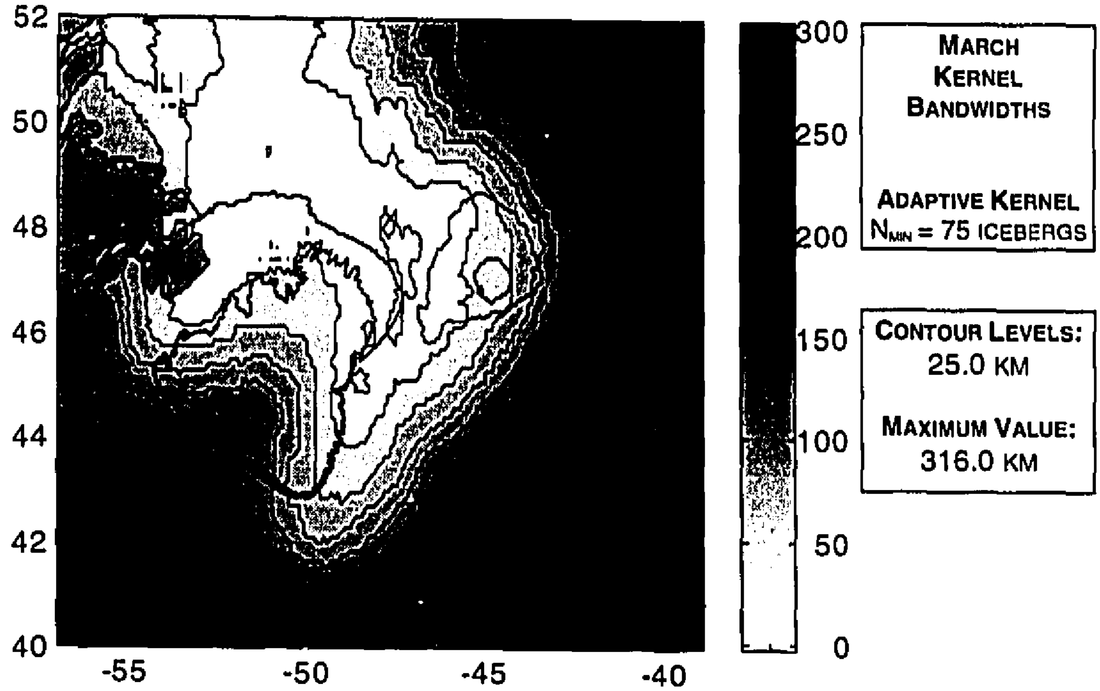

Figure D-3 Regional variation in adaptive kernel bandwidths in estimating iceberg density for March.

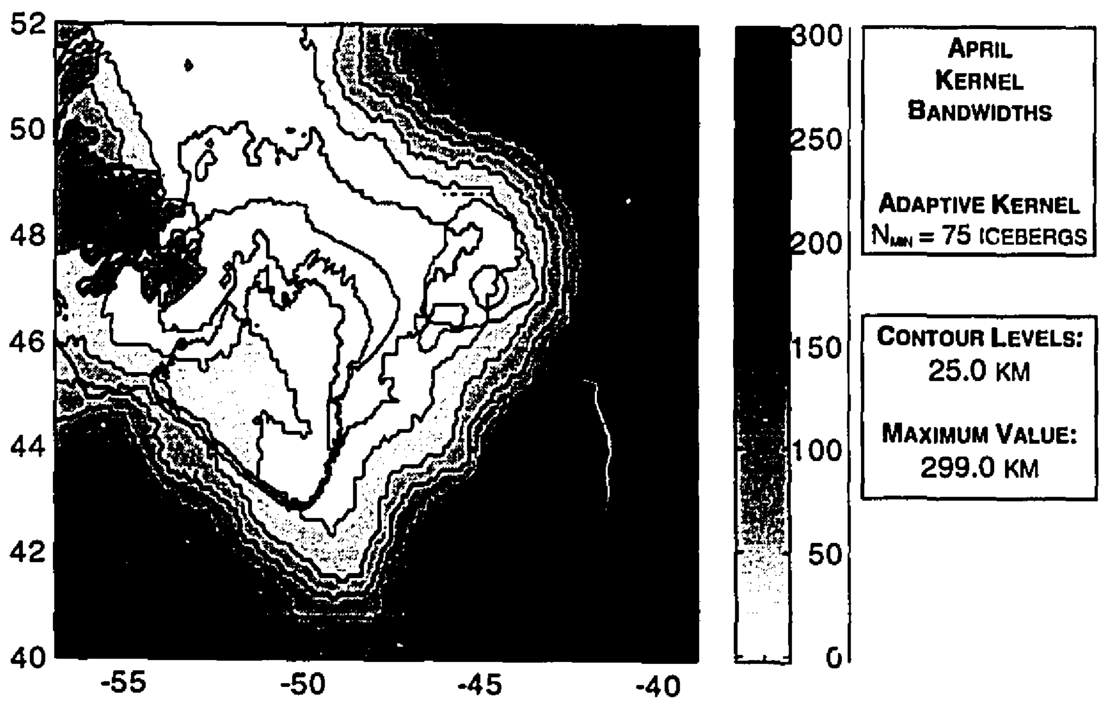

Figure D-4 Regional variation in adaptive kernel bandwidths in estimating iceberg density for April.

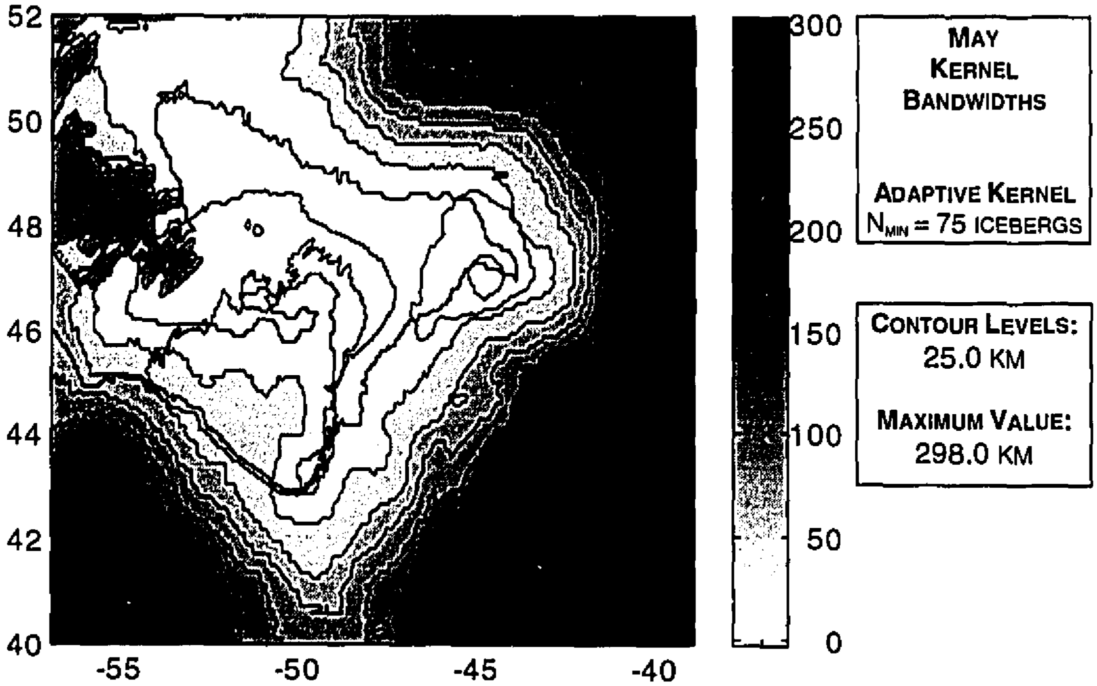

Figure D-5 Regional variation in adaptive kernel bandwidths in estimating iceberg density for May.

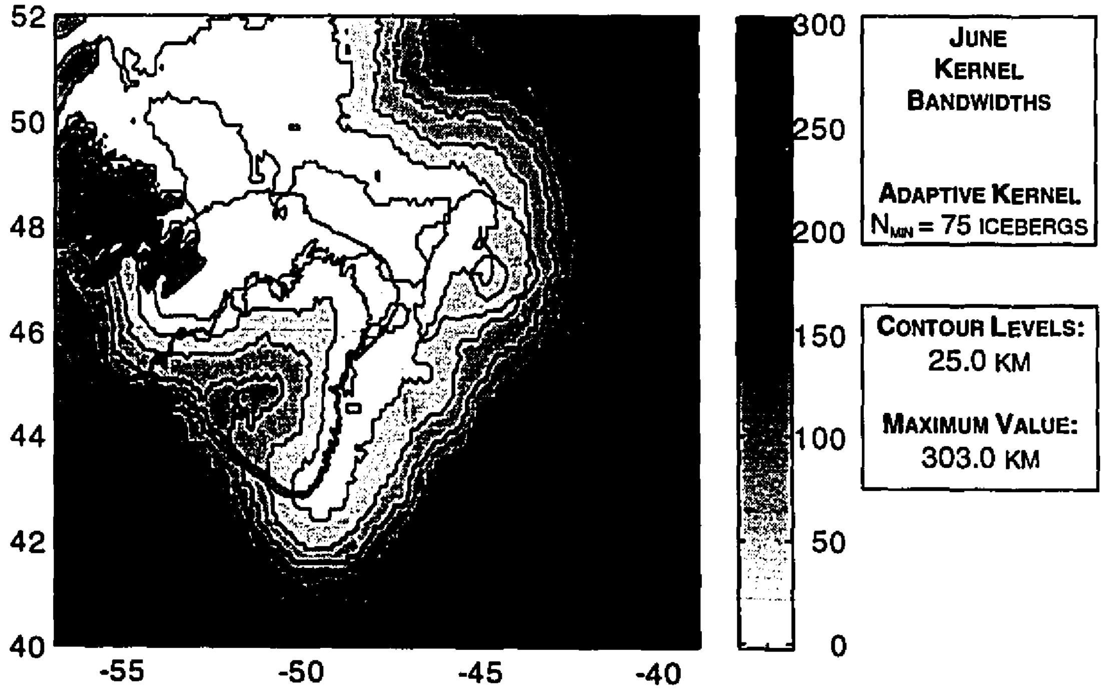

Figure D-6 Regional variation in adaptive kernel bandwidths in estimating iceberg density for June.

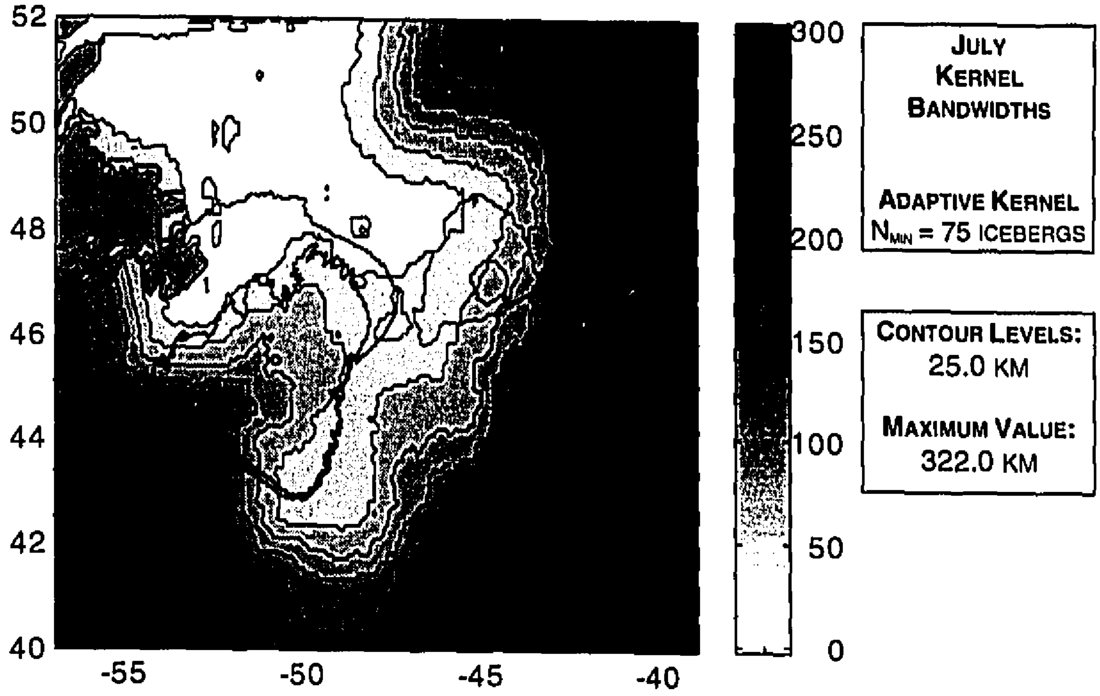

Figure D-7 Regional variation in adaptive kernel bandwidths in estimating iceberg density for July.

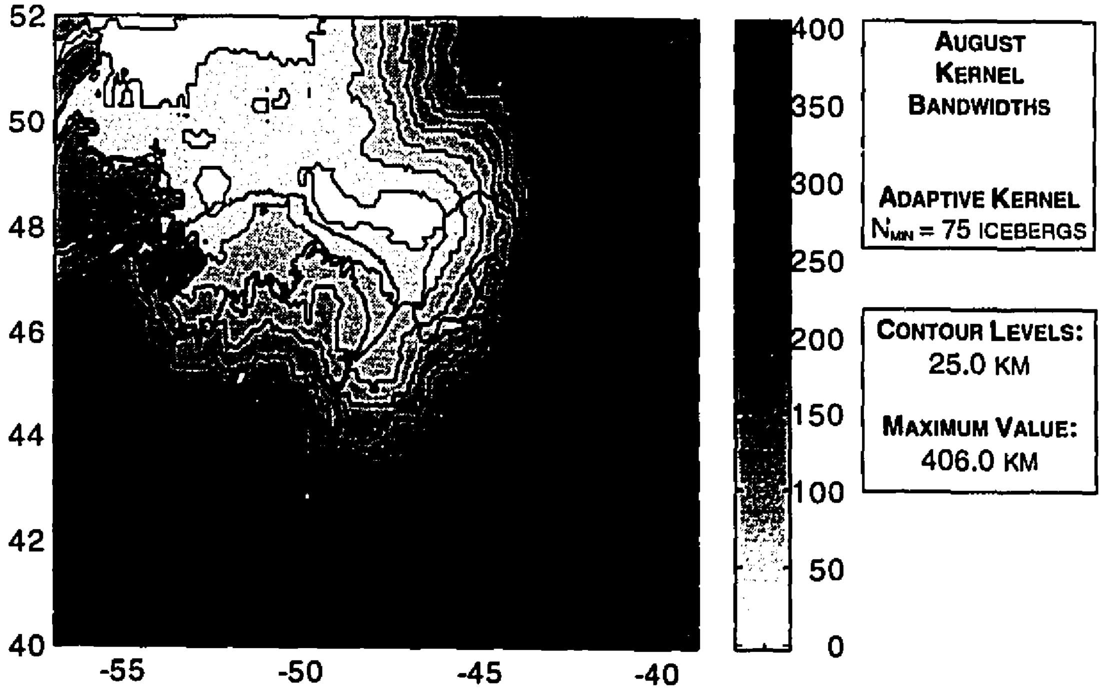

Figure D-8 Regional variation in adaptive kernel bandwidths in estimating iceberg density for August.

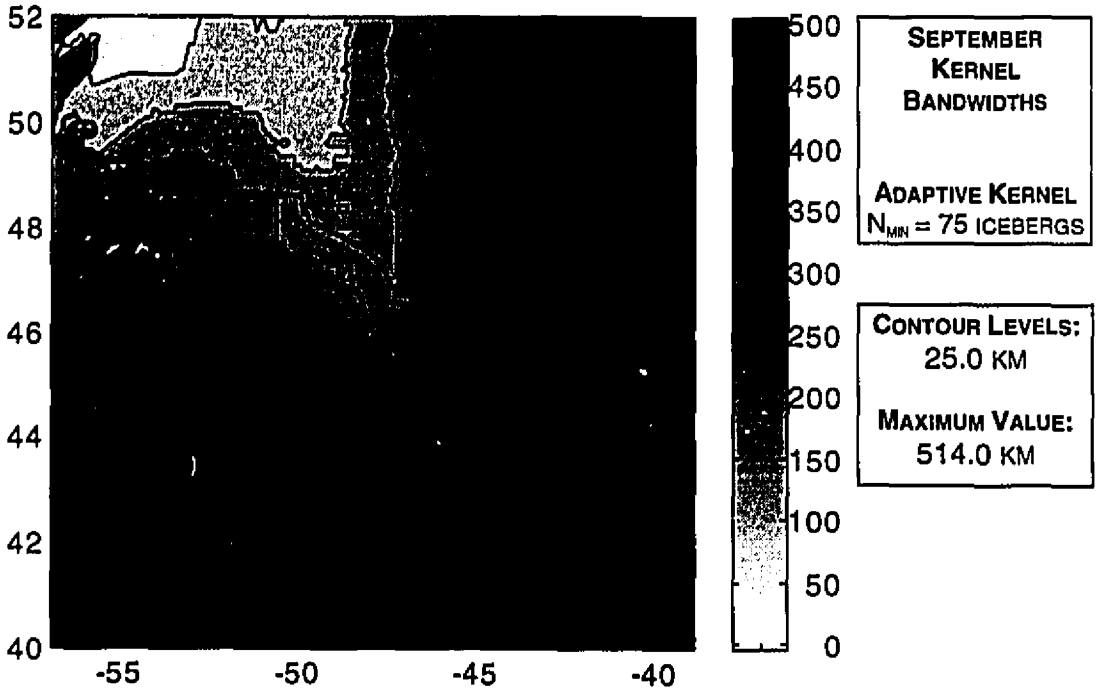

Figure D-9 Regional variation in adaptive kernel bandwidths in estimating iceberg density for September.

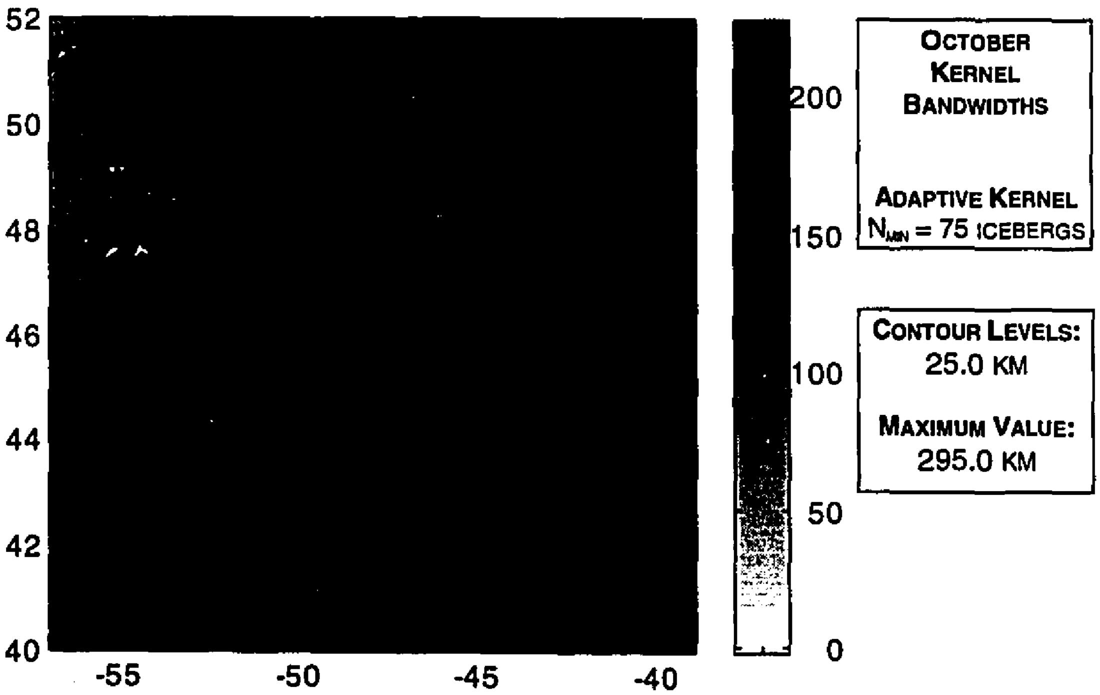

Figure D-10 Regional variation in adaptive kernel bandwidths in estimating iceberg density for October.

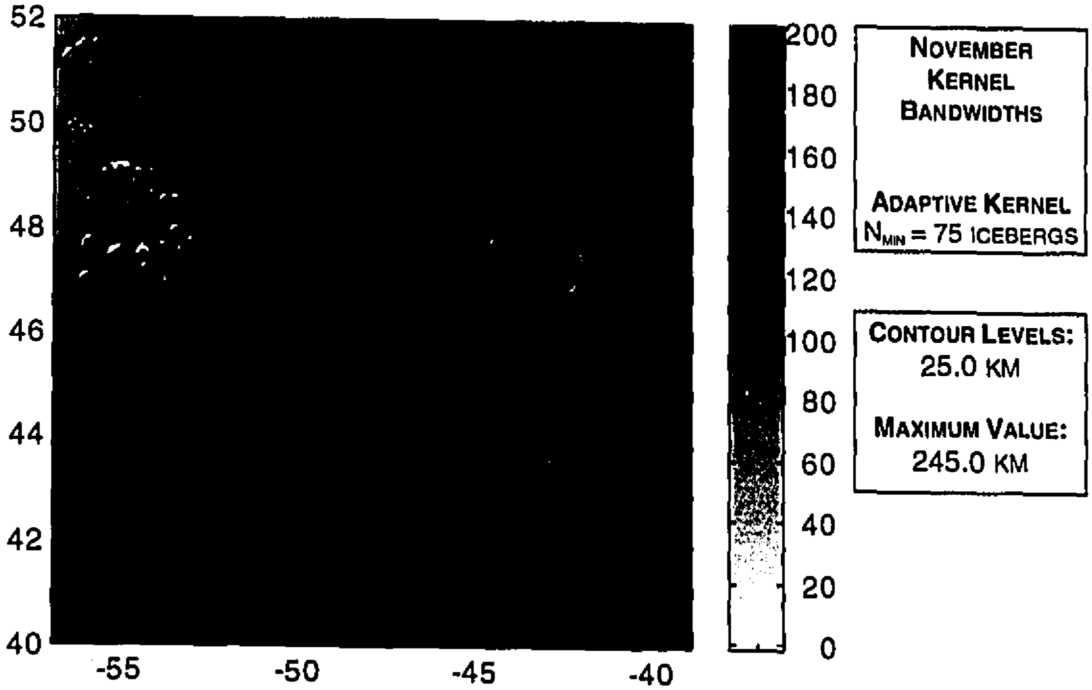

Figure D-11 Regional variation in adaptive kernel bandwidths in estimating iceberg density for November.

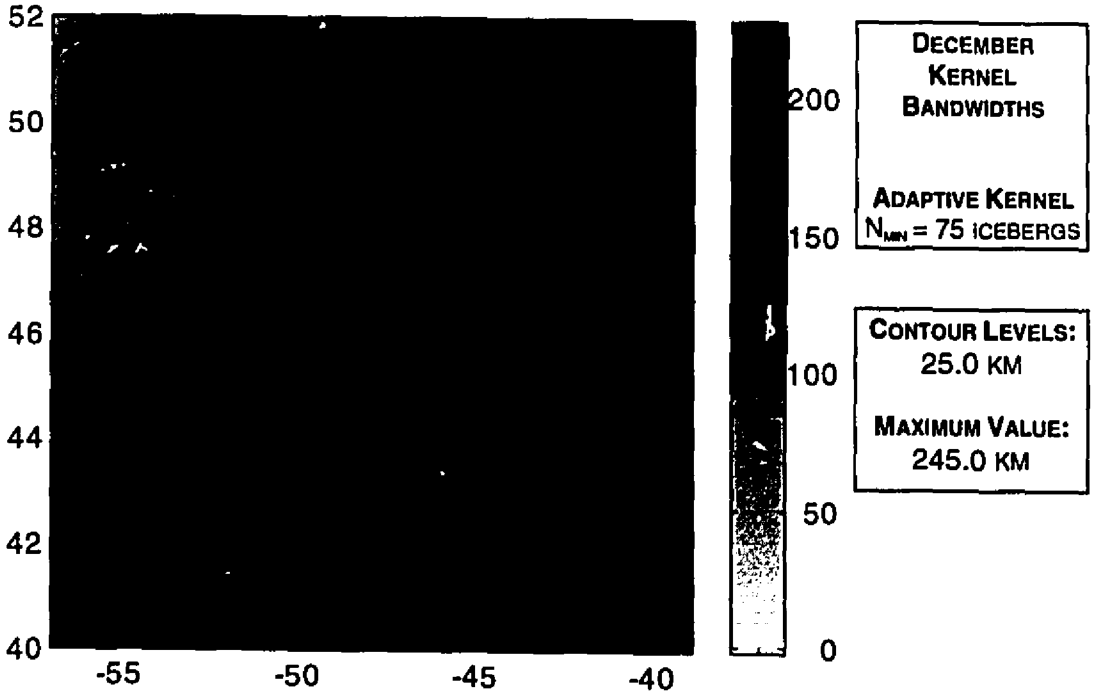

Figure D-12 Regional variation in adaptive kernel bandwidths in estimating iceberg density for December.